MASTER IN BIOCHEMISTRY AND MOLECULAR AND CELLULAR BIOLOGY

Study of xCT expression and localization in the healthy and injured rat spinal cord

Janssen, Pauline

Award date:
2017

Awarding institution:
University of Namur

Faculté des Sciences

STUDY OF xCT EXPRESSION AND LOCALIZATION IN THE HEALTHY AND INJURED RAT SPINAL CORD

Mémoire présenté pour l'obtention

du grade académique de master 120 en biochimie et biologie moléculaire et cellulaire

Pauline JANSSEN

Janvier 2017

Table of contents

Université de Namur
FACULTE DES SCIENCES
Secrétariat du Département de Biologie
Rue de Bruxelles 61 - 5000 NAMUR
Téléphone: + 32(0)81.72.44.18 - Téléfax: + 32(0)81.72.44.20
E-mail: joelle.jonet@unamur.be - http://www.unamur.be

Etude de l'expression de xCT et de sa localization dans un contexte de moelle épinière saine et lésée chez le rat

JANSSEN Pauline

Résumé

Les traumatismes de moelle épinière sont un problème de santé publique majeure. En effet, on compte aujourd'hui 2,5 millions de personnes souffrants de telles lésions dans le monde. Les conséquences fonctionnelles de ces trauma mais aussi leurs impacts psychologiques sont souvent dramatiques, les thérapies actuelles sont inefficaces pour réparer la moelle lésée ou inverser la perte de fonctions motrices. Après trauma, le microenvironnement de la moelle est perturbé et des évènements pathologiques tells que l'excitotoxicité au glutamate et le stress oxidatif contribuent à la perte des cellules neuronales et à la perte de fonctions motrices associée.

Ce mémoire s'intéresse à l'expression et la localization d'une cible thérapeutique potentielle, l'antiporteur cystine/glutamate, nommé système X_c^-, impliqué dans la lutte contre le stress oxidatif et la secretion de glutamate. Nous avons dans un premier temps généré un modèle de trauma médullaire cervical chez le rat. Ensuite, nous avons étudié le profil d'expression génique relative de la sous-unité xCT du système X_c^- qui lui confère sa spécificité à different timings post trauma. Nous nous sommes également intéressés à sa distribution cellulaire dans des moelles épinières lésées et non lésées. Enfin, nous avons investigué une voie de régulation de la transcription du gène *Slc7a11* codant pour le système X_c^- qui est le facteur de transcription Nrf2. De plus, confrontés à des problèmes de spécificité des anticorps anti-xCT, nous avons parallèlement conduit une étude de ceux-ci afin de vérifier leur spécificité. D'abord, nous avons validé le modèle experimental de trauma cervical chez le rat via des analyses fonctionnelles et morphologiques. Ensuite, nous avons démontré une augmentation de l'expression génique relative de xCT dès 4 jours post trauma et jusqu'à 6 semaines après. Les immunomarquages ont montré que les neurones et les cellules gliales expriment xCT et que celle-ci semble augmentée après trauma. De plus, nous avons démontré une augmentation de l'expression génique relative de Nrf2 dès 4 jours post trauma et se poursuivant 6 semaines après. Enfin, l'étude de 4 anticorps différents n'a pas permis de valider leur spécificité à xCT. C'est pourquoi les résultats générés dans ce travail sont les bases d'une étude approfondie de la protéine xCT et devront être confirmés une fois la spécificité des anticorps validées.

Mémoire de master 120 en biochimie et biologie moléculaire et cellulaire

Janvier 2017

Promoteur: C. Nicaise **Co-promoteur:** L. Poncelet

Université de Namur
FACULTE DES SCIENCES
Secrétariat du Département de Biologie
Rue de Bruxelles 61 - 5000 NAMUR
Téléphone: + 32(0)81.72.44.18 - Téléfax: + 32(0)81.72.44.20
E-mail: joelle.jonet@unamur.be - http://www.unamur.be

Study of xCT expression and localization in the healthy and injured rat spinal cord

JANSSEN Pauline

Abstract

Spinal cord injuries (SCI) are a major public health issue. In fact, about 2,5 millions of people in the world are affected by SCI. The functional consequences of SCI as well as their psychological impact are often dramatic, no current therapy is efficient at repairing the lesioned spinal tissue or reverse loss of motor function. Following SCI, the spinal microenvironnement is compromised and pathological events such as glutamate excitotoxicity and oxidative stress contribute to the loss of neuronal cells and subsequent loss of function.

This Master's thesis is focused on the expression and localization of a potential therapeutic target, the antiporter cystine/glutamate, namely the système X_c^-, implicated daily in the protection against oxidative stress and extracellular glutamate release. Initially, we have generated a rat model for cervical SCI. Then, we have studied the relative genic expression profile of the xCT subunit conferring its specificity to the système X_c^- at distinct timings post trauma. Its cellular distribution has been studied in uninjured and injured spinal cords. At last, we have investigated a regulation pathway of *Scl7a11* gene transcription coding for the système X_c^- which is the transcription factor Nrf2. Moreover, confronted to specificity issues concerning the anti-xCT antibodies, we have conducted a study in order to verify their specificity to xCT protein. First, the rat experimental model of cervical SCI has been validated through functional and morphological analysis. Then, we have demonstrated an increased relative expression of xCT mRNA as early as 4 days post SCI and up to 6 weeks after SCI. Immunochemistry has indicated that neurons and glial cells seem to express xCT protein and its expression seems to be increased following SCI. In addition, we have demonstrated an increased relative mRNA expression of Nrf2 as early as 4 days post contusion but also 6 weeks later. Finally, the study of 4 different anti-xCT antibodies has not allowed confirming their specificity. That is why the results generated on this work are the basis of deeper study on xCT protein and must be confirmed once the antibodies specificity has been validated.

Master's thesis in biochemistry and cellular and molecular biology

January 2017

Promotor: C. Nicaise **Co-promotor:** L. Poncelet

Remerciements

Je souhaite tout d'abord remercier monsieur Charles Nicaise de m'avoir accueillie dans son laboratoire durant toute la durée ce mémoire. Merci pour l'ensemble des choses découvertes et apprises, l'acquisition d'une grande autonomie dans mon travail au labo, ses relectures et ses encouragements quand je n'y croyais plus vraiment ! Je voudrais aussi remercier monsieur Luc Poncelet qui m'a accueillie dans son laboratoire de l'ULB et appris à réaliser les analyses neurophysiologiques sur mes rats. Je remercie sa patience et ses nombreuses explications dans ce domaine. Merci également à monsieur Yves Poumay, directeur du laboratoire adjacent au nôtre pour son chaleureux accueil et sa gentillesse.

Même si elle n'était pas mon encadrante je voudrais remercier du fond du cœur Joanna Bouchat, doctorante au LNR, pour sa présence et son aide, son soutien et ses nombreux conseils. Merci d'avoir partagés mes joies et peines pendant ses 10 mois intenses !

Je remercie aussi très chaleureusement les biotechniciens Kathleen De Swert et Benoît Balau. Grâce à eux, j'ai pu profiter d'un apprentissage approfondi des diverses techniques de laboratoire ainsi que de leur expérience dans ce domaine ce qui a été d'une grande aide ! Merci également pour leur soutien et amitié pendant cette période.

Et évidemment … Catherine, ma co-mémorante ! Nous ne nous connaissions pas mais cette expérience a permis la construction d'une belle amitié. Merci pour ces 10 mois passés ensemble dans la joie et la douleur, pour nos fous rires et ses pâtisseries, mais aussi pour ses conseils toujours bienvenus.

Ce mémoire n'aurait pas abouti sans la présence du reste des membres du LabCeti et du LNR dont la passion pour la recherche était très motivante et enrichissante. Emilie, Catherine Lambert, Céline, Valérie, Abdallah, Daniel Van Vlaender, Evelyne, Patrick et Nico, je vous remercie pour l'aide et les conseils apportés mais également de former un groupe de personnes amicales et drôles !

Je remercie également monsieur De Backer de m'avoir ouvert les portes de son laboratoire ainsi que pour ses conseils. Je remercie également les membres de son équipe, en particulier Axelle et Domi qui m'ont été d'une aide précieuse lors des manip, mais également Olivier dont les conseils ont toujours été pertinents.

Enfin, je remercie particulièrement mon compagnon Nils et ma famille qui m'ont encouragée et courageusement supportée pendant cette période.

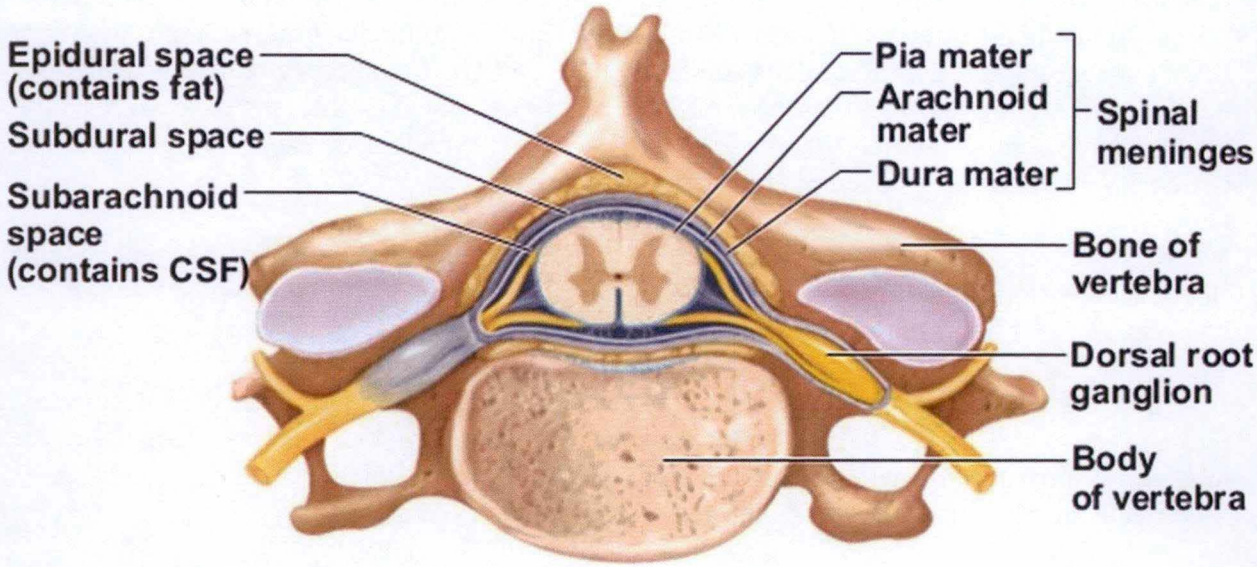

From Collection mémoires et thèses électroniques, Université Laval, Canada, Benoit Barrette (2008)

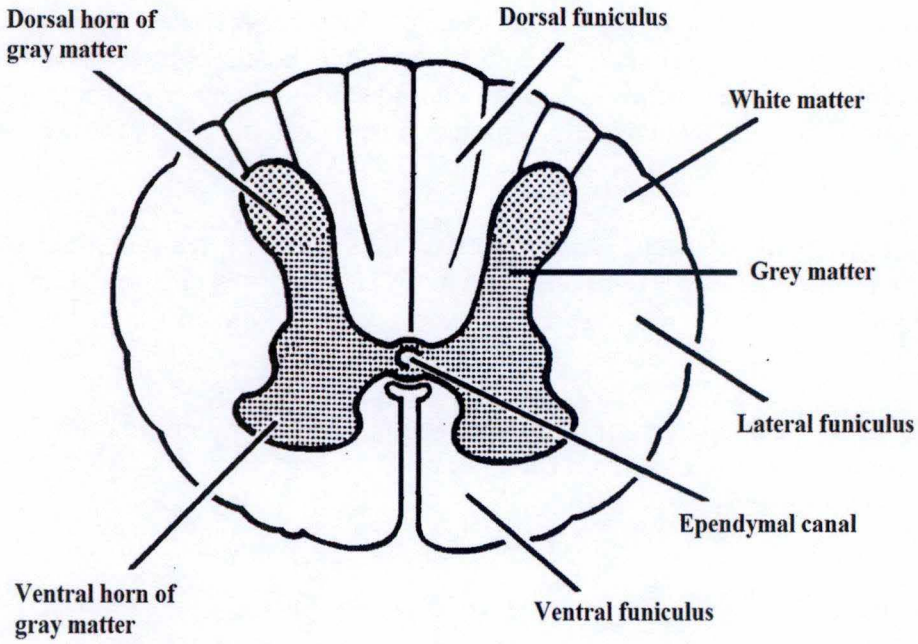

Modified from Nursing course, http://nursing411.org/Courses, consulted on 23-11-2016

Figure 1. Structure of the spinal cord

I. Introduction

1. Structure and function of the spinal cord

1.1. Histology of the spinal cord

The nervous tissue includes the central nervous system (CNS), composed of the brain, the cerebellum, the brainstem and the spinal cord, and the peripheral nervous system, composed of the nerves spreading in the organism and the nervous nodes (Poumay, 2012-2013).

In this work, we are most particularly interested in the spinal cord. This tissue runs through the vertebral canal formed by the vertebra (figure 1). The spinal cord is also protected by non-bone envelops: the dura mater, the arachnoid and the pia mater. These envelops are called spinal cord meninges and are directly in contact with the vertebra (figure 1). (Poumay, 2012-2013)

In spinal cord histological section, two distinct tissues are found.

In one hand, the grey matter occupies the centre area of the section and presents a butterfly shape (Poumay, 2012-2013). The ependymal canal lies in its centre and allows the flow of the cerebrospinal fluid (CSF) thanks to the motion of ependymal cells cilia (Agamanolis, 2016). This one is produced by the choroid plexuses, located in the lateral and fourth ventricles, from arterial blood. Its composition is quite similar to arterial blood. The main difference is that CSF is nearly protein-free (0,3%) and electrolytes levels are a bit modified (Agamanolis, 2016). Indeed, it contains high level of chloride and sodium but is quite poor in potassium and magnesium (Agamanolis, 2016). Three main functions can be attributed to the CSF. First, it has a protective role against trauma (LabCE, 2016). It provides nutrients to the CNS and it removes waste products derived from its metabolism (LabCE, 2016). Glial cells are present in the grey matter (Poumay, 2012-2013). Yet, the motor neurons pericaryons (cellular body), dendrites and the beginning of their axon are only found in the ventral horn of the grey matter whereas the sensory neurons are localised in the dorsal horn of the grey matter (Poumay, 2012-2013). Thus, all the synapses of the organism are located in the grey matter. At last, the space between neurons pericaryon, glial cells and blood capillaries is called the neuropile and is formed by the tangle of axons, dendrites and glial extensions (Poumay, 2012-2013). (figure 1)

On the other hand, the white matter surrounds the grey matter and is composed of a nerve fibres tangle and glial cells. The white matter is divided into the dorsal, the lateral and the ventral funiculus. The term funiculus refers to a large group of nerve fibres located in a given area (Dafny, 2000). Within a funiculus, there are fasciculi which are smaller groups of nerve fibres, with distinct origins but with common features and functions (Dafny, 2000). (figure 1)

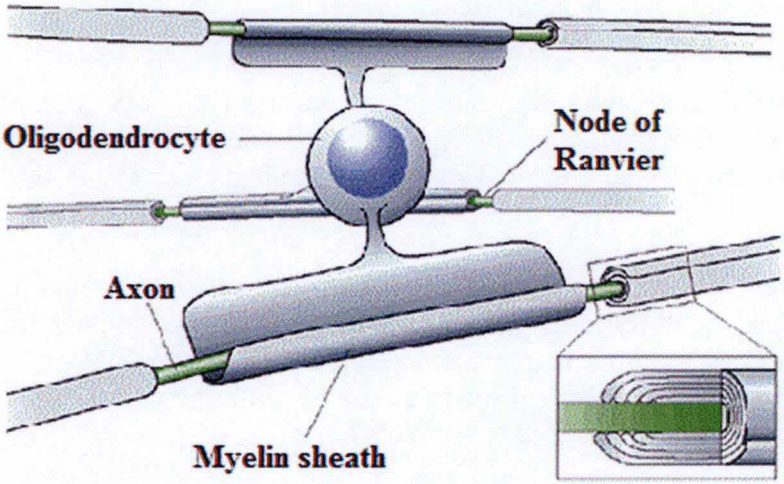

Modified from Popko, *Naturegenetics* (2003)

Figure 2. The myelin sheath is produced by oligodendrocytes

In the CNS, nerve fibres present in the white matter can be of among two types. Unmyelinated fibres are completely lacking myelin sheath and are only formed by their cylindrax. These are the fibres which also run through the grey matter. The second type is the myelinated fibres (figure 2). As its name suggests, in this kind of nerve fibres, the cylindraxe is enwrapped by a myelin sheath produced by the oligodendrocytes (figure 2). Note that the myelin sheath is not continuous around the cylindraxe, but presents interrupted regions regularly spaced. These interrupted areas are called Ranvier's nodes. They are rich in sodium channels allowing the generation of an action potential only at this level. This way of nervous influx conduction is termed salutatory conduction.

The myelin sheath is composed of both proteins (30%) and lipids (70%) (Kettenmann & Verkhratsky, 2011). In particular, the myelin binds lipids components to protein. Axons insulation is the main function of the myelin sheath and allows by this way the high velocity of nervous influx conduction. Thus, there is no synapse in the white matter; its function is the transmission of the nervous influx.

1.2. Cell types of the spinal cord

1.2.1. Neuronal cells

Neurons are the cells involved in the conduction of the nervous influx. Their morphology can be very variable in terms of shape or size. In fact, it can be spherical, pyramidal as well as star-shaped or fusiform. Their size can go from 6µm to 100µm of diameter (Poumay, 2012-2013). Their pericaryon encloses a large spherical nucleus showing a clear nucleoplasm. That suggests the euchromatin is predominant in the nucleus and by this way an active transcription. Neuron cytoplasm also contains distinct organelles. The rough endoplasmic reticulum (RER) is very abundant and disseminated in the entire cytoplasm except in the implantation cone of the axon (Poumay, 2012-2013). It allows active proteins synthesis. Note that some proteins are produced in dendrites but not in the axon (Lodish et al., 2000). In neurons, RER is called Nissl blocks. Then, the Golgi apparatus is well developed and makes a crown around the nucleus (Poumay, 2012-2013). Numerous mitochondria and lysosomes are also found in neuron cytoplasm (Poumay, 2012-2013). The important number of lysosomes is the reflect of a permanent replacement of the plasma membrane and cellular components (Poumay, 2012-2013). In addition, the presence of many mitochondria highlights the heavy metabolism of these cells (Poumay, 2012-2013).

The number of neuronal extensions and their size are likely fluctuating (Poumay, 2012-2013). Dendrites are generally multiples and present arborescence. They receive chemical signals from axon termini of other neurons, transform them into small electrical influx and always carry this influx to the pericaryon (Lodish et al., 2000; Poumay, 2012-2013). In the CNS, dendrites are particularly long and branched. It permits the neuron cell body to create many synapses (up to a thousand) and by this way to receive information from other neurons (Lodish et al., 2000).

The axon, for its part, is unique and longer than the dendrites. It has few ramifications, its diameter is regular and it ends with a bulge called the synaptic button. It emerges from neuron pericaryon in a region called the axon hillock (Lodish et al., 2000). On the contrary to the pericaryon, the axon is poor in organelles and does not contain ribosomes, so it is not able to produce protein. But as dendrites, it is rich in neurotubules (i.e. microtubules) and neurofilaments (i.e. intermediate filaments) (Poumay, 2012-2013).

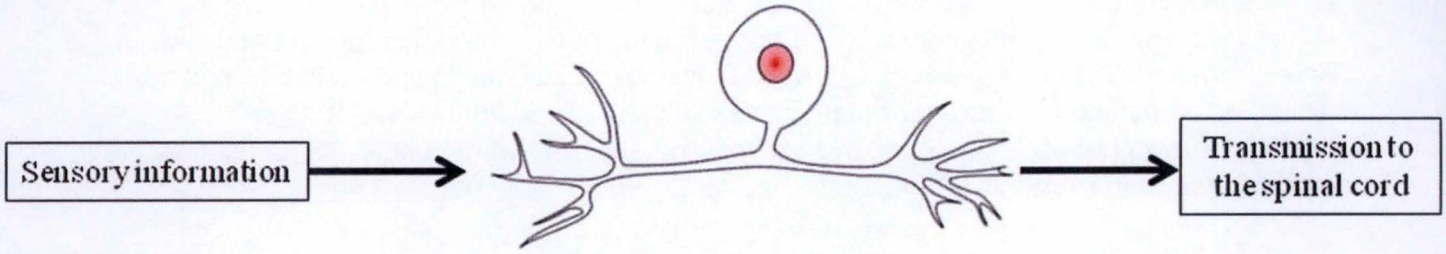

Modified from wikimedia.com

Figure 3. Illustration of pseudounipolar sensory neuron

In the CNS, 3 types of neurons can be distinguished.
The sensory neurons are found in the dorsal horn of the grey matter. They are activated by environmental sensory inputs that can be physical elements such as light, sound, physical contact or chemical signals like taste and smell (Boundless, 2016). Their function is to convert such external stimuli into internal electrical stimuli and to send them to other neurons in the spinal cord through their projections. Most of the time, sensory neurons are pseudounipolar. In fact, their axon takes 2 directions: one side is linked to dendrites receiving sensory signals and the other side is connected to the spinal cord in order to transmit the received information (figure 3) (Boundless, 2016).

The second and most common neurons class present in the spinal cord are the motor neurons. They are exclusively localised in the ventral horn of the grey matter (Poumay, 2012-2013). About their structure, they are composed of a single axon and numerous dendrites and are called multipolar neurons (Boundless, 2016). Thanks to their axon, motor neurons project out of the CNS to reach directly or indirectly muscles. The interface between the synaptic button and the muscle fibre is called the neuromuscular junction.

Finally, the third type of neurons present in the spinal cord is the interneuron. They are neither motor nor sensory. Thanks to their multipolar structure, they establish connections between the other types of neurons in the CNS (Boundless, 2016). They act locally and are connected to near motor or sensory neurons (Boundless, 2016).

1.2.2. Glial cells

Both in the white and grey matters, other cell types are found, called the neuroglia or glia. These cells are not neurons and do not participate directly to the nervous influx transmission. But they have a crucial importance for neurons. In fact, they act as support for neurons and they provide them nutrients and protection. Furthermore, the neuroglia can be divided into two parts: the epithelial neuroglia and the interstitial one. Moreover, the macroglia and the microglia are distinguished in the interstitial neuroglia.

The epithelial neuroglia is organized as a simple epithelium with juxtaposed glial cells. In the spinal cord, it borders the ependymal canal. In this case, these cells are called ependymocytes. Their function seems to be the regulation of exchanges between the CSF and the nervous tissue. They show cilia associated to few microvilli which agitate the CSF.

The interstitial neuroglia is defined as the macro and micro glia. The difference is their embryonic origin. Surely, the macroglia comes from the ectoderm and the microglia has a mesodermic origin.

First, the macroglia corresponds to the astrocytes (protoplasmic and fibrous) and the oligodendrocytes. They are star-shaped cells with ramified thin extensions representing 20% to 40% of the glial population (Verkhratsky & Butt, 2013). These extensions can reach a close neuronal cylindraxe or pericaryon or blood capillaries.

Moreover, fibrous astrocytes are distinct to protoplasmic ones. Indeed, cytoplasm of fibrous astrocytes is rich in glial fibrillary acidic protein which forms intermediate filaments whereas protoplasmic astrocyte cytoplasm is poor of it. Moreover, protoplasmic astrocytes are

preferentially found in the grey matter while the fibrous ones are mostly located in the white matter.

About their functions, they are crucial for neurons migration during embryonic development. In the adult CNS, they offer the micro-architecture of the nervous parenchyma and in case of lesion they proliferate in order to establish a scar (the glial scar). Moreover, astrocytes provide nutrients for neurons via the neurovascular unit. In fact, the vascular endfeet of the astrocyte which is a thin cytoplasmic extension is in close contact with blood capillaries and another extension is in close contact with neuron. It has been found that astrocytes are able to absorb glucose present in the blood and to convert it into lactate (Kettenmann & Verkhratsky, 2011). Then, the produced lactate is given to neurons as energy substrate. A very interesting point is these cells are the only ones in the CNS competent to synthetize glycogen and hence can act as energy suppliers (Kettenmann & Verkhratsky, 2011).

These glial cells are also involved in 80% of the reuptake of extracellular glutamate released by neurons. This function is imperative because accumulation of extracellular glutamate can be neurotoxic. The reuptake occurs through the glutamate/aspartate transporter GLAST and the glutamate transporter-1 GLT-1 in rodent. At last, individual astrocytes are integrated into astroglial syncytia thanks to gap junctions, called connexins, located on their peripheral processes (Kettenmann & Verkhratsky, 2011).

The second cell population included in the macroglia are the oligodendrocytes. These are the prime glial cells corresponding to 75% of the glia (Poumay, 2012-2013). Their main function is the production of the myelin sheath encompassing axonal segments. Myelinating oligodendrocytes are found everywhere in the white matter alongside the myelinated nerve fibres, but it also exists non-myelinating oligodendrocytes called satellite oligodendrocytes (Kettenmann & Verkhratsky, 2011). They are localised in the white matter close to neuron pericayons. Their function is still unclear but it is supposed that they are involved in the ionic homeostasis regulation (Kettenmann & Verkhratsky, 2011). The myelinating phenomenon corresponds to the winding of oligodendrocytes processes around the axon. As astrocytes, oligodendrocytes are interconnected by connexins (Kettenmann & Verkhratsky, 2011).

The microglia represents for its part only 5% to 10% of the glial population (Poumay, 2012-2013). It corresponds to the endogenous CNS immune system and is derived from blood monocytes. Microglia progenitors migrate in the CNS during the foetal life or postnatal period (Poumay, 2012-2013). Once differentiated, they show a small cell body with many long, thin and ramified processes suggesting an ability in antigen presentation (Kettenmann & Verkhratsky, 2011; Poumay, 2012-2013). This phenotype is characteristic of the M2 or neuroprotective state of microgliocytes under physiological conditions. Microglial processes are motile and act as rapid scanning system of the nervous parenchyma (Kettenmann & Verkhratsky, 2011). This motility associated to plasma membrane receptors allows the fast detection of injury and the initiation of the appropriate response. Thus, under pathological conditions, microglia can be activated in their M1or neurotoxic state and their phenotype is progressively modified and characterized by an amoeboid shape and phagocytique ability (Mesci et al., 2015).

1.3.Functions

The nervous system acts in three ways. First, peripheral sensitive nerves collect information received by the organism. Then, they come back to the spinal cord and the information is transmitted to the brain. Further, the brain processes this information and finally it sends response signals through motor nerves in the spinal cord to induce the proper behaviour (Poumay, 2012-2013). Thus, even the spinal cord constitutes only 2% of the total CNS, this tissue is crucial in importance (Dafny, 2000). It carries information both from the brain to the body (efferent pathway) and from the body to the brain (afferent pathway). Indeed, it contains motor neurons in the ventral horn involved in the control of voluntary and involuntary movements as well as neurons mediating most of the visceral functions and sensory neurons which initiate the processing of the sensory information (Dafny, 2000).

2. *Spinal cord injury*

2.1.Epidemiological data

Spinal cord injury (SCI) is a public health problem in 3 ways. First, in the United States of America, 400000 individuals are living with SCI (Melton, 2016). The population at risk is between 16 and 30. However, recent demographic data reveals an increased SCI incidence in elderly people often due to a low energy fall (Oxland et al., 2011). Moreover, 82% of people undergoing SCI are male (Melton, 2016). The most common causes of SCI are in first place car accidents (44%), next the acts of violence, slips and falls, sports-related damages and trampoline accidents (Melton, 2016). Secondly, from a patient's perspective, SCI induces disorders to motor and sensory functions, leading to physical disabilities and to decreased quality of life. Thirdly, from an economic point of view, SCI is expensive to manage: there is an acute phase, needing immediate care and a long-term phase (medical complications, functional rehabilitation), also demanding financial investment (Singh, Tetreault, Kalsi-Ryan, Nouri, & Fehlings, 2014).

2.2.Functional consequences of SCI

SCI are damages to the spinal cord that induces temporary or permanent changes in its function and structure. There are two types of SCI: traumatic SCI (e.g. a car accident) and non-traumatic SCI resulting from degeneration or disease (e.g. cancer); up to 90% of SCI have traumatic causes. Importantly, more than 50% of these traumatic SCI arise at the cervical level. Various combinations of forces are applied to the spine during the serie of events inducing the SCI. When these forces are strong enough, they can disrupt the vertebral column, resulting in vertebra fracture and/or ligaments rupture. This kind of injuries is most of the time (80%) associated to higher energy fracture-dislocations (40%) and burst fractures (30%) with the same frequency (Oxland et al., 2011). In fracture-dislocation case, 2 adjacent vertebra are broken, ligaments are torn, resulting in an offset of the vertebral column axis that induces compression shearing of the spinal cord between the dislocated vertebra (Oxland et al., 2011). In burst fracture situation, the dorsal region of the vertebra body is broken and the bone "bursts" and bone fragments are projected into the spinal cord (Oxland et al., 2011).

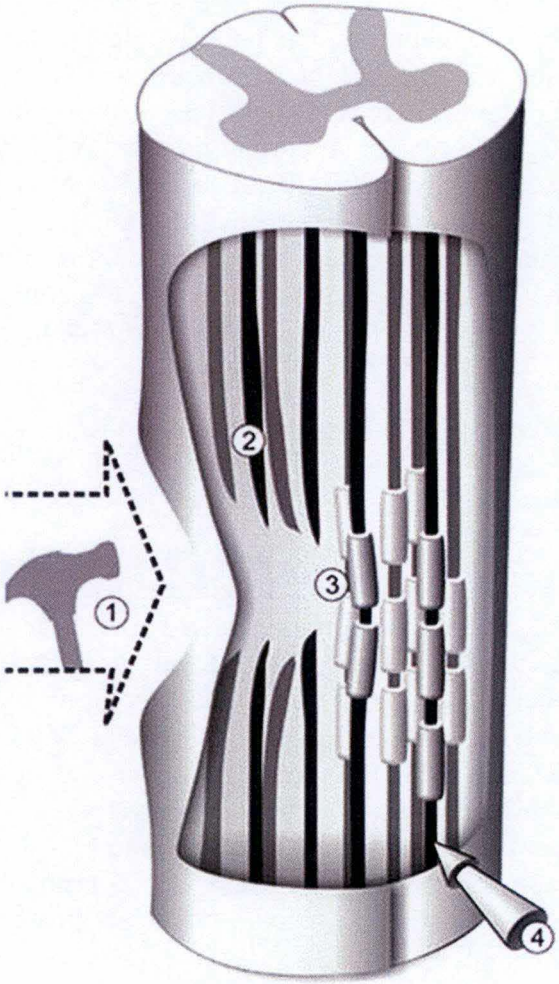

Acute stage:
1. Direct impact
2. Lacerated axons
3. Contused axons
4. Influx of inflammatory cells

Modified from Ronsyn et al., *Spinal cord* (2016)

Figure 4. Schematic presentation of the pathophysiological events following SCI in the acute phase

Following SCI, the spinal cord cannot conduct the nervous influx anymore and motor and sensory functions perturbations appear. Most of the time, the higher on the spinal cord the SCI takes place, the more severe functional consequences will follow. SCI are also classified as complete or incomplete according to whether there are any movements or sensations at or under the level of injury site (Sheperd, 2016). In particular, the permanent loss of motor neurons in the spinal ventral horn is related to loss of motor function in the peripheral muscles. At the cervical level of the spinal cord, two major populations of motor neurons can be found: phrenic motor neurons innervating the respiratory diaphragm and limb motor neurons innervating the forelimb muscles (Nicaise et al., 2013). Thus, cervical spinal cord injury (cSCI) can result in members and trunk paralysis, breathing and sexual disabilities and incontinence (Liverman, Altevogt, Joy, & Johnson, 2005; Sheperd, 2016). Sometimes, speak ability can also be impaired (Sheperd, 2016).

In addition, pain is a common consequence following SCI. In fact, it appears that 60 to 80% of people affected by SCI report chronic pain (Liverman et al., 2005). Chronic pain is so deleterious that depression and suicidal ideation are common in years following the trauma (Augustin, Grosjean, Chen, Sheng, & Featherstone, 2007; Liverman et al., 2005).

2.3.Acute, subacute and chronic phases following SCI

SCI pathophysiology is divided into distinct 3 phases characterised by specific pathological events: the acute phase (seconds to minutes following SCI), the subacute phase (minutes to weeks following the injury) and the chronic phase (months to year after the SCI).

Numerous cells and molecules from immune, nervous and vascular systems are concerned in each phases. Whereas the most engaging cells are already present in the spinal cord, others cells are recruited to the injured site through the blood. There are also up and down regulation of genes involved in the inflammation process, the repair, the neurotransmission and local responses near the injury site (Liverman et al., 2005).

The acute phase, immediately after the trauma, is characterised by both systemic and local events. (figure 4)

At systemic level, a short increase in blood pressure occurs in the seconds following the injury, but rapidly after, a prolonged hypotension state settles. It can be associated to systemic hypoxia if respiration is blocked by paralysis of diaphragm muscle for example (Liverman et al., 2005). The spinal shock results from a lack of oxygen and nutrients provided to the spinal cord tissue and prevent it to function during the first 2 to 24h post injury (Liverman et al., 2005).

However, many events close to the injury site also participate to the spinal shock. First of all, necrosis phenomenon begins as the direct cellular consequence of the trauma and neurons and their axon start to die as well as the endothelial cells covering spinal cord blood vessels walls (Liverman et al., 2005).

In addition, neurons which survived produce series of action potentials leading to significant changes in ion levels. Increase in ion levels is also due the rupture of nervous cells plasma membrane and the further release of their content (Liverman et al., 2005). At last, ions levels can become toxic and induce the death of neurons in their proximity.

In parallel, excess amounts of neurotransmitters are released in the extracellular space and can be toxic for neurons as well. The mechanism involved in this case is called excitotoxicity. Besides, the trauma results in haemorrhage and the subsequently disruption of the blood-spinal cord barrier (Liverman et al., 2005). The consequently local formed oedema occupies the space and by this way endangers even more the nervous cells (Liverman et al., 2005).

Another observed phenomenon is vasospasm, meaning a decrease up to 80% of the blood flow and thrombosis in small blood vessels (Liverman et al., 2005). Thus, vasospasms induce ischemia in the nervous tissue. It has been shown that, following SCI, the grey matter is much more necrotic than the white matter. It can be explained by the fact that the grey matter is richer in blood vessels than the white matter (Liverman et al., 2005; Wolman, 1965).

From minutes to weeks after SCI, **the subacute phase** takes place. This phase is firstly characterised by a significant expansion of the lesion. Necrosis, oedema, ion levels shifts continue during the subacute phase but new elements are added.

In fact, formation of free radicals, reactive oxygen species in particular, begins and is at the origin of oxidative stress.

Furthermore, calcium influx presents disturbance after SCI and calcium levels become dangerously high. This process occurs in 2 steps. First, during the acute phase, there is an infiltration of sodium in cells leading to the subsequent massive import of calcium by sodium-calcium exchangers in the subacute phase (Liverman et al., 2005). High intracellular levels of calcium result in the activation of destructive enzymes and the formation of free radicals (Liverman et al., 2005).

Moreover, secondary axonal degeneration is noticed as well (Park, Velumian, & Fehling, 2004). It is characterised by alterations in neurofilaments architecture and axon membrane integrity. It corresponds to numerous events: a focal perturbation of the axolemma, the swelling of axonal mitochondria, a decrease in intermodal axonal diameter, the loss of axonal neurotubules, the compaction and degeneration of neurofilaments, the separation of the axonal membrane from the myelin sheath associated to the disruption of the myelin sheath and axonal disconnection (Park et al., 2004).

In addition, axonal degeneration is also linked to oligodendrocytes death. Indeed, since one oligodendrocyte myelinates up to 40 distinct axons, the death of many oligodendrocytes after SCI is dramatic for the nearby axons (Park et al., 2004).

SCI also activates the immune system and includes the neutrophils, the monocytes, the T lymphocytes and the resident immune cells of the CNS, the microglia.

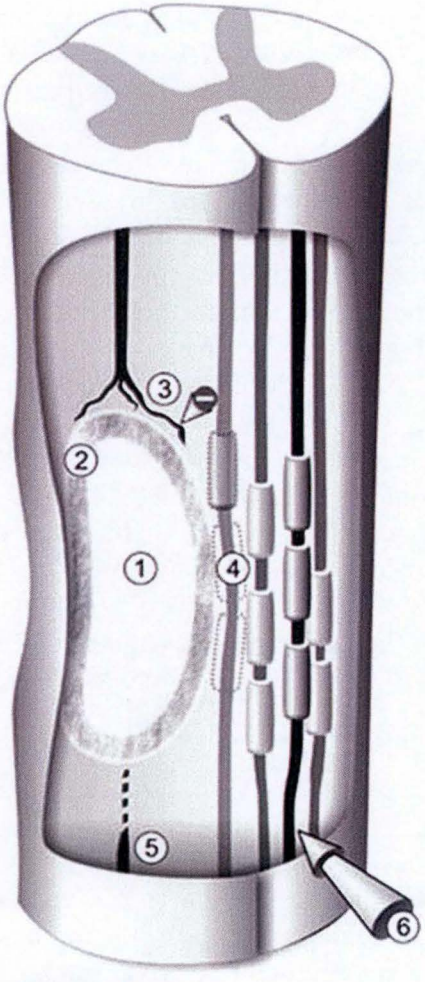

Chronic stage:
1. Central cavity
2. Scar tissue
3. Inhibition of axonal regeneration
4. Demyelination
5. Axonal dieback
6. Influx of inflammatory cells

Modified from Ronsyn et al., *Spinal cord* (2016)

Figure 5. Schematic presentation of the pathophysiological events following SCI in the acute chronic phase

The microglia is activated following injury and starts removing cellular and tissue debris. In addition, microglial cells release pro-inflammatory cytokines and free radicals that participate to the lesion expansion and neurons death (Liverman et al., 2005).

The first immune cells bringing by the circulatory system at the site of injury are the neutrophils. They reach the site thanks to adhesion molecules secreted by the vascular endothelial cells. Their function is to remove microbes and cellular debris, but they also releasepro-inflammatory cytokines and free radicals that reinforce the activation of glial and other immune cells (Liverman et al., 2005).

Over the next 24 hours, monocytes arrive from the circulatory system, enter the spinal cord tissue and turn into macrophages. These cells remove debris by phagocytosis (Liverman et al., 2005).

To finish, the function of T lymphocytes is under debate. Indeed, some suggest that T lymphocytes are destructive autoreactive T lymphocytes which induce demyelination. Other argue the contrary and think that these T lymphocytes protect myelinated axons (Liverman et al., 2005).

The last process occurring during the subacute phase is the apoptotic death of cells. Following SCI, apoptosis affect both neurons and glial cells. Contrary to necrosis where cellular debris are released in the environment and induce damages, the fragments of apoptotic cells are captured by other cells in order to avoid the dispersion of toxic debris in the environment and to reduce the inflammation (Liverman et al., 2005).

The last phase following SCI is called **the acute chronic phase** and covers of months to years after the trauma (figure 5).

Because of the death of oligodendrocytes, demyelination of axons is amplified. Moreover, they undergo alterations of their ion channels resulting in disturbance of the nervous influx conduction (Liverman et al., 2005). These 2 elements are at the origin of the chronic pain.

In addition, the formation of the glial scar takes place during the chronic phase. The scar tissue is formed by a fibrotic part and a glial part. The fibrotic scar corresponds to an invasion of fibroblasts and the formation of a collagen matrix (Yuan & He, 2013). Surrounding the fibrotic scar, the reactive astrogliosis induces the formation of the glial scar containing reactive astrocytes linked to each other, oligodendrocytes and microglial cells. It provides a growing microenvironment that prevents axon regeneration because it forms a thick extracellular matrix formed by a network of proteoglycans (Liverman et al., 2005; Yuan & He, 2013).

Oligodendrocytes express for their part a strong axon growth inhibitor, Nogo-A. At last, activated microglia releases free radicals and pro-inflammatory cytokines in particular (Liverman et al., 2005; Rowland, Hawryluk, Kwon, & Fehlings, 2008).

A.

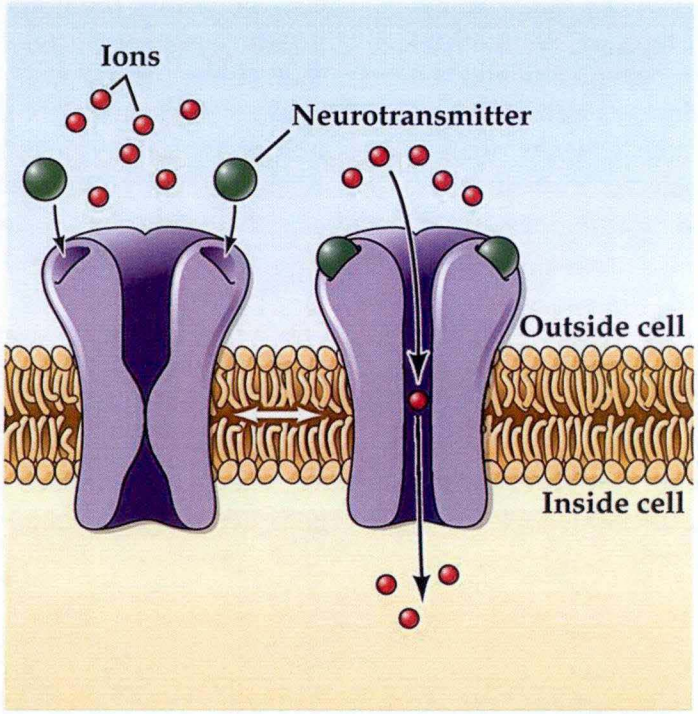

From *Neurosciences*, McGill (2012)

B.

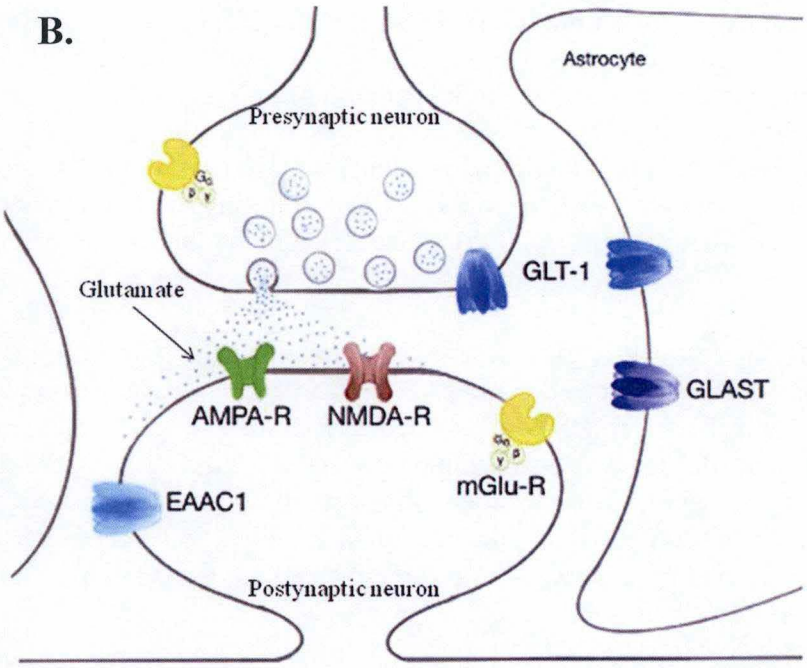

Modified From Rimmele and Rosenberg, *Neuroch. Int.* (2016)

Figure 6. A. Illustration of ionotropic membrane receptor. B. Localisation of astrocytic glutamate transporters at the synaptic cleft level.

2.4. Glutamate excitotoxicity and oxidative stress are involved in SCI physiopathology

Two phenomenons are critical in the SCI physiopathology. It includes glutamate excitoxicity beginning in the minutes following SCI and oxidative stress during the subacute phase (Lopez, Dempsey, & Vemuganti, 2015).

Glutamate excitotoxicity is a "pathological state caused by excessive or prolonged exposure to glutamate resulting in neuronal cells death" (Doble, 1999). Interestingly, this term is applied to neurons which are excitatory cells but also to glial cells. This is surprising because these cells do not present an excitability potential (Xu, Hughes, Ye, Huslebosch, & McAdoo, 2004).

The major excitatory activity of neurons is associated to a release of the glutamate neurotransmitter in the extracellular space induced by the action potentials. The post synaptic cell shows ionotropic membrane receptors to neurotransmitters like NMDA (n-methyl-D-aspartate) or AMPA (α-amino-3-hydroxy-5-methyl-4-isoxazolepropionic acid) receptors. The binding of glutamate to such receptors induces the opening of cation channels leading to an influx of sodium and calcium into the cells associated to a release of potassium in the extracellular space. This ionic flux is at the origin of the excitatory post-synaptic potentials and the following conduction of the received nervous influx. (figure 6A)

Moreover, in order to maintain a proper synaptic transmission and to recycle neurotransmitters, glutamate must diffuse rapidly in the synaptic cleft but also be quickly removed from this space (Rimmele & Rosenberg, 2016).

Under physiological conditions, extracellular glutamate is usually removed from the synaptic cleft by the astrocytes and their glutamate transporters to maintain extracellular glutamate concentration low. So, activity of these glutamate transporters is crucial to preserve the signalling function of synapses, to regulate the activation of the nearby metabotropic glutamate receptors and to control the interaction between excitatory synapses (Rimmele & Rosenberg, 2016). Transport of glutamate against its concentration gradient is allowed by the electrochemical sodium and potassium gradients maintained by the Na/K ATPase as well as the interior negative membrane potential (Rimmele & Rosenberg, 2016).

There are two kinds of sodium-dependent glutamate transporters almost exclusively expressed in processes of astrocytes close to the synaptic cleft (Rimmele & Rosenberg, 2016).

The transporter GLT1 in rodent (equivalent to the human EAAT2) has a key role in glutamate homeostasis and is responsible for 95% of glutamate uptake in the CNS (Lepore et al., 2011; Takana et al., 1997). Note that however, GLT1 seems also to be expressed in axon terminals of neurons (Rimmele & Rosenberg, 2016). The transporter GLAST (equivalent to the human EAAT1), for its part, is the most expressed in the cerebellum and has been shown to be an important part of a macromolecular complex, including mitochondria, glycolytic enzymes and Na/K ATPase, involved in glutamate metabolism (Baeur et al., 2012). Interestingly, *in vitro* and *in vivo* experiments have highlighted that astroglial expression of GLT1 and GLAST are, at least, regulated by neurons (Rimmele & Rosenberg, 2016). (figure 6B)

Following SCI, extracellular levels of the amino acid glutamate increase dramatically up to neurotoxic levels within minutes after the injury (Park et al., 2004).

This extracellular glutamate presents distinct origins. First, after SCI, neurons are damaged, lysed and enter in necrosis and release glutamate in quantity (Park et al., 2004). It has been shown an increased expression of GLT1 and GLAST in a first time following SCI. This could suggest an immediate adaptive response to counter glutamate excitotoxicity (Y. Kim, Park, Cho, Kim, & Yoon, 2011). But, over time, GLT1 and GLAST present a reduced expression and hence a decrease in glutamate re-uptake by glia and/or neurons (Y. Kim et al., 2011).

ROS produced in large amount after SCI seem also been involved in the failure of glial cells to properly reuptake extracellular glutamate (Park et al., 2004).

Moreover, a reversal of the glutamate uptake by glutamate transporters has been highlighted. This reversed transport is attributed to the disruption of ion gradients in the cells and the further failure of the Na/K ATPase (Nicholls & Attwell, 1990; Park et al., 2004).

In addition, this ionic disturbance is characterised by an increased intracellular sodium, potassium and calcium levels leading to an overactivation of metabotropic receptors and the subsequent stimulation of glutamate release in the extracellular space (Park et al., 2004).

Furthermore, microglial cells are similarly prone to release glutamate after SCI (Piani & Fontana, 1993).

The excessive amount of extracellular glutamate leads to the overactivation of ionotropic glutamate receptors (NMDA, AMPA). This overactivation induces a massive calcium influx within the neurons. Such an excessive calcium influx then stimulates the release of intracellular calcium stock. Thus, intracellular concentrations in calcium become highly toxic by activating proteases, nucleases and ROS generation, leading to neurons death (Lopez et al., 2015; Park et al., 2004). In addition, glutamate can induce excitotoxicity in neurons and oligodencrocytes by inhibition of cystine uptake resulting in lower levels of GSH and the subsequent oxidative stress.

As briefly described in the subacute phase, SCI promotes the formation of free radicals and hence induces oxidative stress. **Oxidative stress** is defined as an "imbalance between oxidants and antioxidants in favour of the oxidants, potentially leading to damage" (Zheltova, Kharitonova, Iezhitsa, & Spasov, 2016). The main free radicals produced under such pathological conditions are the reactive oxygen species (ROS) such as superoxide, hydrogen peroxide and hydroxyl radical and reactive nitrogen species (RNS) like nitric oxide and peroxynitrite. These molecules are highly toxic for neurons and are produced in great amount following SCI.

Free radical formation occurs mainly in the mitochondria and is characterised by the loss of a most peripheral electrons of oxygen atoms. Thus, oxygen atoms become odd number electrons molecules. This loss of peripheral electrons makes oxygen atoms very instable, reactive and short lived (Arulselvan et al., 2016; Liverman et al., 2005). The goal for these ROS is to quickly reach a stable state by pulling the electrons of nearby atoms (Liverman et al., 2005).

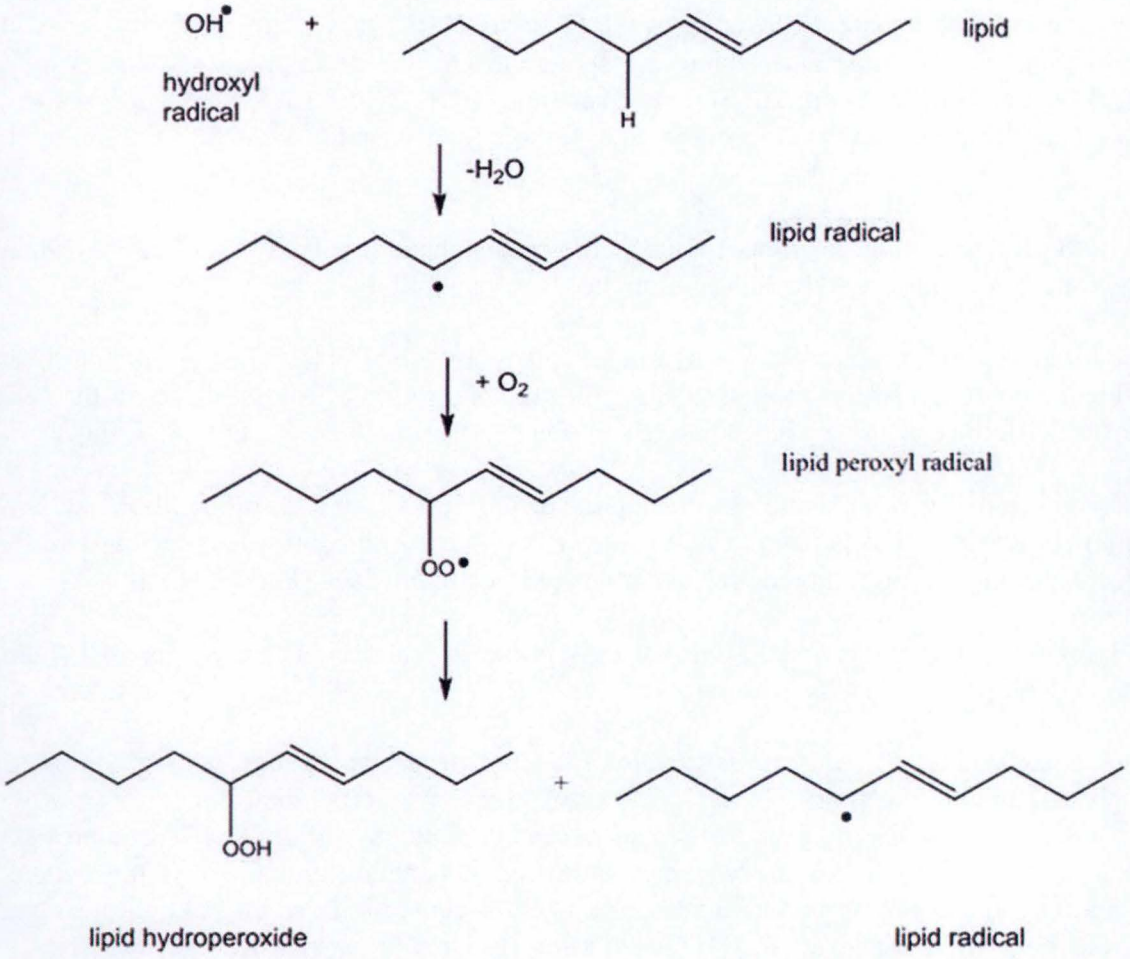

From Butterfield and Reed, *Clinical proteomic Journal* (2016)

Figure 7. Lipid peroxidation. Formation of lipids radicals

The main consequence of free radicals formation is lipids peroxidation. This process occurs in 3 steps: the initiation, the propagation and the termination.

First, ROS attack an allylic carbon of a lipid molecule resulting in the formation of a lipid carbon-centred radical. Then, it reacts with O_2 and becomes a lipid peroxyl radical. Lipid peroxyl radicals are unstable and can in turn react with a nearby lipid and resulting in a lipid hydroperoxide (figure 7). It leads to a chain reaction cascade in the lipids of the plasma membrane terminating by the lysis of the membrane and at the end, the death of the cell (Butterfield & Reed, 2016).

However, under physiological conditions, there is equilibrium between free radical products and antioxidative molecules which protect the organism against these reactive molecules (Arulselvan et al., 2016). Indeed, cells can support a certain level of lipids peroxidation and are able to perform the termination step of the process (Butterfield & Reed, 2016).

On the one hand, lipids peroxidation propagation can be stopped by the formation of a non radical lipid + O_2 by 2 lipid radicals (Butterfield & Reed, 2016).

On the other hand, vitamin E can catch electrons from lipid radicals making them stable again. Vitamin E radical is then brought back to its initial state thanks to the vitamin C or the glutathione (GSH) enzyme (Butterfield & Reed, 2016).

Moreover, ROS also attack membrane enzymes and can disturb ion gradients as well as damage the DNA (Liverman et al., 2005).

At last, the nitrosative stress is a phenomenon associated to oxidative stress and is due to the increase in RNS production (Butterfield & Reed, 2016). The nitration of antioxidant proteins inactivates them and can increase oxidative stress, induce the disruption of the blood-spinal cord barrier and dysfunction in metabolic function and also damage the DNA (Butterfield & Reed, 2016).

Furthermore, it has been shown that the NADPH oxidase and the mitochondrial electron transport chain are over stimulated following CNS injury. Indeed, after insult, NMDA receptors are activated and an important calcium flux into the cell occurs (Nakka & Prakash-babu, 2014). This stimulates the cytosolic NADPH oxidase and the mitochondrial electron transport chain which produce ROS (Lopez et al., 2015).

Yet, free radicals highlight effect at vascular level. In fact, excessive amount of free radicals induce decreased spinal cord blood flow, enhance platelets aggregation, oedema and inflammatory responses (Park et al., 2004).

As suggested in the lipid peroxidation termination process, cells are in fact able to struggle with oxidative/nitrosative stress by regulation of ROS production, elimination of them thanks to antioxidantive enzymes (SOD, catalase, GSH) and scavenger molecules (vitamin E and C) and by the repair of the damaged structures (Manzanero, Santro, & Arumugam, 2012). Unfortunately, following SCI, ROS generation is so important that the antioxidant defence systems are overwhelmed.

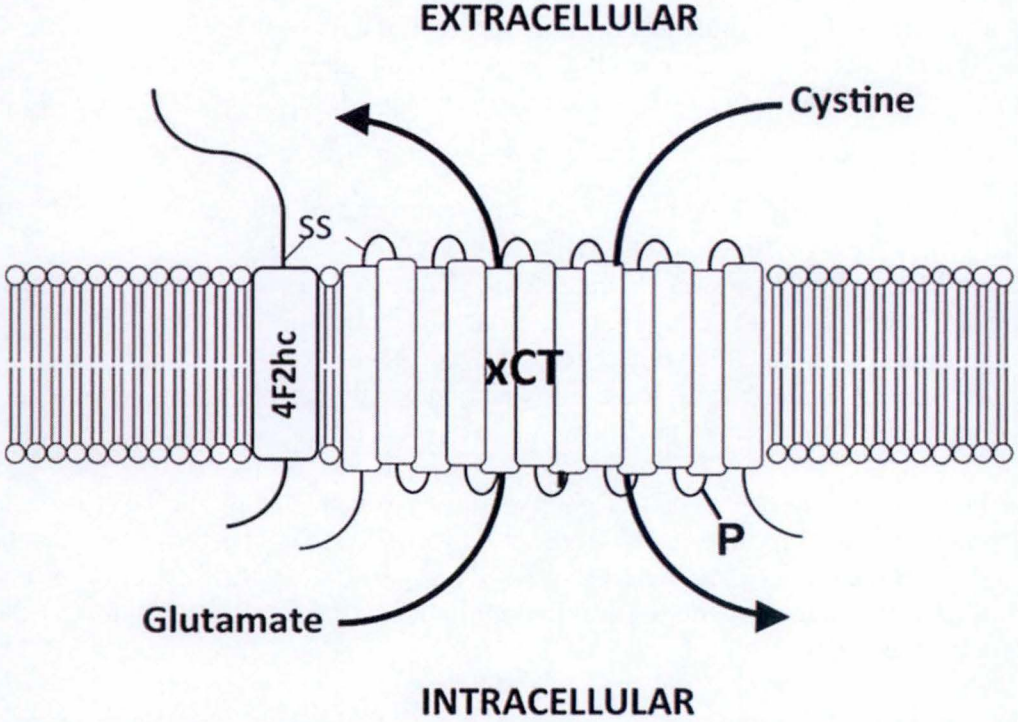

Modified from Massie et al., *J. of Neurochem.* (2015)

Figure 8. Structure of the cystine/glutamate antiporter system xc-

3. *The system X_c^-*

In 1986, Bannai identified for the first time a cystine/glutamate antiporter in human fibroblasts, called systems Xc- (Bannai, 1986). Then, it has been shown that systems Xc- is mostly expressed in the CNS but in intestine and kidneys as well which are organs involved in the cystine homeostasis in the organism (Burdo, Dargusch, & Schubert, 2006). Further, it has been shown by Baker and its team that in the CNS the major source of extracellular glutamate is the cystine/glutamate antiporter system X_c^-.

System X_c^- is a Na^+-independent, plasma bound anionic amino acid transporter encoded by the *Slc7a11* gene on chromosome 2 (Baker, Xi, Shen, Swanson, & Kalivas, 2002). It is composed of one glycosylated heavy chain, 4F2, a subunit common to other amino acid transporters and regulating protein trafficking (figure 8) (Augustin et al., 2007). There is a second subunit called xCT, specific for cystine/glutamate exchange transport (figure 8) (Augustin et al., 2007).

System X_c^- releases one glutamate and takes one cystine up in the cell (figure 8). Cystine is rapidly reduced into cysteine in the cytoplasm which is further used for GSH synthesis. Then, as cystine is a limiting GSH precursor, it was thought for long that the major and critical role of system X_c^- was the uptake of cystine to protect the CNS against oxidative stress. In fact, the brain is notably susceptible to oxidative stress due to its high energy metabolism and even more following SCI (Liverman et al., 2005; McCullagh & Featherstone, 2014). However, it has been shown that loss of xCT does not lead to increased susceptibility to oxidative stress (De Bundel et al., 2011).

But as import of cystine is coupled with an export of glutamate, the role of system X_c^- in extracellular glutamate regulation cannot be denied. Indeed, increasing evidence suggest that at best in the CNS, system X_c^- is a key regulator of non-vesicular extracellular glutamate. Based on system X_c^- duality, it is not surprising that more and more studies argue the involvement of the cystine/glutamate antiporter in neurodegenerative disorders as Parkinson's disease, Huntington's disease, amyotrophic lateral sclerosis or addictive disorders (Kalivas, 2009; Massie et al., 2011; Mesci et al., 2015).

The effect of system X_c^- in neurodegenerative diseases is really interesting.

On the one hand, it has been highlighted that in Huntington's disease system X_c^- activity is decreased, making cells more sensitive to oxidative stress(Massie, Boillée, Hewett, Knackstedt, & Lewerenz, 2015).

On the other hand, it has been shown in the mouse model for Parkinson's disease that dopaminergic neurons of xCT-deficient mice were highly protected against 6-OHDA because of reduced extracellular glutamate (Massie et al., 2011).

System X_c^- can actually participate to glutamate-induced excitotoxicity in the sense that cystine/glutamate antiporter activity is enhanced by various stresses (e.g ROS, amino acids deprivation), leading to an increase in cystine uptake to produce more GSH and in parallel a strong export of glutamate in the extracellular space (Bridge & Patel, 2012; Piani & Fontana, 1993).

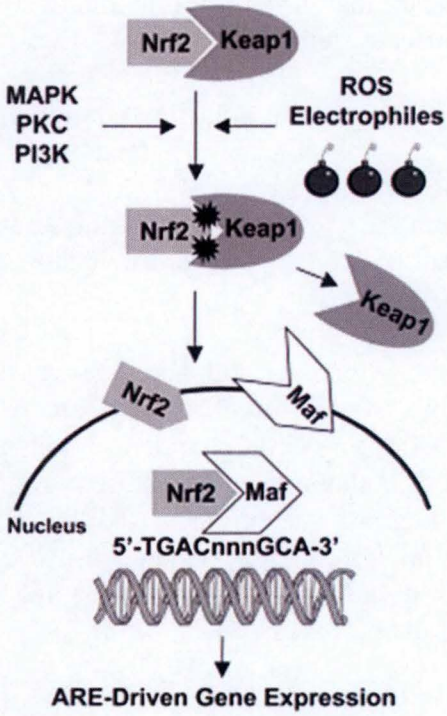

Figure 9. Nrf2 signalling pathhway

Moreover, it has been shown that the promoter sequence of the *Slc7a11* gene (coding for system X_c^- proteins) contains 4 ARE domains (Sasaki et al., 2002). ARE motifs correspond to Antioxidant Response Elements and are the binding site of the nuclear erythroid-2-related factor (Nrf2) (figure 9) (Bridge & Patel, 2012). Nrf2 is also upregulated by oxidative stress through its direct phosphorylation by kinases; this enhances its translocation into the nucleus and the subsequent transcription of genes containing ARE motifs, like *Slc7a11* gene (Bridge & Patel, 2012).

Yet, glutamate excitotoxicity and oxidative stress are involved in SCI pathophysiology, it is therefore interesting to study the system X_c^- after a cervical contusion (Domercq, Etxebarria, Perez-Samartin, & Matute, 2005; Hulsebosch, 2008; Lepore et al., 2011).

4. Aim of the work

Given that glutamate excitotoxicity and oxidative stress were shown as key players during SCI pathophysiology, the system X_c^- is of greatest interest as it imports cystine intracellurlay to be used as anti oxidative precursor while exporting deleterious glutamate extracellularly. We hypothesized that system X_c^- might be dysregulated during SCI condition and contributes to SCI physiopathology.

The first aim of this Master's thesis was the generation of a rat model for cSCI and its functional and histopathological validation.

The second aim was to study the expression and the localization of xCT, the major subunit of system X_c^- in the uninjured and the injured spinal cord. xCT protein has already been described in the healthy brain and during different neurodegenerative conditions but never in the spinal cord nor following spinal trauma. For that purpose, we established a collaboration with Dr Ann Massie at the VUB whose team had previously studied xCT biology in the brain.

As the reader would appreciate along the manuscript, we were faced to major issues related to specific xCT detection in the spinal tissue. The last aim of the thesis was therefore amended by experiments aiming at validating the specificity of anti-xCT antibodies.

II. Material and Methods

1. Rat model for cervical spinal cord injury (cSCI)

1.1. Spinal cord surgery

The study protocol was conducted according to the European Guidelines for Animal Experiments (2010/63/EU) and was approved by the Animal Ethics Committee of University of Namur (16-260). Rats have been divided into 3 groups: 10 animals in the control group receiving laminectomy only (Lam), 10 animals in the C3/4 right cervical contusion group sacrificed 2 weeks (cSCI 2 weeks) after SCI, and 10 animals in the C3/4 right cervical contusion group sacrificed 6 weeks (cSCI 6 weeks) after cSCI. 9 animals have received the impact at C4/C5 level and were followed and maintained alive for 6 weeks. All rats used for the experiment were about 8-10 weeks.

All animals were anesthetised with a mix of saline solution (NaCl 0,9%), xylazine 5mg/kg (XYL-M® 2% VMD, Arendonk, Belgium) and ketamine 100mg/kg (Ketamine 1000 NIMATEK®, Brussels, Belgium). Before starting the surgery, the depth of anaesthesia was evaluated by the loss of reaction after pinching the posterior member and tail as well as by the absence of ocular reflex. We performed laminectomy-only at C3/4 level on animals from the Lam group (n=10) and unilateral spinal cord contusion at C3/C4 level or C4/C5 on animals for the injured group (n=20 and n=9 respectively). The cervical region was shaved and then sanitised with Iso-betadine®. Animals were placed in prone position under a binocular microscope (Olympus SZX9 and Highlight 2100, Tokyo, Japan) for the surgery. A dorsal incision from C3 to C5 spinal cord was made using a scalpel, then we strayed the three first sub-cutaneous muscles layers and we finally removed the para-vertebral muscles above C3/C4. The right side lamina of C3 and C4 were taken away using a specific clamp to expose C3/C4 spinal cord level. Rats were then placed under the spinal cord impactor (IH-0400 IMPACTOR, Precision Systems & Instrumentation, USA) and the exposed spinal cord covered with saline solution NaCl 0,9%. The aim is for this cSCI model to be replicable that is why it is important to define precisely the impact area and to try to impact the spinal cord at the same zone for each animal. In order to have a replicable cSCI, we localized the anterior spinal artery that follows the spinal cord longitudinally and the impactor was positioned right next to the artery. Then we applied a force of 395 kilodyne (equal to 3,95 newton) onto the spinal cord. After the impact the animal's muscles were sewed and the skin was closed with staples.

After each surgery, rats were placed on a heating plate to avoid hypothermia until they were completely awaken. They were given an injection of analgesic buprenorphine 0,03mg/kg (Vetergesic® 0,3mg/ml, Ecuphar, Oostkamp, Belgium) and a 2ml injection of Ringer's liquid (a lactate and physiological serum solution) for rehydration. Animals received an injection of buprenorphine 0,03mg/kg 12 hours post-operative and 24 hours post-operative. Every day up to sacrifice, rats were checked to ensure their health state.

1.2. Assessment of motor function

3.2.1. Grip strength

For this experiment I used a grip strength meter Model GS3 (BIOSEB, Chaville, France). This equipment measures the traction force developed by rat limbs. Because we have done right unilateral cSCI on the animals, I have only measured the right side traction force. Rat was maintained in one hand so that only its right arm can grab the grid of the grip strength meter. With the other hand, the operator pulls rat's tail until the rat releases the grid.

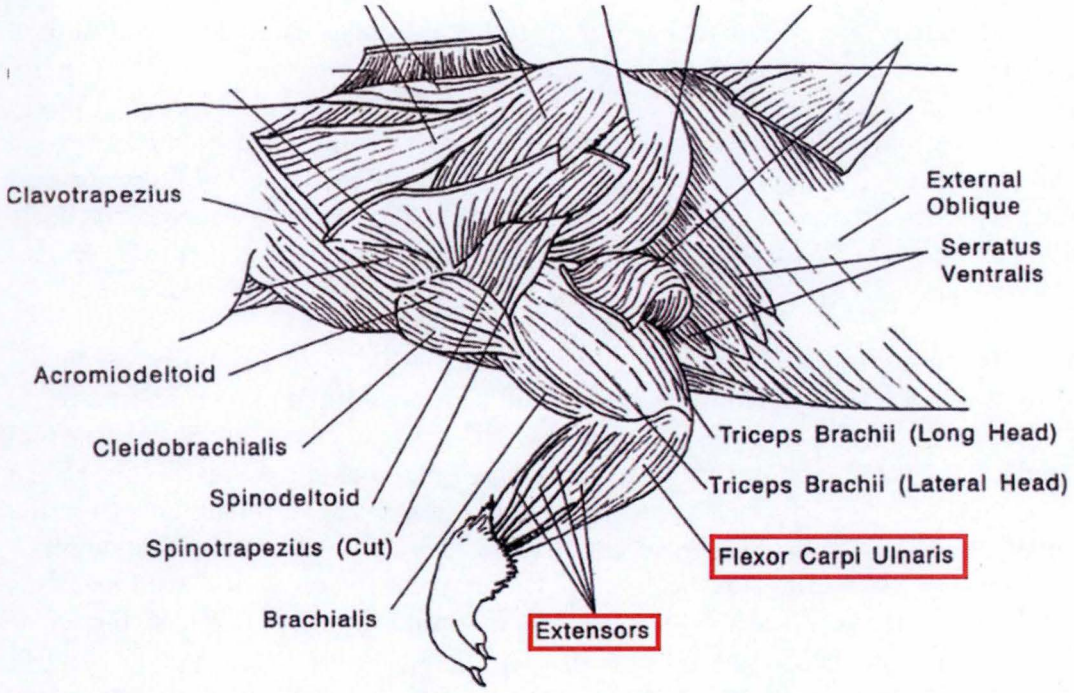

modifed from http://philipdarrenjones.com/web_documents/rat_dissection.pdf

Figure 10. Muscle responses recorded after ulnar and radial nerve stimulation

3.2.2. Cylinder paw preference test

This test has been led on the three rat groups just before their sacrifice. With this experiment I can determine the frequency of right paw use of injured and uninjured rats compared to the left paw. In practice rats were put into a Plexiglas cylinder and video-recorded for 5 minutes. Then the frequency of right, left and both paw use was determined.

3.2.3. Compound muscle action potential (CMAP) and EMG recording

In order to evaluate the functional impairment of ulnar and radial nerves following cSCI, CMAP amplitudes after nerve stimulation were always determined on the right foreleg before the surgery and 2 and 6 weeks after cSCI (n=9). We decided to study ulnar and radial nerves conduction because these nerves emerge from the spinal cord at cervical level and hence could be impacted by the cSCI. Ulnar nerve innervates the deep flexor carpi ulnaris muscle and others hand muscles (figure 10). Radial nerve, for its part, innervates the carpiradialis extensors (figure 10). With this technique I evaluate the muscle amplitude response after specific nerve stimulation and the time between the stimulation and muscle response, this duration is called the latency. This experiment is another way to evaluate functional deficits following cSCI.

Animals were first calmed down with a 0.04ml injection of Sedator® and anesthetized using Isoflurane®. Ulnar nerve conduction was determined at two distinct points. A proximal measure was made in the brachial plexus and a more distal measure was performed at elbow joint level. The recording needle electrode was placed in the inferior part of the palm of the hand, the reference electrode in the superior part of the palm of the hand and the ground needle reference was placed subcutaneously in the wrist. Finally, radial nerve conduction was obtained in the anterior face of the forearm with stimulation slightly above the lateral epicondyle of the humerus. The reference needle electrode was put subcutaneously in the wrist, the recording needle electrode was placed in the one proximal third of the forearm and the ground electrode slightly above the recording electrode. All CMAPs amplitudes were measured baseline to peak using a Sierra Cadwell XP stimulator followed by computer-assisted data analysis.

EMG at rest was also performed. This measure is interesting because it can detect unvolunteer and abnormal activity in the muscle of interest. The recording needle electrode was placed in the deep digitalis flechissor and the muscle activity at rest (i.e. without any stimulation). Both sides were tested to use the left side as control (right unilateral cSCI). At the end of the neurophysiological experiment, rats were awakening using a 0.02ml injection of Antisedan® that counteracts the effect of Sedator®.

3.3. Animals euthanasia

Animals were sacrificed at 2 and 6 weeks post-surgery. They were anesthetised with xylazine 5mg/kg (XYL-M® 2% VMD, Arendonk, Belgium) and ketamine 100mg/kg (Ketamine 1000 NIMATEK®, Brussels, Belgium). After being sure that animals were deeply anesthetized, rats underwent a thoracotomy and the diaphragm was cut to visualise the heart. Then the left ventricle was tubed to a peristaltic pump (FH15, Thermo Fisher Scientific, Whaltam, Masachusetts, USA) and the right atrium was cut off to drain out the blood.

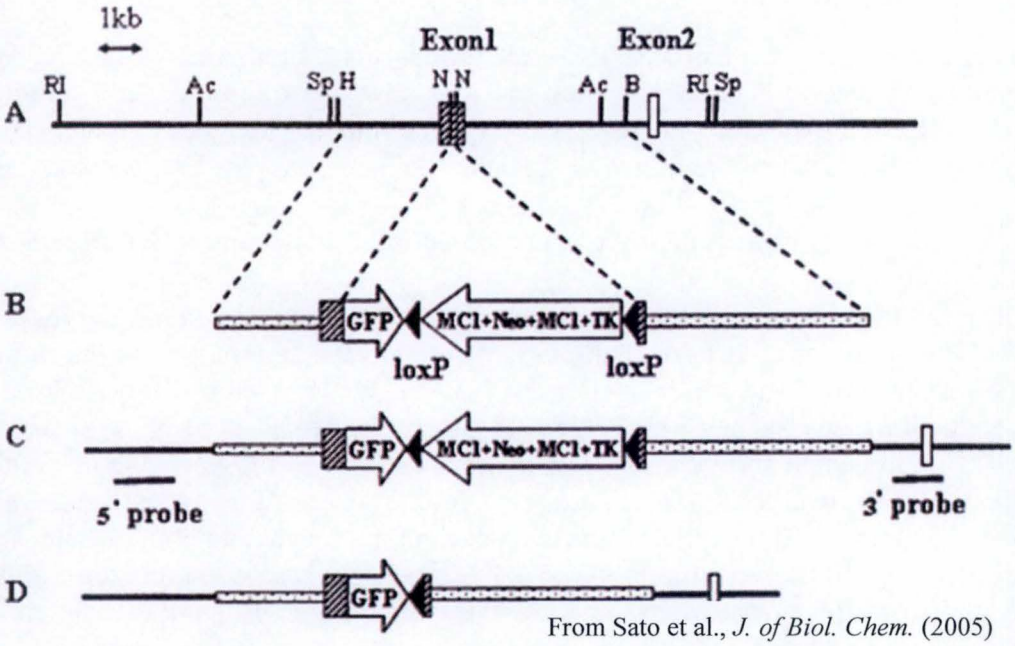

From Sato et al., *J. of Biol. Chem.* (2005)

Figure 11. Gene targeting strategy. Targeting scheme for xCT disruption. The genomic structure of the mouse *xCT* gene is presented at the *top* A. The targeting vector B was designed such that the GFP + Neo cassette replaced the NcoI (*N*) fragment in exon 1. The predicted mutant allele is shown in C. After crossing the homozygous recombinant mice with Cre-recombinase-expressing mice, the predicted allele in which the Neo cassette was deleted is shown in D. *RI*, EcoRI site; *Ac*, AccI site; *Sp*, SpeI site; *H*, HindIII site; *N*, NcoI site; *B*, BamHI site.

The spinal cords have distinct fates. Indeed, some will be used for morphological analysis and immunostaining and others for biochemical experiments. Thus rats used for the histological experiment were first transcardially perfused with cold physiological serum to rinse the blood from the circulatory system (until the liver is pale and the atrial flux is clear) and then perfused with paraformaldehyde 4% (PFA 4%) in order to pre-fix the tissue and to avoid tissue autolysis. Rats intended to biochemical analysis were only perfused with cold physiological serum.

2. xCT knock-out tissue

The laboratory of Ann Massie (VUB, Brussels, Belgium) generously gave us spinal cord samples from xCT-/- and xCT+/+ mice in order to test anti-xCT antibodies specificity. xCT null mice are obtained by homologous recombination where the NcoI/NcoI fragment in the exon 1 is replaced by a GFP as illustrated on figure 11 and described in the paper of Sato(Sato et al., 2005).
Genotyping of animals was performed in Ann Massie's lab according to their protocol.

3. Histological experiments

3.1. Tissue sampling

Rapidly after sacrifice, the spinal cord was removed and transferred into PFA 4% overnight. Next day, spinal cord was rinsed with distilled water and transferred into a sucrose 30% solution for 4 days. Subsequently, a 7mm-portion of spinal cord centred on the epicentre was cut and put into a plastic cup containing OCT (Optimal Cutting Temperature) (Tissue-Tek® SAKURA Finetek, Alphen aan den Rijn, Holland). This viscous liquid is cryoprotectant and avoids the formation of ice spicules. This was then frozen in liquid -80°C methanol and conserved at -20°C. The sample was next processed into 10µm-sections spread over Superfrost + slides (Thermo Scientific, Menzel-Glser, Braunschweig, Deutschland) using a cryostat (Leica Microsystems Gmbh, Wetzlar, Deutschland).

3.2. Eriochrome C / Neutral red staining

The Eriochrome C dye targets proteins associated to the myelin sheath. The Neutral red dye is used as a counterstain and highlights cells nuclei. First, cryostat slides underwent a dewaxing step in order to wash as much as possible the residual OCT/fat from the slides and then are fixed in a formol-acetic solution for 5minutes. After rinsing slides with tap water, they were immersed in the Eriochrome C dye for 30 minutes. The following step was the differentiation stage of Eriochrome C using ammonia water 0,3%. After the immersion in Eriochrome C everything is stained on the slide and the differentiation step is needed to evacuate the aspecific staining. Then, counterstaining was performed by immersing the slides in Neutral red 1% for 5 to 10 minutes. Following counterstaining, slides were dehydrated in two isopropanol bathes before two toluol bathes. Finally, slides were cover-slipped with DPX (VWR, Radnor, Pennsylvania, USA).

Anti-xCT antibodies	Dilution	Publications
ab37185 (Abcam)	1/1000	(Liefferinge, et al., 2016) (Soria, et al., 2016) (Pampliega, et al., Increased expression of cystine/glutamate antiporter in MS, 2011)
home-made antibody (kind gift from Ann Massie's lab)	1/200	(Liefferinge, et al., 2016)
#12691 (Cell Signaling Technology®)	1/100	(Jiang, et al., 2015)
NB300-317 (Novus Biological, Bio-Techne)	1/1000	(Liefferinge, et al., 2016) (Pampliega, et al., Increased expression of cystine/glutamate antiporter in MS, 2011) (Mesci, et al., 2015)

Table 1. List of anti-xCT antibodies tested, their dilution and publications using these antibodies.

3.3. Morphological analysis

Once sections are stained as described above, they are photographed with a Leica 2450 microscope (Leica Microsystems Gmbh, Germany). The picture are analysed with ImageJ software in order to quantify lesion size rostrally and caudally from its epicentre. The percentage of damaged surface is then calculated with the software based on the total surface of spinal cord hemi-section. The epicentre is defined as being the section with the highest damaged surface and is the point 0 on the representation shown in the results part of this work. The volume of the lesion has also been calculated 2 and 6 weeks following cSCI using Cavalieri estimation: $V=[\Sigma(A_1+A_2+...+A_n) \times D]-[A_{max} \times Y]$ with A=damaged surface (μm^2), D=distance between 2 sections (150µm) and Y=section thickness (10µm).

3.4. Peroxydase immunostaining

With this experiment I have tested the specificity of different commercial anti-xCT antibodies and an in-house antibody generated in Ann Massie laboratory. I used sections of xCT+/+ mouse spinal cord and xCT-/- mouse spinal cord generously offered by Ann Massie team as well as rat spinal cord sections.

Cryostat slides are dried at room temperature and fixed in PFA 4% for 10 minutes. After rinsing in PBS once, slides undergo two glycine 0,1M bathes for 3 minutes in order to wash PFA residues. Slides are immersed in a H_2O_2 3% solution for 10 minutes and rinsed. Then, slices are saturated using PBS-BSA 0,2%-Triton0,02% for 1 hour at room temperature. Next, they are incubated with primary anti-xCT antibody diluted in PBS-BSA 0,2%-Triton0,02% overnight at 4°C or 1 hour at room temperature. The next day or one hour after, slides are rinsed with PBS-BSA 0,2%-Triton0,02% and incubated for 1 hour with biotinyled IgG1/100 (VECTASTAIN). The mix Streptavidine-Peroxydase is prepared at equal volumes and at a final dilution of 1/200 in PBS-BSA 0,2%-Triton0,02% and slides are incubated with it for 1 hour. After three PBS-BSA 0,2%-Triton0,02% rinsing, a drop of chromogene DAB+ is added on the slides. Revelation on the positive control slide is observed live with a microscope and timed. The revelation is stopped by plunging the slides in distilled water. The same revelation time is performed on the other sections. For the counterstaining, slides are immerged in Hemalun dye for 10 seconds and are washed in tap water for 5 minutes. In order to cover-slip the slides, we have to go to an organic phase using an isopropanol bath for 6 minutes and a toluol bath for 6 minutes. Slides are cover-slipped with DPX (VWR, Radnor, Pennsylvania, USA). Anti-xCT antibodies tested and their dilutions are listed in table 1.

To further confirm the specificity of the anti-xCT antibody from Novus Biological (NB300-317) in immunostaining, a peptide competition protocol has been conducted with the immunizing peptide used to produce the anti-xCT antibody NB300-317. First, the antibody is raised to a concentration of 1µg/ml in PBS-BSA 0,2%-Triton0,02%. The diluted antibody is divided into two tubes. In one tube the blocking peptide is added at a ratio of 5:1, an equivalent volume of PBS-BSA 0,2%-Triton0,02% is added in the second tube. Both tubes are incubated 1hour at room temperature. Then, the protocol is the same as described above. Staining patterns between the blocked and unblocked antibodies are compared.

3.5.Double immunofluorescence

The aim of this experiment is to identify which cells in the spinal cord express the xCT protein and where there is co localization. I focused on astrocytes and microglial cells because the question of their xCT protein expression is under debate (Soria, et al., 2016). Furthermore, laminectomy slides were used as control. First, cryostat slides are dried at room temperature and fixed in PFA 4% for 10 minutes. After rinsing in PBS once, slides undergo two glycine 0,1M bathes for 3 minutes. Then, slides are saturated with PBS-BSA 0,2%-Triton 0,02% for 1 hour at room temperature. Slides are further incubated with primary antibodies diluted in PBS-BSA 0,2%-Triton0,02% overnight at 4°C :

- Anti-xCT antibody (NB300-317, rabbit) 1/1000 and mouse anti-GFAP antibody 1/50 (GA5 clone, Sigma Aldrich) to determine whether there is a co localization between xCT protein and astrocytes.
- Anti-xCT antibody (NB300-317, rabbit) 1/1000 and mouse anti-CD68 antibody (Biorad) 1/200 which is a marker of microglial activation.

The next day, after rinsing in PBS-BSA 0,2%-Triton0,02%, slides are incubated with the secondary antibodies 1/1000 diluted in PBS-BSA 0,2%-Triton0,02% for 1h. For GFAP and CD68 a goat anti-mouse-Alexa 594 (Life Technologies) is used and for xCT it is a goat anti-rabbit-Alexa 488 (Life Technologies). At last, nuclei are stained with Hoechst 1/100 diluted in PBS-BSA 0,2%-Triton0,02% for 15 minutes followed by a last rinsing with PBS. To finish, slides are cover-slipped using Mowiol in a dark room.

4. Gene and protein expression

4.1. Tissue sampling

Rapidly after sacrifice, the spinal cord and brain were removed. The spinal cord was divided into 2mm-long hemicord fragments surrounding the epicentre of impact, rostrally and caudally (picture 4 modified from Li et al., 2014). The spinal cord segments were then snap-frozen in liquid nitrogen and kept at -80°C.

4.2. Relative mRNA expression using RT-qPCR

Spinal cord samples are homogenised in 1ml Tripure reagent (Life Technologies, Bleiswijk, The Netherlands) in screwed-top tubes containing ceramic beads using the Magnalyser (Roche Diagnoctics, Mannheim, Deutschland) at 6500rpm for 50 seconds. This technic allows grinding and crushing the sample properly. This first step provides solubilization of biological samples and protein denaturation. After homogenization, samples are incubated at room temperature for 5 minutes and centrifuged at 13000rpm for 10 minutes. Supernatants are withdrawn and mixed with 200µl chloroform RNase free. Chloroform addition induces phase separation with protein in the organic phase and RNA in the aqueous phase (Rio, Ares, Hannon, & Nilsen, 2010). This mix is vortexed and centrifuged at 13000rpm for 15 minutes at 4°C. 300 to 350µl of supernatant are collected in a new Eppendorf and the same volume of ethanol 70% is added. The mixture is transferred on the column supplied by the kit and centrifuged for 30 seconds at 13000rpm. Then 100µl DNase is added on the column and it is incubated at room temperature for 15 minutes. The last steps are alternating of specific buffers addition (High Pure RNA Tissue Kit, Roche Diagnostics, Basel,

Gene target	Sequence forward 5'→3'	Sequence reverse 5'→3'	Product size (bp)	Accession number
xCT (Rat)	CCTGGCTTTTG GACGCTACAT	TCAGAATTGCT GTGAGCTTGCA	182	NM_001107 673.2
xCTexon1 (Mouse)	TGCCTGTGGAG TACTGTCACTT	AAGGACCAAAG ACCTCCAGAAT	110	NM_011990 .2
xCToutexo n1 (Mouse)	CCTGGCATTTG GACGCTACAT	TCAGAATTGCT GTGAGCTTGCA	182	NM_011990 .2
Nrf2 (Rat)	GCTGTGATCTG TCCCTGTGTAA	GGAAGACTCCA CAGAGTGCTCT	137	NM_031789 .2
HPRT	GGACCTCTCGA AGTGTTGGAT	CCAACAACAAA CTTGTCT	70	S79292.1

Table 2. List of used primers

Switzerland) and centrifugation. Determination of RNA concentrations was made by using a spectrophotometer Nanodrop 1000 (Thermo Scientific, Bleiswijk, Netherlands).

After extraction, total RNA is reverse-transcribed with the Super Script II RNase H Reverse Transcriptase Kit (Invitrogen, Merelbeke, Belgium). All samples are first raised at the same concentration in a final volume of 11µl. A first mix is prepared as follows for one sample: 1µl dNTPs (Invitrogen), 0,1µl oligo-dT (hybridizing the polyA tail of mRNA in order to specifically reverse transcribe them) (Invitrogen) and 0,9µl RF H_2O. This mix is added to every 11µl samples. The solution is then incubated 5 minutes at 65°C in the Thermocycler equipment (2720 Thermal Cycler, Applied Biosystems, Life Technologies) to allow hybridization of oligo-dT to polyA tail. Samples are next cool on ice. A second mix is prepared as follows per sample: 4µl First Strand Buffer 5x (Invitrogen), 2µl 0,1M DTT 10x (Invitrogen), 0,1µl Reverse Transcriptase enzyme (Invitrogen) and 0,9µl RF H_2O (Invitrogen). This mix is added to samples and again placed in the Thermocycler equipment. They undergo the following program:

- 50 minutes at 50°C
- 15 minutes at 70°C
- At least 5 minutes at 4°C

Obtained cDNA is diluted 5x and conserved at -20°C.

Specific genes were further amplified from the obtained total cDNA using the Takyon SYBR Green Kit in the Light Cycler 96 Real-Time PCR system (Roche Diagnostics, Mannheim, Germany). The reaction mix is prepared per sample as follows and is put in a 96 wells plate:

- 10µl SYBR Green
- 2,5µl of each primer at a concentration of 2,4µM
- 5µl 1/5 cDNA

The 96 wells plate in the Light Cycler 96 Real-Time PCR system undergoes the following program:

- 600 seconds at 95°C
- 10 seconds at 95°C
- 10 seconds at the mean melting temperature of primers } x40
- 20 seconds at 72°C
- 10 seconds at 95°C
- 1 minute at 65°C
- 1 second at 97°C
- 30 seconds at 37°C

Primers sequences are compiled in table 2. Reference gene is HPRT gene (hypoxanthine guanine phosphoribosyl transferase).

Anti-xCT antibodies and dilution	Secondary antibodies and dilution	Protein loaded (µg)	Publications
ab37185 (Abcam) 1/4000	HRP-conjugated anti-rabbit IgG (Vectastain) 1/10000	10	(Liefferinge, et al., 2016) (Pampliega, et al., Increased expression of cystine/glutamate antiporter in MS, 2011)
ab37185 (Abcam) 1/4000	HRP-conjugated anti-rabbit IgG antiserum (Dako) 1/50000	10	
home-made antibody (offered by Ann Massie's lab) 1/10000	HRP-conjugated anti-rabbit IgG antiserum (Dako) 1/50000	10	(Liefferinge, et al., 2016)
#12691 (Cell Signaling Technology®) 1/1000	HRP-conjugated anti-rabbit IgG antiserum (Dako) 1/50000	25	(Starheim, et al., 2016) (Naik, Sajja, Prasad, & Cucullo, 2015)
NB300-317 (Novus Biological, Bio-Techne) 1/400	HRP-conjugated anti-rabbit IgG antiserum (Dako) 1/50000	25	(Liefferinge, et al., 2016) (Linher-Melville, Haftchenary, Gunning, & Singh, 2015)

Table 3. Description of antibodies used for Western blot experiments and publications

4.3. Western blot analysis

Samples were first homogenized at 4°C in extraction buffer (60mM Tris base buffer, SDS 2%, 100mM DTT, pH 7,5, phosphatase inhibitor cocktail 3 (Sigma-Aldrich, ref P0044), SIGMAFAST™ Protease Inhibitor Cocktail Tablets EDTA-Free (Sigma-Aldrich, ref S8830)). Protein concentration was determined using Pierce method. Equal amounts of protein were loaded on 10% polyacrylamide gel and separated by SDS-PAGE (1h30, 120V). After separation, proteins were transferred to a polyvinylidene fluoride membrane. Non-specific binding was blocked by incubating the membrane in NFDM 5% TBS-Tween 0,2% blocking agent for 1h at room temperature. Membranes were incubated o/n with different anti-xCT antibodies. The next day, the membrane was washed three times with TBS-Tween 0,2% and incubated for 1h15 with the secondary antibody. Finally, immunoreactive proteins were revealed with BM chemiluminescence blotting substrate (POD) (Roche, Mannheim, Germany) and images were analysed using Imagequant Las4000 mini (GE Healthcare, Bukinghamshire, UK). All information about antibodies used is compiled in the table 3.

Moreover, I have also performed a Western Blot experiment in Ann Massie's laboratory with one of her PhD student using one of their home-made anti-xCT antibodies (1/1000). The protocol is almost identical but protein samples was diluted in XT Reducing Agent 20x (Biorad, #161-0792) and XT Sample Buffer 4x (Biorad, #161-0791), the blocking agent used was ECL 5% (ECL Prime Blocking Agnrt, GE Healthcare, #RPN418V) and finally the secondary antibody used is the one from Dako (1/60000).

4.4. Construction of a plasmid expression vector

Because of the specificity problems I met with the anti-xCT antibodies, we decided to test their specificity using an expression vector containing a HA-tag (Human influenza hemagglutinin). The idea is to create a recombinant xCT protein associated to the HA-tag in transiently transfected eukaryotic cells. Anti-xCT antibodies and anti-HA antibody will then be applied on eukaryotic cells to validate the specificity of anti-xCT antibodies.

4.4.1. Reverse transcription

At the beginning of the experiment xCT amplification by PCR was made with rat prefrontal cortex cDNA samples obtained by reverse transcription as describe in the "quantitative PCR" part. However, after the PCR and the electrophoresis nothing was detected at the expected size of xCT CDS (data not shown). To resolve the problem a new RT was conducted using this time random oligonucleotides with GoScript™ Reverse Transcription System kit (Promega).

4.4.2. xCT amplification by PCR

To begin, specific primers were designed considering following parameters: primers must hybridize the extremities of xCT CDS, restriction sequences (EcoRI and KpnI) are added to the primers sequences as well as 5 random nucleotides before restriction sequences. These are the primers designed:

- xCTtot forward : 5'-CCATGGAATTCATGGTCAGAAAGCCAGTTG-3'
- xCTtot reverse : 5'-GTACCGGTACCTAATTCTTTAGAGTCTTCTGGTAC-3'

First, xCT amplification was conducted using a low-fidelity polymerase for the PCR in order to validate the designed primers. Mix in a tube:

- 1µl of each primer at a concentration of 10µM
- 1µl of 1/20 diluted rat prefrontal cortex cDNA
- 10µl of mix DreamTaq 2X
- 7µl RNase free H_2O

A 120V electrophoresis on a 1% agarose gel is performed to verify the PCR results. A clear signal is obtained at 1500bp which is the expected size of xCT CDS (data not shown).

After this verification, the xCT amplification is performed by PCR using a high-fidelity polymerase, the Q5 enzyme. The following components are mixed in a tube:

- 5µl of Q5 reaction buffer
- 0,5µl of dNTPs
- 1,25µl of each primer at a concentration of 10µM
- 1µl of 1/20 diluted rat prefrontal cortex cDNA
- 0,25µl of Q5 polymerase
- 16µl RNase free H_2O.

4.4.3. xCT insert extraction and purification

This step is performed with the Wizard® SV Gel and PCR Clean-Up System (Promega). xCT insert-containing gel is first dissolved by addition of Membrane Binding Solution and incubated at 55°C until gel slice is entirely dissolved. Then, the mixture is transferred into a SV Minicolumn. After a short incubation at room temperature, the Minicolumn is centrifuged at 10000xg for 1minute. cDNA is now bound the Minicolumn and is washed twice by addition of Membrane Wash Solution and centrifugation at 10000xg. The final step is the elution step where the Minicolumn is put on a clean microcentrifuge tube, 50µl of Nuclease-free water is added and then centrifuged at 10000xg.

4.4.4. pCMV-HA digestion, dephosphorylation and purification

Before the ligation of the xCT insert in the vector, this one must be linearised. Restriction sites chosen for the digestion are EcoRI (5'-GAATTC-3') and KpnI (5'-GGTACC-3') sites. The digestion is made in a 100µl mix as followed:

- 5µl of non digested pCMV-HA
- 10µl of Fast Digest buffer
- 2,5µl of EcoRI restriction enzyme
- 2,5µl of KpnI restriction enzyme
- 80µl Rnase Free H_2O

This mix is incubated 25 minutes at 37°C. To ensure the efficiency of the restriction, 5µl of the mix is loaded in a 1% agarose gel. Negative control for the electrophoresis is provided by 5µl of non-digested pCMV-HA.

In cloning, a dephosphorylation step of the vector is interesting to prevent religation of the linearised pCMV-HA. The vector pCMV-HA is then dephosphorylated by addition of Shrimp Alkaline Phosphatase (NEW ENGLAND BioLabs® Inc.). The mix is incubated 1hour

at 37°C. Then, EDTA 0,5M is added to neutralize the phosphatase and the solution is incubated 15minutes at 65°C.

The purification step must be done in a volume of 400µl, so 300µl of RF water is added to the 100µl of digested and dephosphorylated pCMV-HA. Then, 400µl of phenol is added and the mix is centrifuged 4minutes at 10000xg. The supernatant is collected (about 400µl), added to 400µl of chloroform and centrifuged at 10000xg. The about 400µl of supernatant containing pCMV-HA DNA is transferred into a new tube.

4.4.5. Precipitation of pCMV-HA and xCT insert

Ethanol 100% and sodium acetate (NaOAc) 3M are added to pCMV-HA DNA obtained previously and to the solution of purified xCT insert as followed: 2,5x the volume of ethanol 100% and 1/10 volume of NaOAc 3M. The two tubes are put at -80°C for at least 45minutes. After, tubes are centrifuged at 10000xg for 15minutes and ethanol is removed carefully to avoid detaching the DNA cap. Ethanol 70% is now added in the two tubes and they are centrifuged again at 10000xg. Ethanol is removed even more carefully than before to avoid detaching the DNA cap. Then, tubes are dried and 10µl of RF water is added. After this step, DNA (insert and vector) is enough concentrated to allow the ligation of the xCT insert into the pCMV-HA vector.

4.4.6. Ligation of xCT insert in pCMV-HA

The following mix is prepared:

- 1µl of pCMV-HA
- 6µl of xCT insert
- 2µl of ligase buffer
- 1µl of ligase enzyme
- 10µl of RF H_2O

This is incubated over-night at 16°C. This step is also verified by electrophoresis on 1% agarose gel.

4.4.7. Bacteria electroporation

A specific strain of Escherichia coli, called DH5α, has been used for the electroporation. This strain is electrocompetent.

2µl of ligation product is added in a DH5α aliquot without making bubbles, which can block the electroporation, and the solution is gently mixed. 60µl is withdrawn and put in the CelljeCT basin equipment. Then, a 2350V electrical current is triggered which allows the expression vector to get into bacteria. Lysogeny broth (LB) medium is provided to the electroporated bacteria and they are incubated at 37°C for at least 1h. Finally, 100µl of electroporated bacteria is seeded on culture medium and incubated over-night at 37°C.

4.4.8. Bacterial colonies screening

Once bacterial colonies have grown, it must be verified whether colonies have been transformed with the expression vector. 48 colonies are resuspended individually in 20µl of

RF water. The 48 samples undergo a PCR using the DreamTaq polymerase and the following primers:

- xCT criblage forward: 5'-ACCCAAGTGGTTCAGACGAT-3'
- M13 reverse: 5'- CAGGAAACAGCTATGAC-3'

5. Statistical analysis

Statistical analysis was carried out by using non-parametric Mann-Whitney test and non-parametric Kruskal-Wallis test with GraphPad Prism 6 software. p values $< 0,05$ were considered significant and symbolised with *.

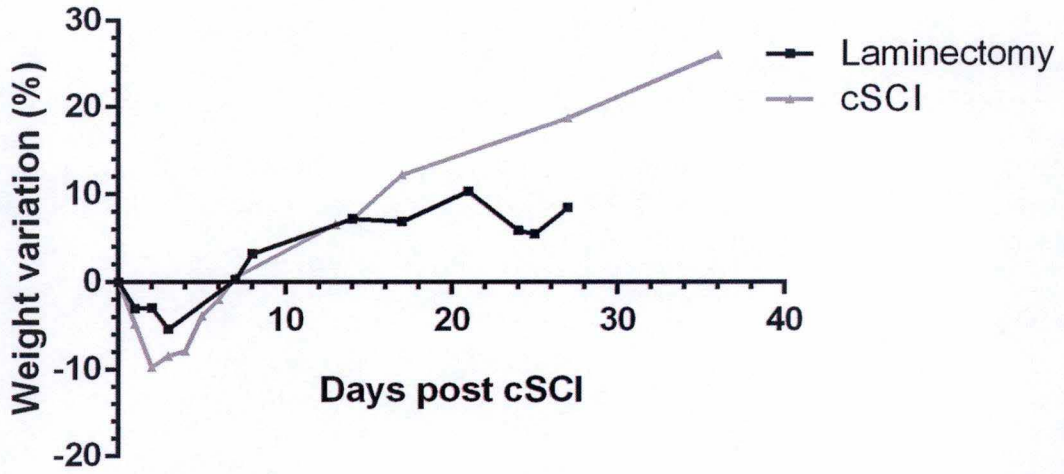

Figure 12. Evolution of rats weight after laminectomy or cSCI

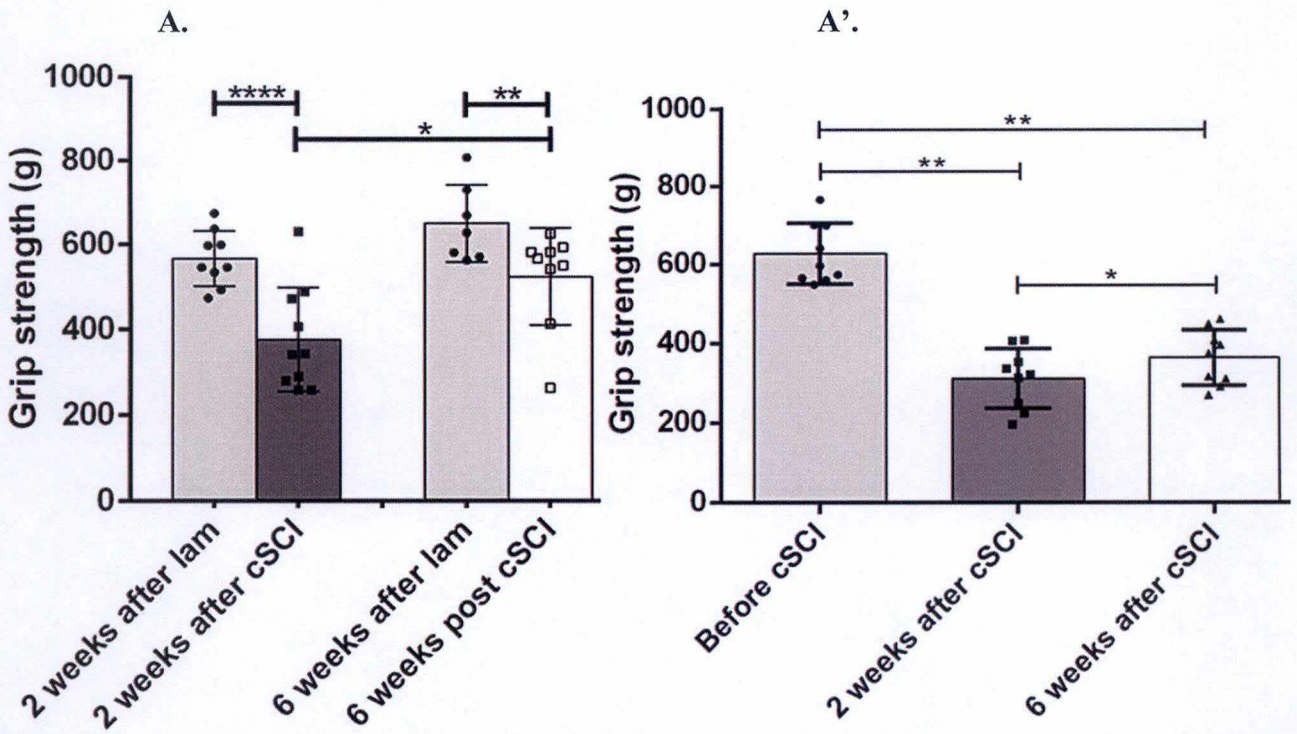

Figure 13. Grip strength experiment. A, A'. Evaluation of rats grip strength 2 and 6 weeks after SCI or laminectomy (lam), mean values and strandard deviation (SD) are represented (n=10 in each group in A and n=9 in A').

III. Results

1.1. Validation of cSCI model

An important component of my Master's thesis was the *in vivo* part. Indeed, the idea was to study xCT protein expression and localization at different time points following SCI. First, we had to validate our animal model for cSCI. This verification is based on rats' daily observation, evaluation of motor function using behavioural experiment, and neurophysiological and morphological analysis.

1.2. Phenotypic observations

Immediately after impact on the cervical spinal cord, a right hemiplegia and reduced right diaphragm breathing amplitude is noticed. Rats in their cages are observed daily and show a progressive recovery of mobility, starting from 5 days after cSCI. Hemiplegia is more pronounced at the level of the right forelimb than of the right hindlimb due to the cervical localization of impact. The motor recovery has always begun with the hind leg and is rapid at this level. On the other hand, the motor recovery of the right foreleg is slower and is fluctuating from a rat to another.

Following the surgery, rats' appetite declines and they lose substantial weight. This can be explained by the general state of animals after the surgery - they need a bit of time to recover – as well as by their right hemiplegia which restrains them eating. To evaluate the weight loss and gain in the cSCI group and the laminectomy group I use the following formula: *[(D day weight – weight before cSCI)/ weight before cSCI] x 100*. Not surprisingly, mean weight loss percentage after the surgery is less important in the laminectomy group than in the cSCI group: day 3 post cSCI, rats from the laminectomy group present a mean weight loss of 5,34% and those from the cSCI group a mean weight loss of 8,38% (figure 12). From day 14 after the surgery, mean weight gain percentage seems to be greater in the cSCI group than in the laminectomy group (figure 12). It could be suggested that impacted rats have enough recovered 2 weeks after cSCI and can now eat again normally.

1.3. Assessment of motor function

Two behavioural experiments were conducted to evaluate the motor function following cSCI. The grip strength test provides information about the traction force of animals. The second behavioural experiment led is called the cylinder paw preference test. It indicates the frequency of paw use (right, left and both paws).

1.3.1. Grip strength test

Initially this experiment has been conducted on the three following groups: laminectomy group (Lam) (n=10), cSCI 2 weeks group (n=10) and cSCI 6 weeks group (n=10). Two weeks after the impact, injured animals show a significant decrease of their grip strength ipsilaterally to the impact compared to laminectomy animals (figure 13A, $p<0,0001$). Moreover, 6 weeks after the impact rats still show reduced grip strength but the difference with the control group is less pronounced (figure 13A, $p<0,05$). Besides, the grip strength is significantly improved in animals 6 weeks after impact compared to animals 2 weeks after impact (figure 13A, $p<0,05$). In a second phase, 9 rats were followed individually before and after the impact. As

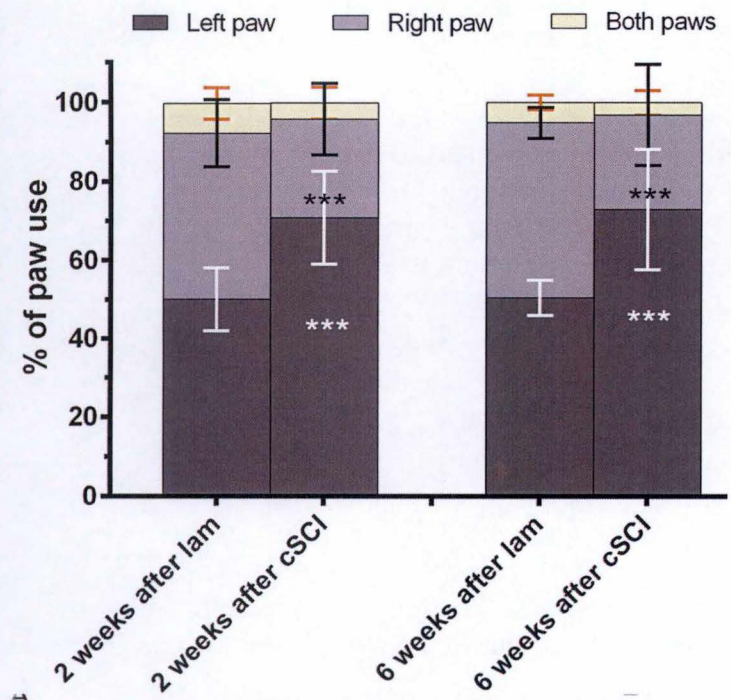

Figure 14. Cylinder paw preference test. Evaluation of paws use frequency 2 and 6 weeks after SCI or laminectomy (lam), mean values and SD are represented (n=10 in each group).

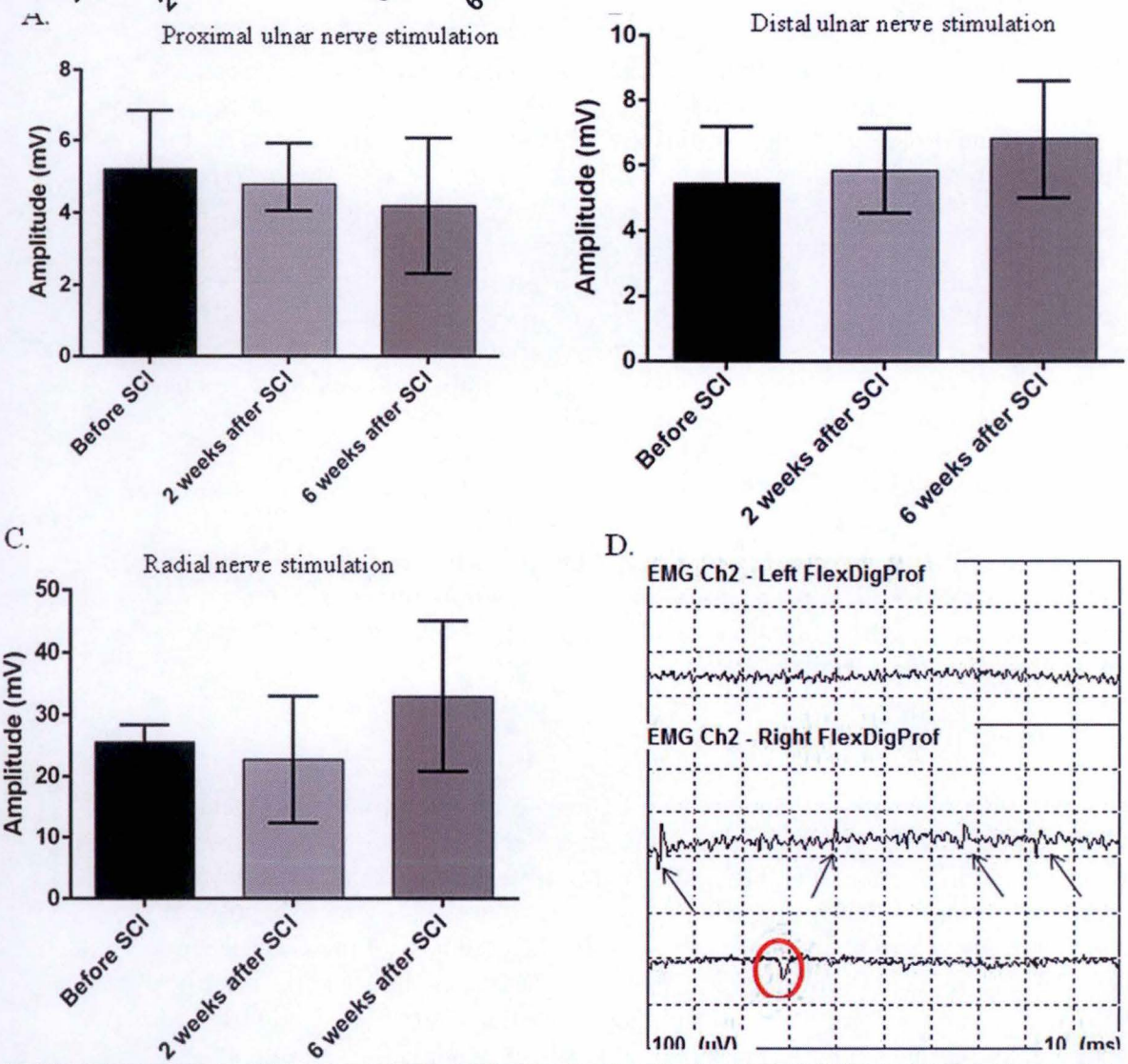

Figure 15. Neurophysiological analysis. A, B, C. CMAPs evaluation before and after cSCI. The mean amplitude values and SD of muscle response following proximal and distal ulnar nerve stimulation and after radial nerve stimulation, are respectively represented (n=9). Measures have been performed before and 2 and 6 weeks after cSCI D. Comparison of EMG at rest recorded in the left deep digitalis flechissor (Healthy side providing normal EMG record) and in the right deep digitalis flechissor (pathological EMG record). Black arrows tip fibrillation potentials and red circle positive sharp waves.

noticed with the distinct rats groups just above, the grip strength is also significantly decreased 2 and 6 weeks after the cSCI (figure 13A' $p<0,05$ in the both cases). These animals also show a significant enhancement in their traction force 6 weeks after cSCI compared to 2 weeks after cSCI (figure 13A' $p<0,05$). Results obtained by comparison of injured and uninjured groups and by following individuals over time before and after impact are consistent with each other.

1.3.2. Cylinder paw preference test

This experiment has been conducted on the laminectomy group and cSCI groups (2 and 6 weeks post impact). Results further strengthen the motor impairment in the right forelimb, showing a significant change in the frequency of paw use. In fact, at both 2 weeks and 6 weeks after the impact, rats use significantly less their right paw ipsilaterally to the lesion ($p<0,05$ for the 2 weeks cSCI group and $p=0,0001$ for the 6 weeks cSCI group) and more their left paw compared to control ($p<0,05$ 2 and 6 weeks post cSCI) (figure 14).

1.4. Neurophysiological analysis

1.4.1. CMAPs evaluation

Because of gray matter motor neuron loss following SCI, it is interesting to measure neurophysiologically nerve-elicited compound muscular action potentials (CMAPs). CMAPs peak-to-peak amplitudes were recorded in the palmar muscles and brachioradialis muscle before and after cSCI (2 and 6 weeks post impact), using ulnar and radial nerves stimulation respectively.

Palmar muscle amplitudes after proximal stimulation of the ulnar nerve show a decreasing tendency 2 and 6 weeks following impact (figure 15A). However, results are not significant ($p>0,05$). There is no significant difference in muscle amplitudes before and following cSCI after distal stimulation of the ulnar nerve as well as after radial nerve stimulation ($p>0,05$) (figure 15 B, C).

Onset latency to muscle response was also recorded before and after cSCI. For the two stimulated nerves there is no significant difference of the onset latency 2 weeks post impact and 6 weeks post impact either (data not shown).

Furthermore, muscle response records after proximal and distal stimulation of the ulnar nerve allow the estimation of the nervous influx velocity before and after cSCI. However, no significant difference can be highlighted between uninjured and injured state (data not shown).

1.4.2. Abnormal EMG at rest following SCI

At rest (i.e. without any electrical stimulation), no activity from muscular fibres should be detected by the recording concentric electrode as demonstrated in the EMG at rest performed on the left deep digitalis flechissor. Such an EMG is characterised by a silent baseline (figure 15D).

The same records made 2 and 6 weeks after cSCI show obvious EMG abnormalities. Indeed, two types of electrical activities are detected. Fibrillation potentials (figure 15D, black arrows), are short duration spontaneous action potentials generated by the muscular fibres

Figure 16. Morphological aspect of uninjured and injured spinal cord stained with Eriochrome C/Neutral red. a,b. Morphological aspect of spinal cord section after laminectomy. GM : grey matter, WM : white matter, black arrow : motor neuron, white arrows : glial cells in the grey matter, yellow arrows : glial cells in the white matter, black circle: myelinated nervous fibre, black rectangle unmyelinated nervous fibre. **c,d.** Morphological aspect of spinal cord 2 weeks after cSCI at epicentre level. Black arrow: glial cells asterix : distroyed nervous tissue, red arrow : vacuole. e,f. Morphological aspect of spinal cord 6 weeks after cSCI at epicentre level Red arrow : vacuole.

Laminectomy

a

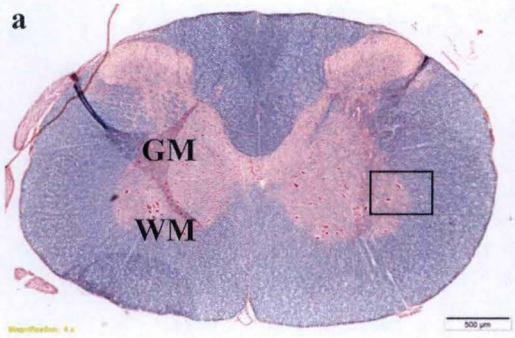

b

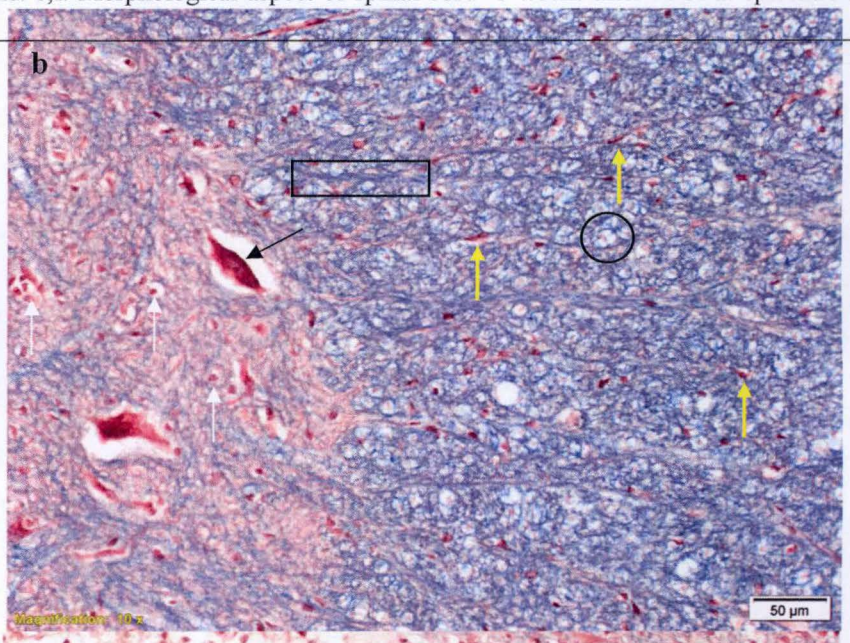

2 weeks post cSCI

c

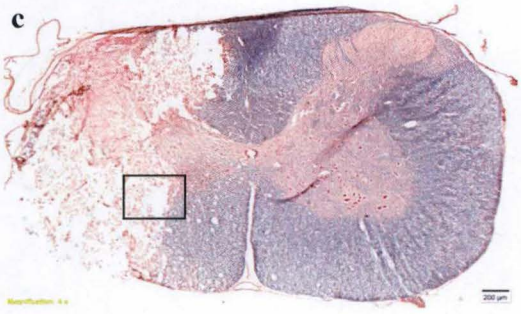

d

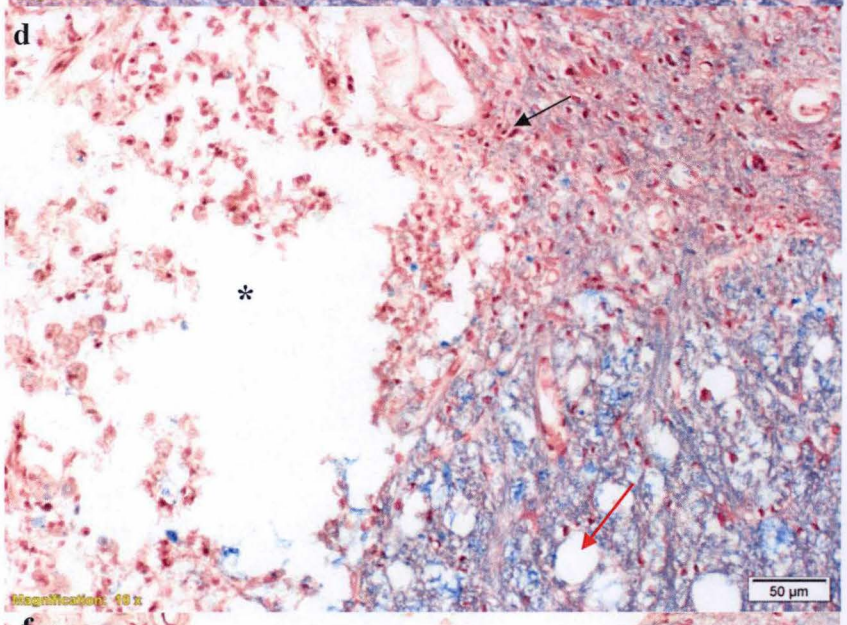

6 weeks post cSCI

e

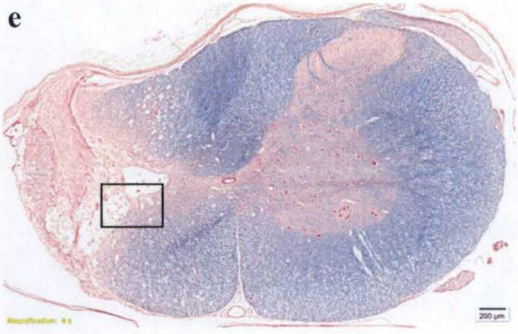

f

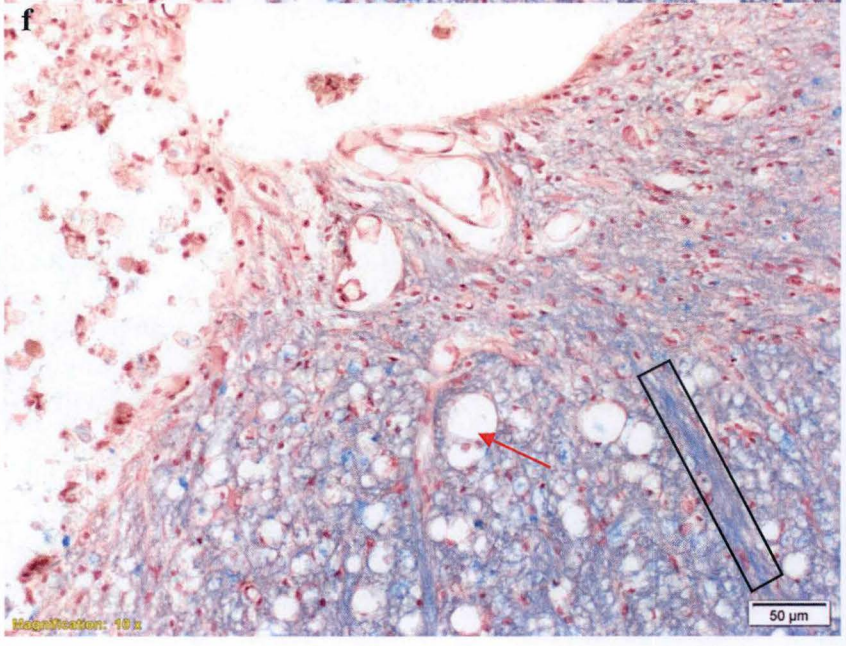

(individual to a few close together) (Nerve study, 2016). The second pathological electrical activities are positive sharp waves (figure 15D, red circle). They are also spontaneous actions potentials but slightly longer than fibrillation ones and they are thought to be initiated by individual muscle fibres (Nerve study, 2016).

1.5. Morphological analysis of the injured spinal cords

1.5.1. Morphological aspect of uninjured and injured spinal cord

Aspect of spinal cord sections of the laminectomy group is typical of healthy spinal cord (figure 16a). White and grey matters are clearly delimited (figure 16a, GM, WM). In the ventral horn of the grey matter motor neurons can be observed as well as glial cell small nucleus surrounding them (figure 16b). Glial cells are also found in the white matter (figure16b). This white matter presents a cracked and spongious aspect highlighting the nerve fibres paths ascending or descending along the spinal cord. The unmyelinated and myelinated fibres can be differenciated (figure 16b). Indeed, white circles giving the spongious aspect are typical of myelinated fibres and result from the solubilisation of the lipids composing the myelin sheath during the staining protocol (figure 16b, black circle). Because unmyelinated fibres are not surrounded by myelin sheat they are stained and are detected near the grey matter (figure 16b, black rectangle).

Following right cSCI, architecture of the nervous tissue is disrupted unilaterally due to the impact. Even macroscopically the impact point is visible. Indeed, after dissection a clear round zone, pinkish in colour due to local hemorrhage, can be seen and associated to a small depression in the same zone of the spinal cord. At microscopic scale; both 2 and 6 weeks post cSCI (even if far more pronounced 2 weeks after the impact), the spinal cord shows a burst aspect on the injured side with holes where the tissue is completely destroyed (figure 16c,d,e,f). White and grey matters are undistinguishable under such pathological conditions (figure 16c,e). Numerous small to large vacuoles are evident in both white and grey matters (figure 16d,f). In damaged regions sensory and motor neurons have disappeared and many cells seem to colonize injured zones (figure 16d). Note that the burst aspect of the injured spinal cord decreases the further from the epicentre you go along with the tissue vacuolisation process.

1.5.2. Quantification of the lesion size

Computer-assisted analysis of the pictures from microscope has allowed establishing a quantification of the lesion extension rostro-caudally from its epicentre 2 and 6 weeks after cSCI. The percentage of damaged spinal cord on both sides from epicentre is quite comparable 2 and 6 weeks post cSCI (figure 17A). However, from 600µm caudally to the epicentre, the percentages mean values tend to be inferior 6 weeks after cSCI than 2 weeks post cSCI but the difference is not significant ($p>0,05$). Two weeks following cSCI, the lesion represents 76% on average of the total hemi-section at the epicentre and 6 weeks later, this value is 58% on average.

The volume has also been calculated following cSCI. Two weeks after impact, the lesion presents a mean volume of 5109241mm^3, whereas 6 weeks post cSCI this volume is reduced to 3050795mm^3. But the decrease is not significant ($p>0,05$, figure 17C).

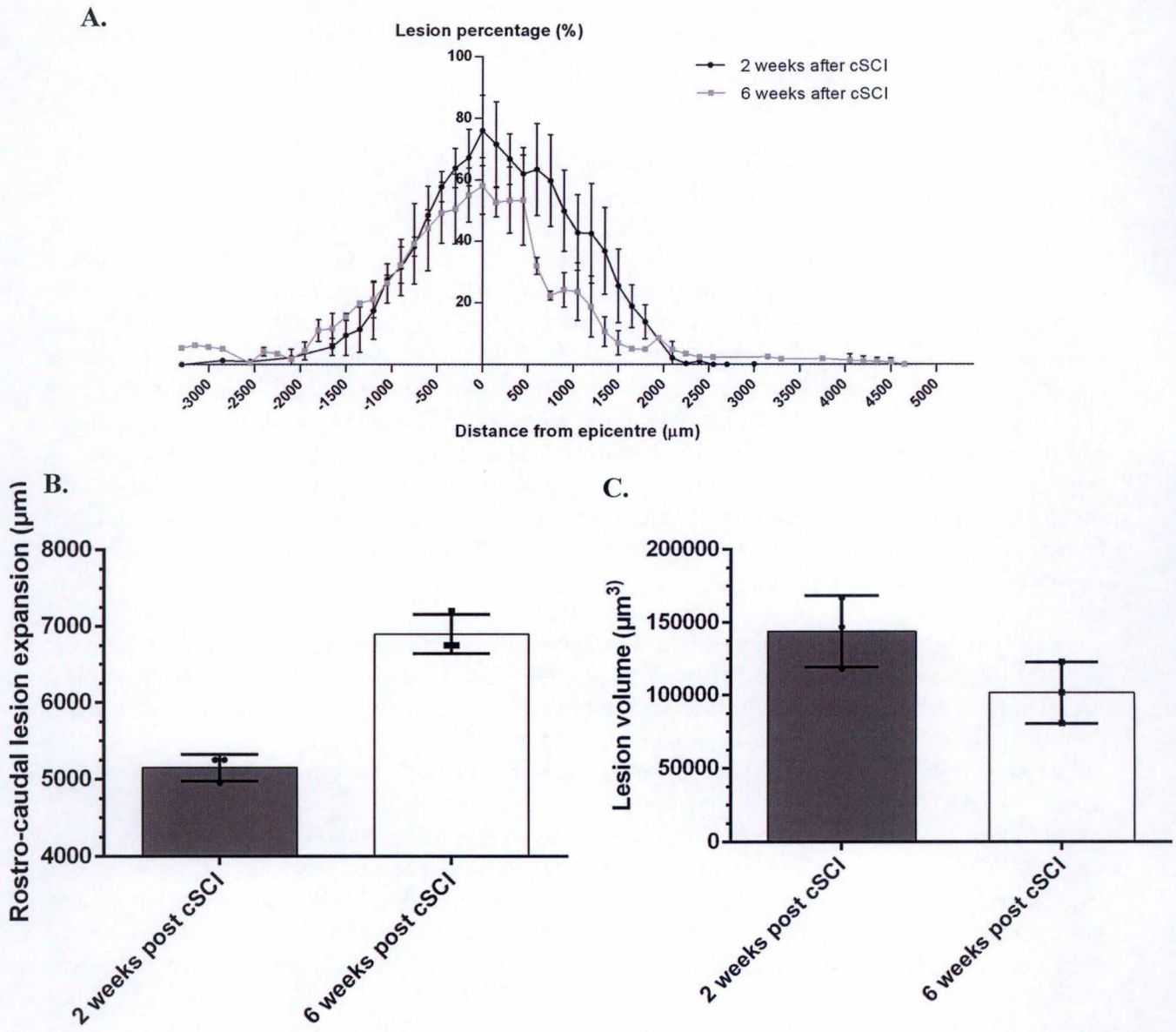

Figure 17. Quantificatio of the lesion size. A. Surface percentage of damaged spinal cord hemi-section rostrally and caudally from epicentre (x=0), mean percentage values and SD are represented (n=3 in each group). B. Volume of the lesion 2 and 6 weeks after cSCI, mean values and SD are represented (n=3 in each group). C. Rostro-caudal expansion of the lesion 2 and 6 weeks after cSCI, mean values and SD are represented (n=3 in each group).

It is also interesting to compare the expansion of the lesion both rostrally and caudally from the epicentre. This expansion is estimated by measuring the distance between the most rostral section and the most caudal section where the lesion begins to appear as small vacuoles. Two weeks following cSCI, the mean rostro-caudal expansion is 5150µm whereas 6 weeks after cSCI it is 6900µm. There a 34% increase of the expansion in one month but this difference is not significant ($p>0,05$, figure 17B).

2. xCT expression and localisation in the heathy and injured spinal cord

In the second main part of this Master's thesis, system X_c^- is investigated in distinct ways. Because it is the xCT protein that gives its specificity to the cystine/glutamate antiporter, the experiments were focused on it. The goal was to characterise xCT protein (expression, localisation) but also its gene expression and regulation in the case of spinal cord trauma.

2.1. xCT mRNA relative expression following cSCI

Relative expression of xCT mRNA is analysed in laminectomy case, 4 days, 2 and 6 weeks after cSCI. xCT relative expression shows a rapid and significant increase of a factor 17,2 as early as 4 days after the cSCI ($p<0,05$, figure 5). This increase of a factor 15,5 is still highly significant 2 weeks following cSCI ($p<0,05$, figure 5). Six weeks post cSCI, there is still a increase of a factor 8,2 in xCT mRNA relative expression compared to laminectomy group but the difference is not significant ($p>0,05$, figure 5). Furthermore, these results suggest that xCT relative expression tends to decrease in the weeks following cSCI (figure 5).

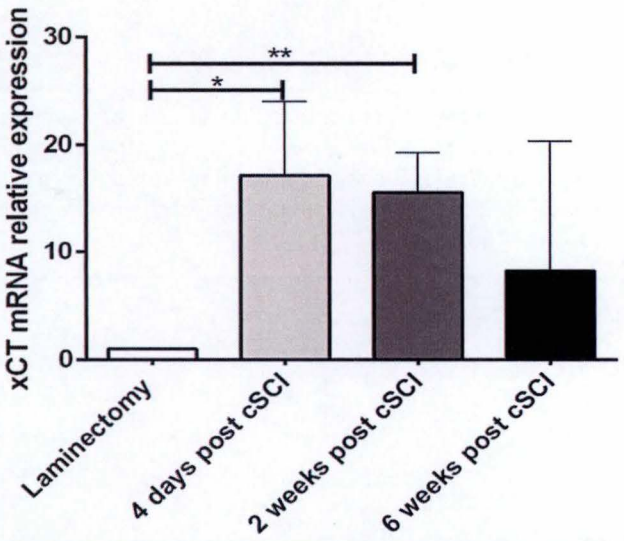

Figure 18. xCT mRNA relative expression following cSCI. Relative quantification in the distinct samples are homogenised using the house-keeping gene HPRT. Mean values and strandard deviation are represented.

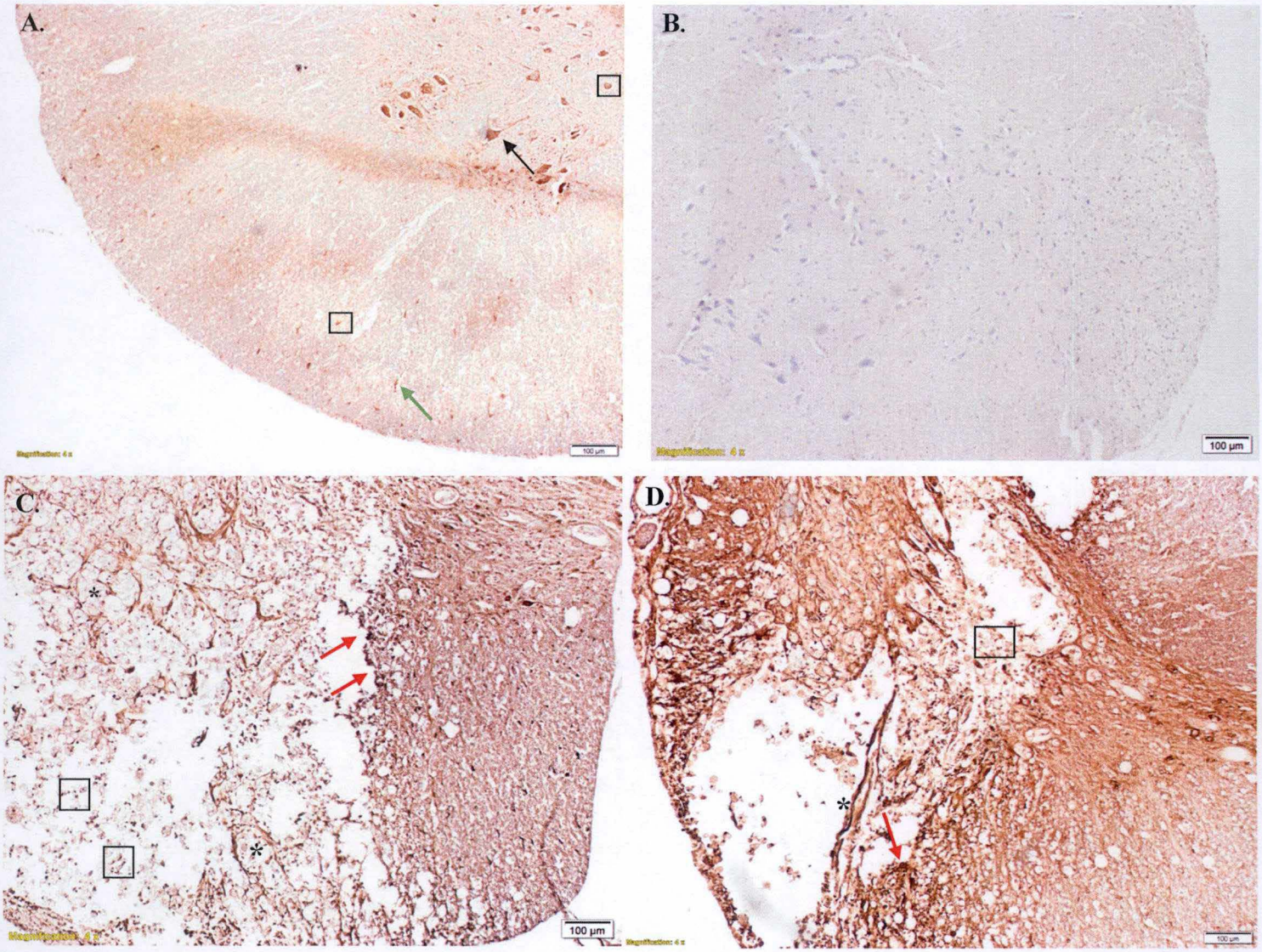

Figure 19. xCT protein cellular distribution following cSCI. A. xCT cellular distribution in laminectomy spinal cord section. B. Technical control without anti-xCT antibody. C. xCT cellular distribution in spinal cord section 2 weeks after impact at epicentre level. D. xCT cellular distribution in spinal cord section 6 weeks after impact at epicentre level. Black arrow : motor neuron, green arrow : radial glia, black rectangle : glia, red arrow : strong staining of xCT protein in border of the lesion site, black asterix : xCT protein immunostaining appears as ramified network. The anti-xCT antibody used here is NB300-317

2.2. xCT protein cellular distribution following cSCI

In the first place, a technical control has been performed without the anti-xCT antibody. The result confirms the specificity of the secondary antibody because there is no immunostaining of any structure (figure 19B).

Then, the laminectomy rat spinal cord section shows a light staining of xCT protein in glial cells in grey and white matters (figure 19A). xCT protein seems also be present in the radial glia at the periphery of the white matter (figure 19A). Motor neurons of the grey matter's ventral horn exert an immunostaining of xCT protein as well (figure 19A).

Following cSCI, the immunostaining appears stronger and in greater amount (figure 19C,D). This could suggest an increased expression of xCT protein. The staining is important in border of the injury site both 2 and 6 weeks post cSCI (figure 19C,D). Moreover, stained glial cells are much more abundant and appear grouped near the lesion site whereas they are disseminated in nervous tissue in laminectomy case (figure 19A,C,D). Another interesting point is that xCT protein immunostaining appears as ramified network near the lesion (figure 19C,D). With this technique xCT protein is detected in injured and uninjured spinal cord.

However, glial cells expressing xCT protein cannot be distinguished. That is why, to refine the analysis, double immunofluorescence has been conducted. Indeed, the aim is to detect whether there is co localization between glial cells (astrocytes using GFAP marker and activated microglial cells using CD68 markeur) and xCT protein.

In laminectomy section, white and grey matters are clearly separated which is not the case anymore after cSCI (figure 20a). xCT protein appears in the grey matter and slightly in the white matter (figure 20a). Astrocytes are also immunostained and their expansions can be noticed in the white matter (figure 20b, white arrows). Moreover, it seems that astrocytes don't co localize with xCT protein (figure 20a,b,c, black arrow, black and white rectangles). But this remark is questioned after observation of the spinal cord 2 and 6 weeks post cSCI. Indeed, the immunostaining suggests co localization between xCT protein and astrocytes (figure 20d to i, white squares). Following cSCI, there is an increase in astrocytes number and they seem to tend to concentrate in lesioned areas (figure 20). The fluorescent immunostaining also highlights black regions where the tissue has disappeared (figure 20f) because of the impact as well as the vacuolisation phenomenon (figure 20i) emerging at epicentre level and spreading rostro-caudally from it.

About microglia fluorescent immunostaining, the first thing to notice is the absence of staining in laminectomy spinal cord section (figure 21b). xCT staining in laminectomy spinal cord section is very discrete (figure 21a, whites arrows) In cSCI condition, CD68 marker is surexpressed and induces a strong staining both 2 and 6 weeks post injury (figure 21e,h). Microgliocytes presents an amyboid shape different from their resting shape (figure 21e,h). Moreover, it seems that microglial cells progressively colonize area where the nervous tissue has disappeared (figure 21h, white asterix). A strong xCT protein staining is also detectable in this area as well as elsewhere in the spinal cord section following cSCI (figure 21d,g). A clear co localization between activated microglia and xCT protein emerges following cSCI (figure 21f,i).

6 weeks post cSCI
2 weeks post cSCI
Laminectomy
xCT
GFAP
Merge
a
GM
WM
b
c
d
e
f
g
h
i

Figure 20. Fluorescent immunostaining of xCT protein (green) and astrocytes (red). a,b,c. Laminectomy spinal cord section. GM: grey matter, WM: white matter, white arrows : astrocytes, black arrows: absence of co localization between xCT and astocytes, black rectangles: xCT protein staining, white rectangles: GFAP staining. d,e,f,. 2 weeks post cSCI spinal cord section. White asterix: region where the tissue is completely destroyed, white rectangles: co localization between xCT protein and astrocytes. g,h,i. 6 weeks post cSCI spinal cord section. Rred asterix: vacuolization process, white, rectangles: co localization between xCT protein and astrocytes.

At last, another phenomenon has been noticed in spinal cord sections following cSCI and is particularly visible in fluorescent immunostaining. Indeed, the presence of numerous cells nearby the lesion site is observed but not in the uninjured side of the spinal cord (figure 22, white rectangles). We were wondering whether these cells are astrocytes or activated microglia. The immunostaining using the CD68 marker indicates the presence of some activated microglyocytes in this cells cluster but they are in minority (figure 22A). So, we can conclude that these invading cells do not belong to the microglia. Furthermore, the immunostaining of GFAP shows very few GFAP-positive cells in the invading cells population (figure 22B). Again, we can conclude that these cells are not astrocytes.

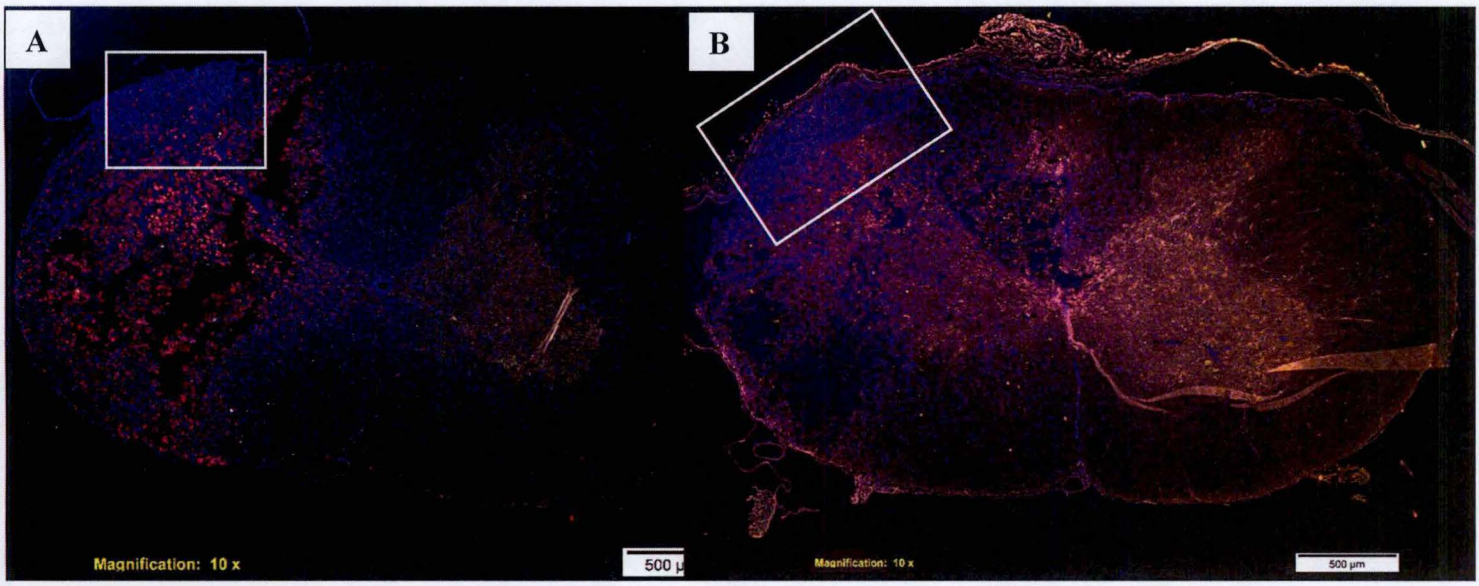

Figure 22. Double fluorescent immunostaining on rat spinal cord 2 weeks post cSCI. A. Immunostaining of CD68 marker (red), xCT protein (green) and cells nuclei (blue). B. Immunostaining of GFAP marker (red), xCT protein (green) and cells nuclei (blue).
White rectangle: invasion of the lesion by CD68 and GFAP negative cells

6 weeks post cSCI
2 weeks post cSCI
Laminectomy
xCT
CD68
Merge

Figure 21. Fluorescent immunostaining of xCT protein (green) and microglyocytes (red). a,b,c. Laminectomy spinal cord section. White arrows: xCT protein staining. d,e,f,. 2 weeks post cSCI spinal cord section. White rectangles: co localization between xCT protein and microglyocytes. g,h,i. 6 weeks post cSCI spinal cord section. The white asterix: region where the tissue has been destroyed and which is colonised by microglial cells, white circles: co localization between xCT protein and microglyocytes.

2.3. xCT transcription activator relative expression following cSCI

Nuclear factor (erythroid-derived 2)-like 2 (Nrf2) is a transcription factor present in a resting state in every cells of the body. It has been shown that under certain conditions Nrf2 can migrate in the nucleus, bounds to ARE (antioxidant response element) region of the DNA and activates xCT transcription (Soria, et al., 2016).

An increased relative expression of xCT mRNA after cSCI has been demonstrated previously, that is why the Nrf2 gene relative expression is interesting to investigate after cSCI. Similarly to xCT relative expression, there is a significant and rapid increase in Nrf2 relative expression 4 days post cSCI ($p<0,05$, figure 23). This significant increase continues 2 and 6 weeks post cSCI ($p<0,05$, figure 23).

Otherwise, it is interesting to notice that the factor of increase is far less important than in xCT gene relative expression. In fact, post cSCI, the factor of increase in Nrf2 mRNA relative expression turns around 2,3 (figure 23).

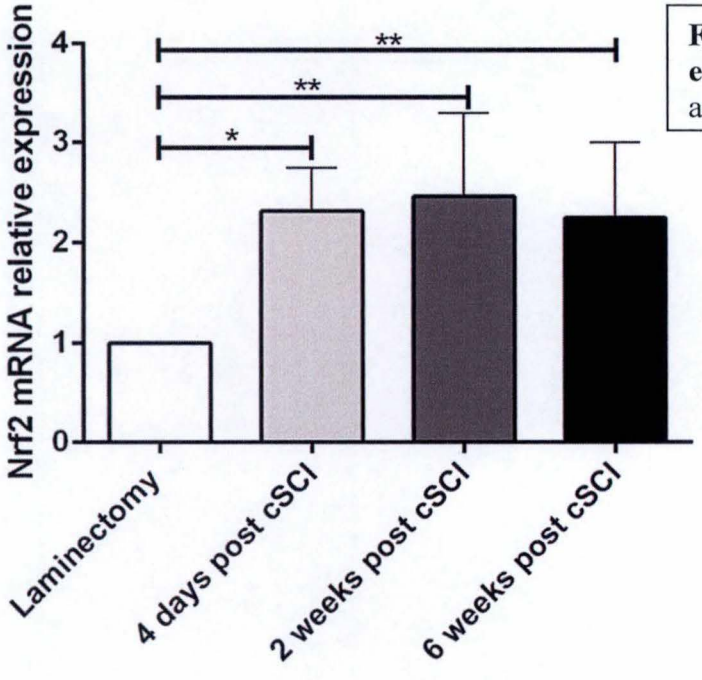

Figure 23. Nrf2 mRNA relative expression following cSCI. Mean values and standard deviation are represented.

3. Study of anti-xCT antibodies specificity

The specificity of available commercial anti-xCT antibodies is questioned in literature (Liefferinge, et al., 2016) and I was confronted to it during the experiments. That is why different techniques were conducted in order to confirm the specificity of our anti-xCT antibodies.

3.1. xCT-/- and xCT+/+ mouse tissue acquisition

xCT know-out and wild type mice brain and spinal cord were generously offered from Ann Massie's laborotary. To confirm the genetic status of these animals they send us the result of their genotyping (figure 24). A signal at 950bps is detected in xCT+/+ sample

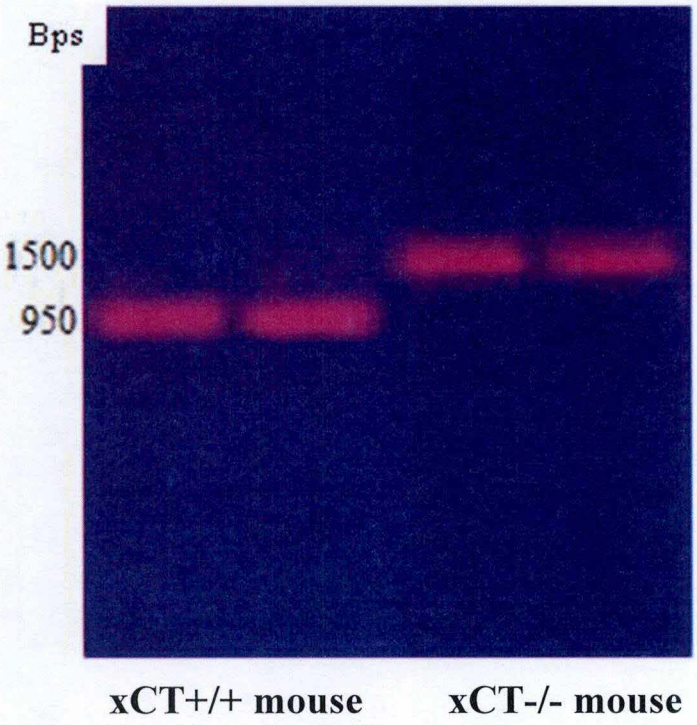

Figure 24. Genotyping results of xCT+/+ and xCT-/- mice. A piece of tail is used to perform the genotyping. Bps: base pairs

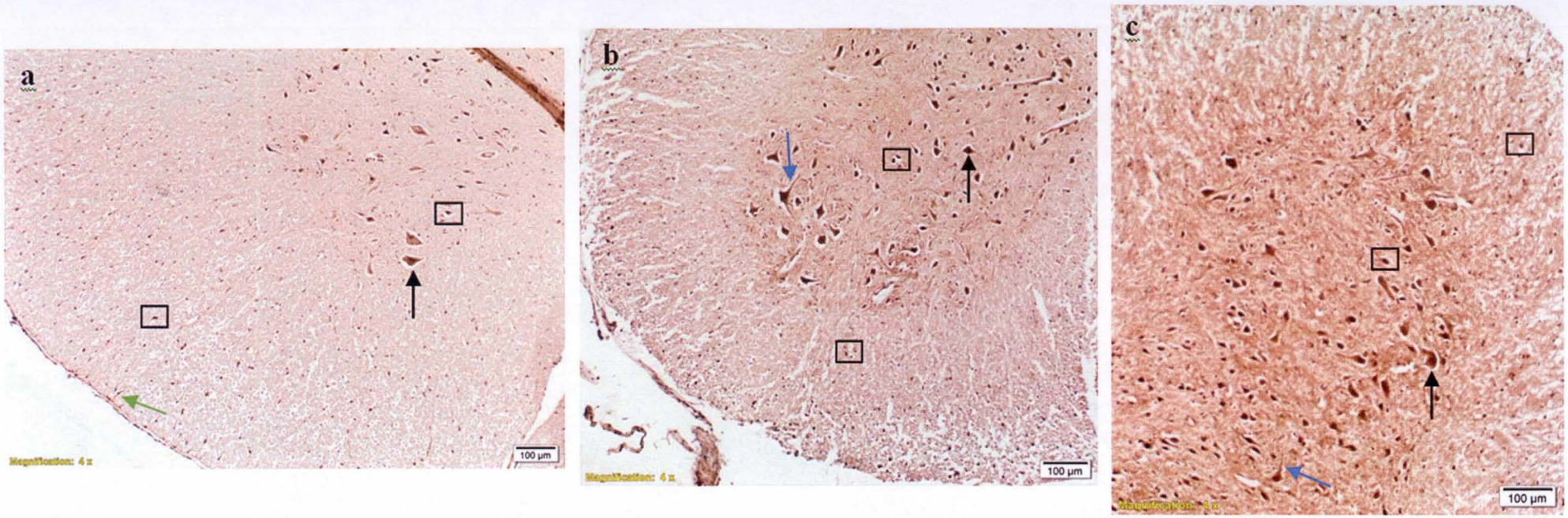

Figure 25. Peroxidase immunostaining obtained with anti-xCT ab37185 antibody 1/1000. a: rat spinal cord section, b: xCT+/+ mouse spinal cord section and c: xCT-/- mouse spinal cord section. Black arrow : motor neuron somata, blue arrow : motor neuron dendrite or axon, black rectangle : glia

Figure 26. Peroxidase immunostaining obtained with home-made anti-xCT antibody 1/200. a: rat spinal cord section, b : xCT+/+ mouse spinal cord section and c : xCT-/- mouse spinal cord section. Black arrow : motor neuron somata, black rectangle : glia

corresponding to a fragment of xCT mRNA located around exon 1. The amplification in xCT-/- sample used the same forward primer than in the XCT+/+ one and the reverse primer binds to the GFP cassette which leads to an amplicon of approximately 1500bps. As the GFP cassette is specific of KO animals, these genotyping results confirm the genetic status of our samples.

3.2. xCT protein detection by immunostaining

The immunostaining technique has been employed to test and to verify the specificity of our anti-xCT antibodies. For these experiments xCT-/- mouse spinal cord section acts as negative control and xCT+/+ mouse spinal cord and laminectomy spinal cord sections as positive control. Different slides treatments have been performed to improve the immunostaining protocol. Immunostaining on floating frozen sections, Triton100 permeabilised sections, antigen unmasked section (using citrate buffer) no convincing results (data not shown).

Furthermore, types of cells in the CNS expressing system X_c^- are still under debate. It seems that system X_c^- is expressed in motor neurons somata, dendrites and axon. xCT protein has also been highlighted in oligodendrocytes soma and processes and in microglia but not in astrocytes (Soria, et al., 2016).

Globally, background noise is strong with all the anti-xCT antibodies tested but mostly in the mouse spinal cord tissue (figures 25 to 14).

The use of anti-xCT ab37185 provides an immunostaining of neurons somata and dendrites and glial cells and their expansion in the grey matter in rat spinal cord and xCT+/+ mouse spinal cord sections (figure 25a,b). In the white matter of rat spinal cord section, radial glia is detected in periphery and is characterised by bipolar expansions. In both rat spinal cord and xCT+/+ mouse spinal cord sections white matter, glial cells are stained but cannot be determined precisely (figure 25a,b). Similarly, this anti-xCT antibody induces an immunostaining in the xCT-/- mouse spinal cord section of motor neurons somata as well as a very discrete staining of glial cells in both white and grey matters (figure 25c).

The second anti-xCT antibody tested is a home-made one in Ann Massie's laboratory (VUB, Brussels). First, it provides no staining in the rat spinal cord section (figure 26a). Furthermore, in the xCT+/+ mouse spinal cord section, motor neurons somata and glial cells are stained in the grey matter; glial cells with expansions can also be noticed in the white matter (figure 26b). Again, in xCT-/- spinal cord section, motor neurons somata are stained as well as glial cells in grey and white matters (figure 26c).

The anti-xCT #12691 antibody commercially available gives similar staining as previously which means a staining of neurons somata and dendrites and glial cells in the grey matter of rat and xCT+/+ mouse spinal cord sections (figure 27a,b). Glial cells and radial glia are similarly noticed in the white matter (figure 13a). The same staining is found again in the xCT-/- mouse spinal cord section (figure 27c).

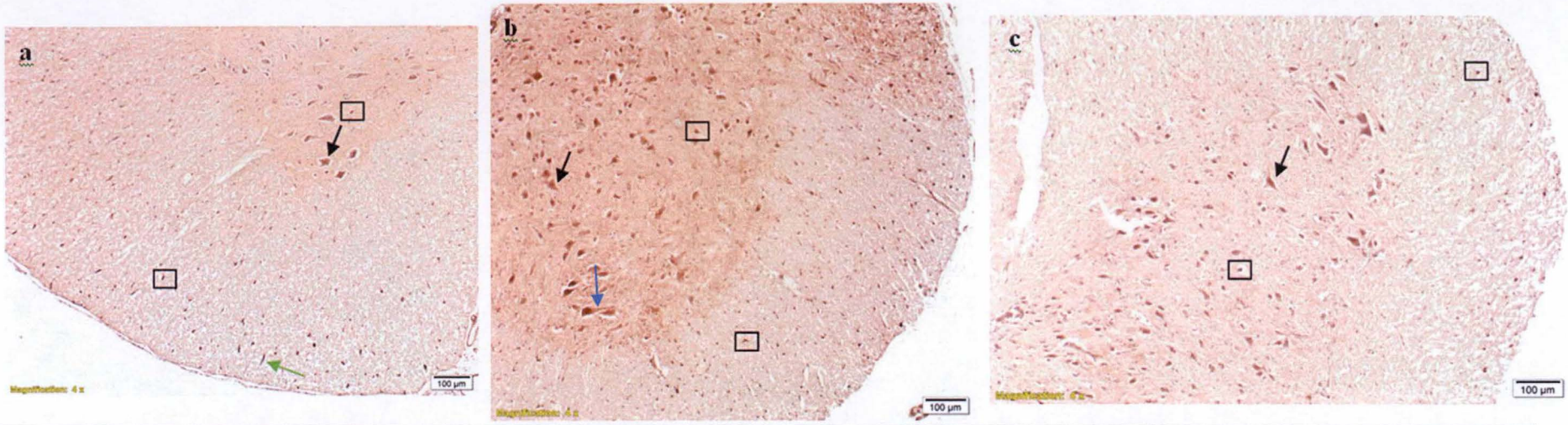

Figure 27. Peroxidase immunostaining obtained with anti-xCT #12691 antibody 1/100. a : rat spinal cord section, b : xCT+/+ mouse spinal cord section and c : xCT-/- mouse spinal cord section. Black arrow : motor neuron somata, blue arrow : motor neuron dendrite, green arrow : radial glia, black rectangle : glia

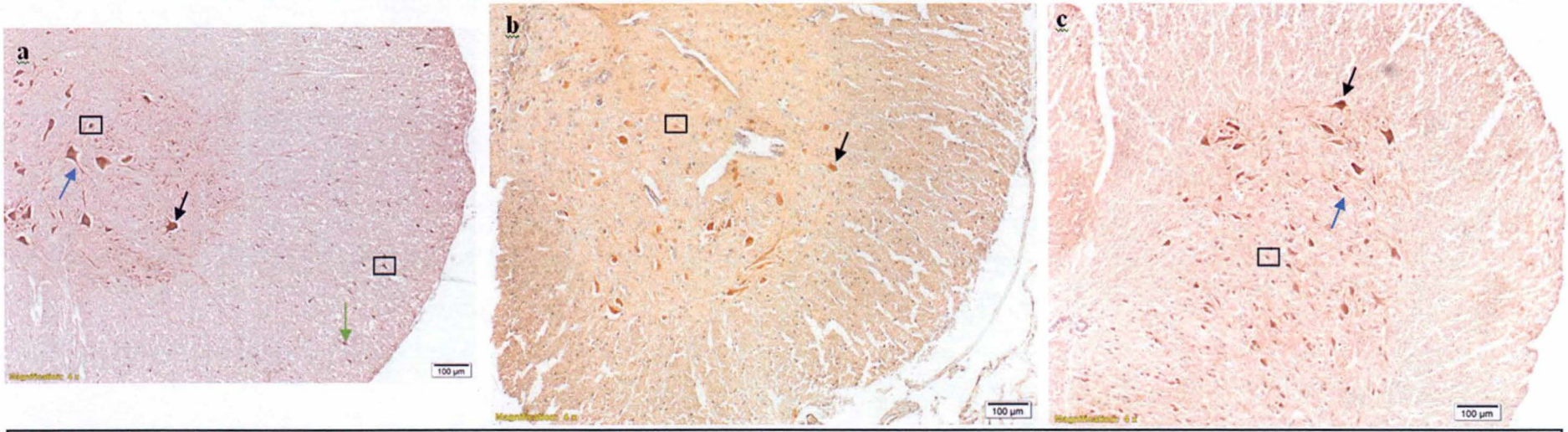

Figure 28. Peroxidase immunostaining obtained with anti-xCT NB300-317 antibody 1/1000. a: rat spinal cord section, b: xCT+/+ mouse spinal cord section and c: xCT-/- mouse spinal cord section. Black arrow: motor neuron somata, blue arrow: motor neuron dendrite or axon, black rectangl : glia

Then, the anti-xCT NB300-317 antibody offers staining of motor neurons dendrites and somata as well as glial cells of both white and grey matters (figure 28a). In xCT+/+ mouse spinal cord section, motor neurons and glial cells of the grey matter seem to be stained but there is no staining in the white matter (figure 28b). The grey/blue points observed in the white matter are cells stained by hemalun (figure 28b). Once again, there are still motor neurons and grey matter's glial cells staining in the xCT-/- mouse spinal cord section (figure 28c).

Unfortunaletely, we cannot be sure of the specificity of the anti-xCT antibodies we have. However, the antibody from Novus Biological (NB300-317) seems to provide a bit better immunostaining than the others, that's why it has been used to study xCT localization following cSCI.

In addition, peroxidase immunostaining has been conducted using peptide competition protocol. This technique permits the validation of the antibody specificity thanks to the immunizing peptide. This experiment has tested the anti-xCT NB300-317 antibody. Without antibody blocking by the immunizing peptide, staining are similar to the previous ones in both xCT+/+ and KO mouse spinal cord sections (figure 29a,c). Motor neurons soma and dendrites are stained in the grey matter. On the other hand, glial cells are clearly detected in the grey matter but the staining of white matter's glial cells is discrete in the xCT+/+ mouse spinal cord section and seems absent in the xCT-/- mouse spinal cord section (figure 29a,c). With a previous incubation of the antibody with the immunizing peptide, the staining completely disappeared both in XCT+/+ and KO samples (figure 29b,d). It means that this anti-xCT antibody is truly specific to immunizing peptide derived from xCT protein.

3.2.xCT protein detection by Western blotting

The Western blot protocol has been designed and adapted to central nervous system tissue expressing xCT protein. In literature, it has been found that squeletal muscle doesn't express xCT protein (Kim, et al., 2001), so it has been used as negative control at the beginning of Western blot protocol development. After the acquisition of xCT-/- and XCT+/+ tissue, these samples were included in the experiments as negative and positive control.

During the establishment of the optimal experimental conditions for Western blot protocol, distinct blocking agents have also been tested (BSA 3%, ECL 5%) but NFDM 5% gives the best results (data not shown). An unexpected observation was the real improvement when blocking agent was associated with TBS-Tween instead of PBS-Tween (data not shown).

Five Western blot results have been selected among all the tested conditions.

First, in contrast to publication of Ann Massie's team (Liefferinge, et al., 2016), no clear band at 35kDa is detected in any condition tried (figure 30A,B,C,D, E).

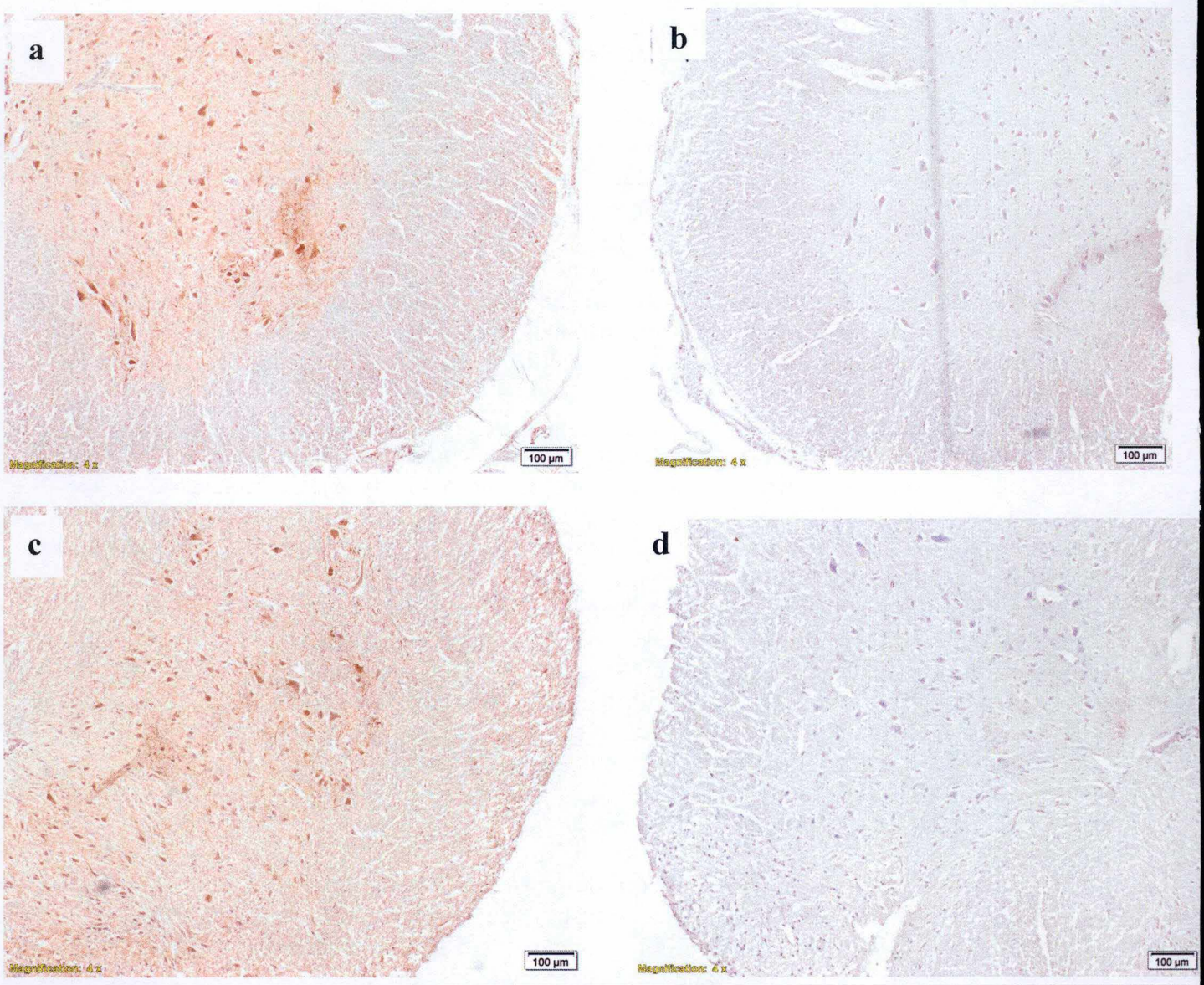

Figure 29. Peroxidase immunostaining obtained following peptide competition against anti-xCT NB300-317 antibody. a : xCT+/+ mouse spinal cord section without blocking peptide, b : xCT+/+ mouse spinal cord section incubated with blocking peptide, c : xCT-/- mouse spinal cord section without blocking peptide, d : xCT-/- mouse spinal cord section incubated with blocking peptide

The ab37185 anti-xCT antibody combined with the secondary antibody from Vectastain shows band at 55kDa as said in its data sheet (figure 6A) in each samples except in skeletal muscle. The comparison of the aspect of the 55kDa bands in the prefrontal cortex, the hippocampus and the spinal cord seems to suggest that the hippocampus is richer in xCT protein than the other samples (hippo>CPF>SC). The same antibody combined with the secondary antibody from Dako presents a 55kDa band only in the rat hippocampus sample (figure 30B) and strictly nothing in the rat spinal cord sample. This can be explained by less material available in the spinal cord sample.

Bands at 110kDa are also detected in the prefrontal cortex, the hippocampus and the spinal cord under the conditions of figure 30A and only in prefrontal cortex and the hippocampus under the conditions of figure 30B (for the same raison suggested just above). This band doesn't appear in squeletal muscle sample in both conditions (figures 30A,B).
In addition, the secondary antibody manufactured by Dako gives better results in term of ratio signal/noise than the one from Vectastain (figures 30A,B).

The use the #12691 anti-xCT antibody provides numerous bands in the KO sample compared to the XCT+/+ sample that was unexpected (figure 30C). No 55kDa band is detected in any sample. Bands at 130 and 170kDa are found again in all samples expect in squeletal muscle sample.

Concerning the Ann Massie's home-made anti-xCT antibody, no band is detected in skeletal muscle and one band is detected in the three others samples at about 130kDa as well as at 170kDa (Figure 30D).

The NB300-317 anti-xCT antibody seems to provide a signal at 35kDa in the rat spinal cord but the band is quite thick (figure 30E). A signal at 55kDa is observed in the xCT-/- and XCT+/+ mice spinal cord tissue but also in the rat spinal cord sample. Bands at about 100kDa are noticed in all spinal cord samples. A strong signal is also observed around 70kDa in the 3 spinal cord samples. In the muscle sample, there are no signals also found in the spinal cord samples. A fuzzy band is detected at about 110kDa in spinal cord samples but not in the xCT-/- samples.

A band at about 95kDa is also noticed in rat prefrontal cortex, rat hippocampus, xCT-/- and XCT+/+ mice and rat spinal cord, but not in the squeletal muscles samples with all antibodies (figure 30A,B,C,E).

In addition, I have performed Western blotting experiments with the team of Ann Massie in their laboratory. In brain samples of rat and xCT+/+ mice, the considered specific band at 35kDa was detected whereas this band disappeared in the xCT brain KO sample (data not shown). The same protocol was applied on spinal cord samples (rat, xCT+/+ and KO mice) and very surprisingly nothing was detected at 35kDa in XCT+/+ samples of spinal cord and many bands were detected in the xCT-/- spinal cord (data not shown).

Unfortunately, it seems that no anti-xCT antibodies we have at our disposition are specific for xCT protein and we are not able to be 100% sure that we actually detected xCT proteins in our samples with the Western blot technique.

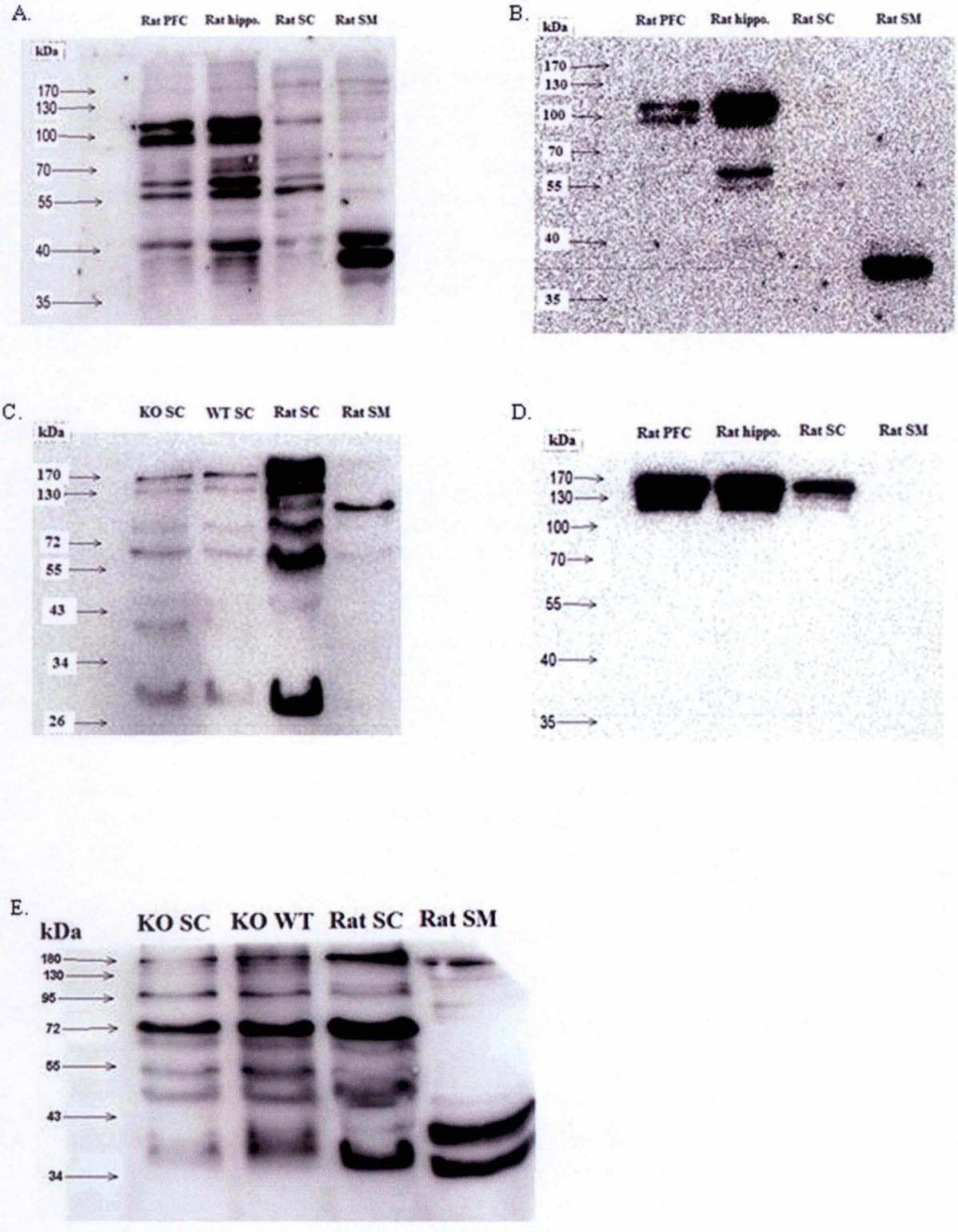

Figure 30. xCT protein detection using Western blot in the CNS tissue.
A. Western blot result using ab37185 anti-xCT antibody (1/4000)c and secondary antibody from Vectastain (1/10000). B. Western blot result using ab37185 anti-xCT antibody (1/4000) and secondary antibody from Dako (1/50000). C. Western blot result using #12691 anti-xCT antibody (1/1000) and secondary antibody from Dako (1/50000). D. Western blot result using home-made anti-xCT antibody (1/10000) and secondary antibody from Dako (1/50000). E. Western blot result using NB300-317 anti-xCT antibody 1/400) and secondary antibody from Dako (1/50000).

3.4. Construction of plasmid carrying Slc7a11 and HA reporter gene

The last technique developed to verify the specificity of our anti-xCT antibodies is the construction of an expression vector. The aim is to transiently transfect eukaryotic cells with recombinant pCMV-HA containing xCT insert encoded by the *Slc7a11* gene.

First xCT CDS has been amplified with the Q5 polymerase. The electrophoresis performed on the PCR product shows a clear signal at 1500bp which is the expected xCT CDS size (figure 31A).

Before the ligation of xCT insert in the pCMV-HA, this one must be linearised using restriction enzymes. The typical aspect of a non-digested plasmid (circular shape) on gel after electrophoresis is 2 distinct spots and a linearised plasmid is characterised by a clear and single band on gel. Thus, a single signal at 3750bp is noticed after pCMV-HA restriction and 2 spots are detected in the non digested pCMV-HA sample (figure 31B).

Once the efficiency of the plasmid restriction is confirmed, ligation of xCT insert into the linearised pCMV-HA is performed. Verification electrophoresis highlights a band at about 5300bp in the ligation solution which confirms the presence of the xCT insert into the pCMV-HA (figure 31C).

Unfortunately, this experiment has not got further the bacterial colonies screening, question of time. Indeed, the screening of bacterial colonies gave no results, so the protocol to construct this expression vector needs some improvement.

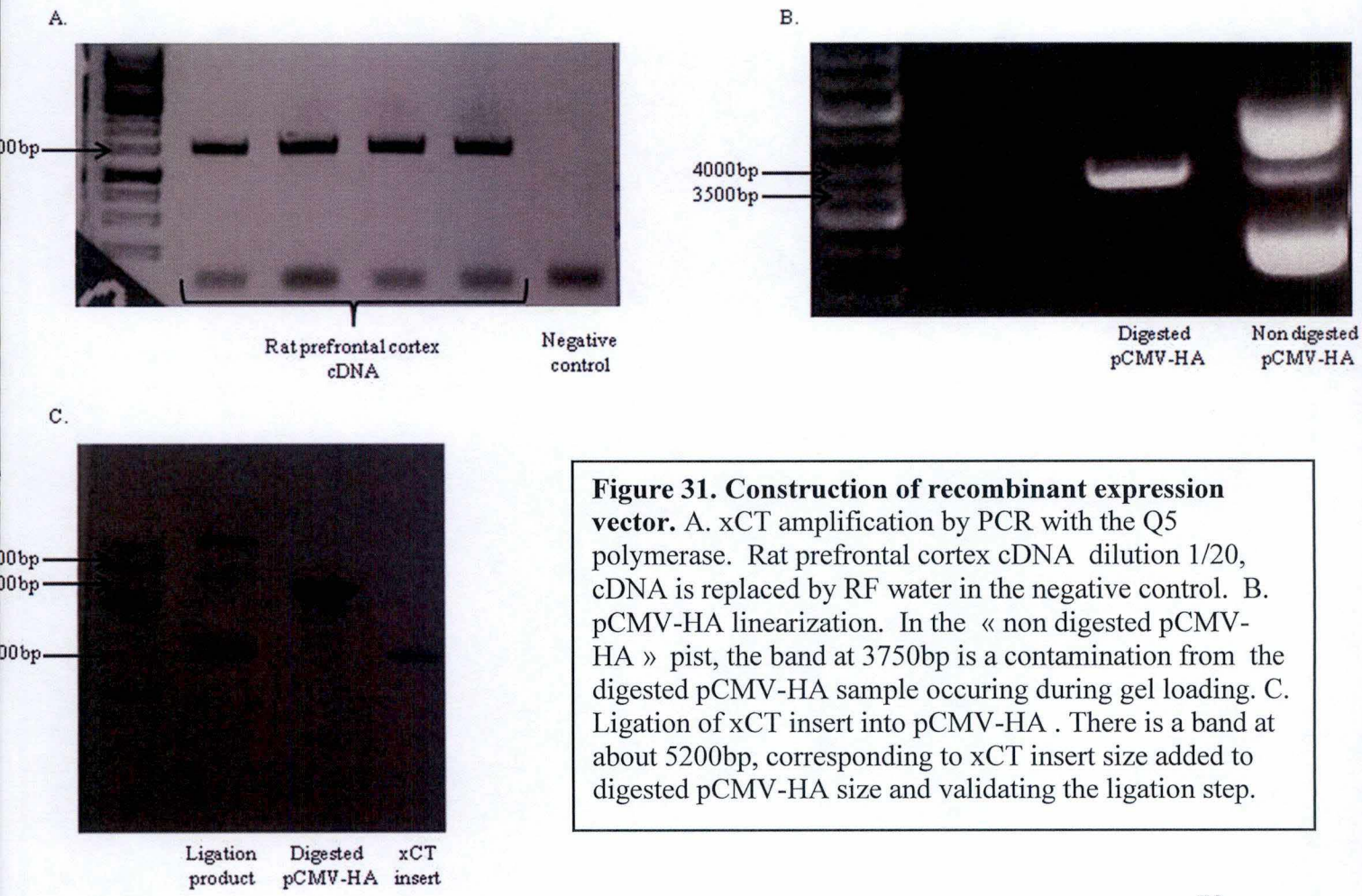

Figure 31. Construction of recombinant expression vector. A. xCT amplification by PCR with the Q5 polymerase. Rat prefrontal cortex cDNA dilution 1/20, cDNA is replaced by RF water in the negative control. B. pCMV-HA linearization. In the « non digested pCMV-HA » pist, the band at 3750bp is a contamination from the digested pCMV-HA sample occuring during gel loading. C. Ligation of xCT insert into pCMV-HA . There is a band at about 5200bp, corresponding to xCT insert size added to digested pCMV-HA size and validating the ligation step.

IV. Discussion and perspectives

In this work, we have developed a rat model for cSCI and studied xCT protein and gene expression as well as its cellular distribution in the spinal cord. Moreover, because of non specific xCT detection in immunohistochemistry and Western blot during the experimentation, we have assessed different anti-xCT antibodies and started the construction of a plasmid carrying xCT insert (encoded by the *Slc7a11* gene) coupled to reporter gene, the HA-tag.

Following experimental cSCI, unilateral hemiplegia and breathing impairment are immediately noticed after the impact and confirm that it has properly unilaterally damaged the spinal cord at mid-cervical level. The substantial weight loss post cSCI is another indicator of the physical impairment of injured rats.

Behavioural experiments have been conducted to evaluate the motor function of animals that underwent the cSCI. The traction force measuring using the grip strength test reveals a significant decrease 2 and 6 weeks post cSCI. Thus, the cervical contusion induces a striking loss of motor function in the forelimb unilaterally to the contusion. Yet, we can notice a highly significant increase in grip strength force 6 weeks after the impact compared to animals 2 weeks after the impact. It supports the idea that there is a progressive motor recovery over time after a SCI (Li et al. 2014).

These results are reinforced by the follow-up of the same animals before, 2 and 6 weeks post cSCI, which similarly present a significant decrease of their traction force post contusion as well as a significant improvement of their grip strength 6 weeks post cSCI compared to 2 weeks post lesion.

However, despite significant results, it appears that the grip strength test could not be as representative of cSCI impact as thought at the beginning. In fact, it's strongly advised to train animals with the grip strength unit before the experiment but due to lack of time our rats have not been trained. Another point is that this test measures the maximum isometric strength of the hand and forearm muscles. But, cervical nerves at C3/4 level innervate mainly scapula extensor muscles and not skeletal muscles involved in gripping abilities. So, effects of cSCI observed on the rat's traction force could be due to a spread of spinal cord damage around the impact area or are an overall loss of scapular muscles force.

The second behavioural experiment, the cylinder paw preference test, consists in the evaluation of the frequency of each paw use after cSCI. The obtained results strengthen the motor function impairment noticed by the grip strength test. Indeed, following cervical contusion, rats use significantly more their left paw instead of their right paw.

To validate the rat cSCI model, neurophysiological experiments have also been performed before and after cervical contusion. First, these analysis have been conducted on uninjured rats in order to collect preSCI CMAPs measures and to confirm that records are reproducible. Given the short latencies and the monophasic signal observed for each nerve tested before cSCI, we can conclude that ulnar and radial nerve conduction can be measured precisely and specifically. These experiments allow the detection of nerve conduction impairment after impact, due to the loss of motor neurons of the spinal cord grey matter. Thus, 2 and 6 weeks post injury, it seems that CMAPs amplitudes of palmar muscles are reduced after ulnar nerve proximal stimulation. But, no significant statistical difference can be

shown in this case and likewise after distal stimulation of ulnar nerve and radial nerve stimulation. Similarly, we are not able to show a significant difference of the onset latency after cSCI. Finally, the estimation of nerve conduction velocity does not present any statistically significant difference between uninjured and injured animals.

The lack of significant results in the CMAPs evaluation can be attributed to the stimulation of nerve not directly impacted by the cSCI. Indeed, even if these nerves are indirectly affected by the spinal cord contusion, the damages are maybe not important enough to induce a change in the amplitudes and the onset latency of muscle response.

However in literature, these parameters have been shown to be modified following cervical contusion in both humans and animals SCI models. Indeed, on the one hand, amplitude of muscles response appears to be decreased and on the other hand, the onset latency of muscle response is extended (Curt & Ellaway, 2012) (Thirumala, et al., 2015).

Yet, the lack of significant results could also be attributed to the low number of rats included in the neurophysiological analysis (n=3).

It would have been interesting to conduct this experiment earlier after cSCI. Indeed, significant differences have been demonstrated in CMAPs amplitudes and onset latency as early as 1 days post contusion (Thirumala, et al., 2015). In this work, the experiment has been conducted 2 and 6 weeks after cSCI and considering the rapid recovery of rats motor function after cSCI, neurophysiological analysis may have been more pertinent earlier following the impact.

Using EMG recordings of forelimb muscles at rest, we detect slow potentials denervation following cSCI. The detection of these abnormal potentials underlies a hyperexcitability of muscular fibres resulting in the generation of spontaneous action potentials (10). They are usually secondary to acute denervation and begin to appear 2 to 3 weeks post SCI (10). They are thought to come from metabolic perturbations within the muscle fibres following SCI or from an increased sensitivity of synaptic receptors to acetylcholine after denervation process (10).

Finally, as noticed in human SCI, the architecture of the rat spinal cord tissue is extensively damaged after the contusion (Nicaise, et al., 2013). The grey and the white matters cannot be distinguished anymore whereas they are clearly delimited in laminectomy and healthy spinal cord. In addition, there are areas completely lacking nervous tissue.

At cellular level, the loss of both sensory and motor neurons and the multiplication of glial cells are characteristic of SCI (Nicaise, et al., 2013).

The size of the lesion has also been evaluated at epicentre level but also rostrally and caudally around it.

In one hand, 6 weeks post impact, the lesion in the epicentre is less important (≈58%) than 2 weeks post cSCI (≈76%) in spite of unsignificant results. In addition, the volume of the lesion is also reduced 6 weeks post cSCI (≈3050795mm^3) than 2 weeks post cSCI (≈5109241mm^3). This suggests a phenomenon of spinal tissue remodeling (Silva, Sousa, Reis, & Salgado, 2013).

On the other hand, a rostro-caudal expansion of the lesion from the epicentre occurs in the weeks following the injury and is more pronounced 6 weeks post cSCI than 2 weeks post after. This could be surprising because we have previously shown a reduction of the lesion size in the weeks following the cSCI.

Spinal cord tissue remodelling is undeniable but it is not incompatible with a rostro-caudal expansion of the lesion. Indeed, this could be explained by the fact that the repair process takes time and is in some ways inhibited by the release of neuronal inhibitory growth factors whereas the lesion expansion process is faster and starts before the repair processes (Silva, Sousa, Reis, & Salgado, 2013).

Consequently to all these results, we can argue that we have successfully generated an animal model for cSCI.

Using the aforementioned rat model of cSCI, we have quantified the relative mRNA expression of xCT 4 days, 2 and 6 weeks post cSCI. In the early acute phase following contusion, xCT mRNA relative expression shows a rapid and important enhancement of a factor 17,2 compared to xCT mRNA relative expression in laminectomy rats. Two weeks post injury, xCT mRNA relative expression is still significantly higher than in laminectomy case with a factor of 15,5 but a bit reduced compared to 4 days post cSCI. Finally, 6 weeks post cSCI xCT mRNA relative expression tends to decrease compared to early timing post cSCI.

These results are consistent with what is found in literature. Indeed, system X_c^- is strongly activated by oxidative stress and pro-inflammatory cytokines in microglial cells under pathological conditions (Pampliega, et al., 2011) (Piani & Fontana, 1993). Thus, the increase in xCT mRNA relative expression following cSCI might be attributed the activation of the microglia and the necessity to struggle against free radicals via an intensified systhesis of GSH. But, the import of cystine within the cell is coupled with the release of glutamate inducing a massive secretion of glutamate in the extracellular space (Piani & Fontana, 1993).

Thus, system X_c^- activation also contributes to glutamate excitotoxicity following cSCI. Furthermore, it has been shown that excessive extracellular glutamate concentrations inhibit the activity of system X_c^- and lead to deficient supply of GSH precursor (cystine) in the microglia, this results in more damages due to free radicals (Massie, et al., 2008). This phenomenon is called oxidative glutamate toxicity (Massie, et al., 2008). This inhibition of system X_c^- by excessive amount of glutamate could explain the decreasing xCT mRNA relative expression 6 weeks post cSCI in our experimental model.

Then, immunochemistry has allowed us to characterize the cellular distribution of xCT protein before and after cSCI. First, in a physiological situation, xCT protein appears to be expressed by motor neurons in the grey matter, glial cells in both grey and white matters and radial glia in the white matter periphery. The radial glial cells are progenitor cells able to differenciate into neurons, astrocytes and oligodendrocytes during the embryonic CNS development. In the adult after CNS injury for instance, radial glial cells can differentiate into mostly astrocytes, maybe into oligodendrocytes and some of them into neurons of the upper-layer of the cortex (Barry, Pakan, & McDermott, 2014). But at this stage, we cannot precisely define which type of glial cells express xCT protein.

Furthermore, xCT immunostaining following cSCI is stronger than in laminectomy case with a focus on border of the lesion epicenter. Moreover, xCT expressing cells seem to form a network near damaged zones. This network aspect may be associated to the presence of astrocytes and their cyplasmic expansions (Piani & Fontana, 1993).

Then, we have tried to identify the type of glial cells expressing xCT protein using fluorescent double immunostaining. We have used the GFAP marker to identify astrocytes and the CD68 marker for the activated microglia.

First, no co localization between xCT protein and astrocytes is demonstrated in the laminectomy case. But following cSCI, it seems to be co localization between xCT protein and astrocytes. In literature, xCT expression by astrocytes is currently under debate (Albrecht, et al., 2010) (Burdo, Dargusch, & Schubert, 2006).

In addition, the GFAP immunostaining shows an increased number of astrocytes near damaged areas following cSCI as already described in the literature (Liverman, Altevogt, Joy, & Johnson, 2005).

About CD68 immunostaining, no activated microglial cells are detected in laminectomy group. This is explained by the choice of marker used to identify microgliocytes. Actually, CD68 is a marker of activated microglia so such result is not surprising because this spinal cord is not injured. Then, in laminectomy case, xCT fluorescent immunostaining is not pronounced which is not surprising again because it is the uninjured condition.

Following cSCI, the lesioned spinal cord is invaded by CD68 positive cells, mostly located in border of disrupted regions. Thus, we demonstrate the strong activation of microglia following cSCI (Liverman, Altevogt, Joy, & Johnson, 2005). xCT fluorescent immunostaining is very strong as well and highlights a clear co localization with CD68-positive cells. These results are consistent with the literature where activated microglia strongly expresses xCT (Pampliega, et al., 2011) (Shih, et al., 2006).

The last thing we have pointed with the fluorescent immunostaining is the invasion of the injured tissue by numerous cells GFAP- and CD68-. The use of CD68 and GFAP markers reveals that these cells are neither activated microglial cells nor astrocytes.

Following SCI, a progressive scar of the lesioned spinal tissue is built up. This scarring tissue includes reactive astrocytes, glial precursors, activated microglial cells and a newly synthesized extracellular matrix. This glial scar is also in part constituted by invading fibroblasts forming the fibrotic scar (Yuan & He, 2013). Thus, these invading cells could be the invading fibroblasts. These fibroblasts are derived from perivascular and meningeal cells (Yuan & He, 2013).

To pursue this study in order to precisely define which cells express xCT, we could have added a double fluorescent immunostaining using anti-xCT antibody and the neuronal marker MAP2. Similarly, the nature of the invading cells suspected to be fibroblasts could be further investigated.

Thus, we demonstrate here an increased relative expression of xCT mRNA rapidly after the cSCI suggesting a quick adaptive response of the glial cells in particular against oxidative stress but also a decreasing xCT relative mRNA expression 6 weeks post cSCI potentially due to the excessive amount of extracellular glutamate resulting in system X_c^- inhibition.

Moreover, using immunohistochemistry experiments, we detect xCT protein in motor neurons somata and dendrites/axon as well as in glial cells and radial glia.

In addition, following cSCI, xCT protein expression appears stronger, mostly around the lesion and there is compelling co localization with CD68-positive cells. A co localization between xCT protein and GFAP-positive cells is similarly detected but only under cSCI conditions.

All these experiments to characterize xCT protein in cSCI situation have been conducted on samples located at the epicentre of the lesion. So, all of them could be performed again on samples more distant to the lesion epicentre.

Moreover, it has been shown that xCT gene expression is under the control of the transcription factor Nrf2. Globally, Nrf2 is involved during oxidative stress and stimulates the transcription of antioxidative factors, including the *Slc7a11* gene coding for system X_c^- (Shih, et al., 2006) (Bridge & Patel, 2012).

In this work, we have quantified the relative Nrf2 mRNA expression in laminectomy case and after different timings post cSCI. Like xCT mRNA relative expression, Nrf2 relative mRNA expression shows a significant and rapid increase as early as 4 days post cSCI and continues until 2 weeks post injury. Six weeks later, Nrf2 mRNA relative expression is still elevated but seems to begin to slightly reduce. These results are consistent with the relative expression profile of xCT mRNA in the same timings post cSCI.

This investigation could be continued by the quantification of Nrf2 protein in laminectomy case and at different timings post cervical contusion using Western blot experiments. Moreover, as suggested for xCT protein, it could be interesting to see how Nrf2 expression evolves rostro-caudally from the injury epicentre.

Similarly, we would have wanted to quantify the expression of xCT protein in laminectomy case and following cSCI by Western blot, but unfortunately the protocol still presents unsolved issues despite of the numerous improvement attempts. That is why, no xCT protein quantification has be conducted on cervical injured and uninjured rat spinal cord samples in order to preserve them until the Western blot protocol is completely developed.

At last, the involvement of system X_c^- in cSCI could be studied in xCT-/- and xCT+/+ mice. Because of the duality of system X_c^-, it could be interesting to perform the behavioural and neurophysiological tests described here and to study whether the deletion of system X_c^- induces a more important deterioration of the motor function following cSCI or presents a neuroprotective effect. Indeed, it has been shown for example, that the deletion of system X_c^- slows the symptoms in a mice model of amyotrophic lateral sclerosis (Mesci, et al., 2015).

In the same line, involvement of system X_c^- in the motor function impairment after cSCI could be investigated by administration of system X_c^- inhibitor like sulfasalazine to a group of rats. However, this technique will require other control because such inhibitors may present some aspecificity (Mesci, et al., 2015).

During this work, I have been confronted to some unexpected issues concerning the specificity of the anti-xCT antibodies. Such issues have been very recently pointed out in the literature (Liefferinge, et al., 2016). I have tested 4 anti-xCT antibodies. In order to validate their specificity towards xCT, I have conducted 3 distinct control experiments: the use of xCT-/- samples, a peptide competition protocol and the construction of an expression vector containing the xCT insert.

Firstly, anti-xCT antibodies were tested on xCT-/- and xCT+/+ mice tissue in peroxidase immunostaining in addition to healthy rat spinal cord section. These mice spinal cord tissues allow verifying the specificity of our anti-xCT antibodies particularly because xCT-/- spinal cord offers an undeniable negative control.

Generally, every anti-xCT antibodies induce a staining in the xCT-/- mice spinal cord sections. Motor neurons are always strongly stained in the ventral horn of grey matter and glial cells are similarly immunostained but more slightly function of the anti-xCT antibody tested. Such immunostaining of xCT-/- tissue really questioned the specificity of commercially available anti-xCT antibodies as well as the one provided by Ann Massie s lab. In fact, if these antibodies were actually specific to xCT protein, strictly no staining is supposed to be detected in xCT-/- tissue.

In addition, immunostaining experiments were completed by a peptide competition protocol in order to confirm that one anti-xCT antibody is specific to its immunizing peptide derived from xCT protein. This synthetic peptide is based on the N-terminus sequence of xCT protein between residues 1 to 50.

Pre-incubation of the anti-xCT antibody with its immunizing peptide induces the disappearance of immunostaining both in xCT+/+ and xCT-/- spinal cord sections. So, this suggests that the anti-xCT antibody is specific to the N-terminus part of xCT protein.

In literature, the generation of xCT-null mice is not described in deep details (Sato, et al., 2005). Indeed, it is only specified that the GFP sequence is inserted in xCT gene region including the translation initiation site and its 5'-flanking region (Sato, et al., 2005).

It can be supposed that the early beginning of the xCT protein is translated before the following GFP translation. Our commercial anti-xCT antibodies (except the one from Cell Signalling, #12691) are obtained from an immunizing peptide corresponding to the N-terminus region of xCT protein comprised between the first and the 50^{th} residues. Thus, a hypothesis proposed to explain the staining in xCT-/- tissue is that the antibodies recognize a very small part of the translated N-terminus sequence of xCT protein. However, such a reactivity observed in the immunostaining suggests that this hypothesis is unlikely to be true. The most likely is that the anti-xCT antibodies also recognize something else distinct from xCT protein strictly speaking.

In the comparative study of various anti-xCT antibodies (Liefferinge, et al., 2016), a fuzzy band is detected in brain xCT+/+ samples at 35kDa and disappears in the xCT-/- samples in Western blot experiments. Based on this result, Liefferinge et al argue that this band is the only one specific to xCT protein (Liefferinge, et al., 2016). However, our experiments have never given such results, even "fuzzy", except maybe with the NB300-317 antibody in the rat spinal cord sample.

Moreover, it is important to note that in their study, the revelation final step is performed for 45minutes to 1hour to detect this "fuzzy" band which is considerable. In fact, the more you expose the Western blot membrane, the more elements appear and their specificity can be discussed.

In addition, in the paper of Liefferinge et al., xCT-/- mice tissue is used as negative control even for the comparison with other species like rats or human (Liefferinge, et al., 2016). It is true that xCT-/- samples should be the best negative control but our experiments highlight numerous bands in the xCT-/- spinal cord sample although nothing is expected.

Furthermore, it has been shown that some organs do not express xCT protein like squeletal muscle (Kim, et al., 2001). In the experiments conducted in this work, there are few bands in the rat squeletal muscle systematically and no bands are also found at the same size in spinal cord samples.

In addition, based on the number of amino acids of xCT protein (502 amino acids), its molecular weight is expected at 55kDa. This 55kDa band is observed with almost all antibodies tested but also in the xCT-/- samples. A hypothesis based on Kim's publication (Kim, et al., 2001) is that the band detected at 55kDa is a modified form of xCT due to alternative splicing.

There is a detection of a signal at 95kDa with different antibodies in the CNS samples but not in the squeletal muscle. This band is also described in literature and is thought to be non specific to xCT protein (Shih, et al., 2006).

Bands are also detected at about 110 and 130kDa. A hypothesis is that our proteins extraction method is not reducing enough. In fact, xCT forms a dimer with 4F2hc thanks to strong disulfide bonds. Consequently, bands at 110kDa and bands at about 130kDa could represent the xCT/4F2hc heterodimer (4F2hc subunit MW=80kDa) (Shih, et al., 2006).

The most surprising element observed during Western blotting experiment are the results obtained in the lab of Ann Massie with their home-made anti-xCT antibody. In fact, the protocol was efficient and the proper band for xCT protein (i.e. at 35kDa) is detected in rat and mouse brain and disappeared in the xCT-/- brain sample. But under the same experimental conditions, the obtained results on spinal cord samples are disappointing because of the numerous bands present in all samples, in particular in xCT-/- mice spinal cord sample. We are still not able to explain why in brain samples the detection is optimal and not in the spinal cord samples.

Such problems to detect xCT protein were really unexpected. Results obtained in immunohistochemistry and Western blot experiments in order to validate the specificity of our anti-xCT antibodies were not convincing and hence, we have decided to construct an expression vector containing the xCT insert.

During the allocated time, we have properly developed a recombinant plasmid containing the xCT gene. Unfortunately, the screening following the bacterial transformation does not present any colony having incorporated the recombinant plasmid so far.

In perspectives, after the isolation of successfully transformed colonies and the purification of the cDNA, the recombinant plasmid is then transfected into eukaryotic cell cultures. Eukaryotic cells are then supposed to express a recombinant HA-tagged xCT protein. Western blot experiments would have been performed using anti-HA antibody (very

specific) and our anti-xCT antibodies. In theory at least, bands detected with the anti-HA antibody should be specific to the recombinant xCT protein and could be used as control. Comparison of the molecular weight bands provided by the anti-HA antibody and the anti-xCT antibodies would have allowed to determine which bands are specific for xCT protein.

Another important point is that at the beginning of the vector construction, HA-tag was thought to be in the C-terminal part of the plasmid and the primers design was based on it. But pCMV-HA sequencing has revealed that the HA-tag is actually placed in the N-terminal part. In addition, it has also highlighted that after the EcoRI restriction site there are 2 nucleotides which do not hybridize to anything. This means that the reading frame is shifted and, in this case, our recombinant xCT protein would never have been translated. Thus, new primers have been designed but they have not been tested, question of time. In these new primers, 2 nucleotides are added after EcoRI site to align the reading frame as well as a stop codon after the KpnI site.

Unfortunately, despite different techniques used, I am unable to affirm that our antibodies specifically detect xCT protein, both in Western blot and in immunochemistry. Furthermore, these intriguing results stress out the validity and scientific quality of previously numerous published papers about xCT expression and localization using commercial antibodies, in absence of appropriate controls like xCT-/- tissue (Burdo, Dargusch, & Schubert, 2006) (Tomi, Hosoya, Takanaga, Ohtsuki, & Terasaki, 2020) (Piani & Fontana, 1993). In addition, some publications advise not to use commercial anti-xCT particularly in immunohistochemistry because of the risk to stain aspecific elements and to perfom proper controls (Liefferinge, et al., 2016) (Shih, et al., 2006).

To continue the study of anti-xCT antibodies specificity, I really would have had the time to finish the construction vector experiment. I would also have performed, in immunochemistry in particular, double immunostaining using antibodies raised against xCT protein and against the heavy chain of system X_c^-, 4F2. Thus, co localization between xCT and 4F2hc could be an evidence of anti-xCT antibodies specificity. Moreover, it appears in literature that home-made anti-xCT antibodies are more specific than commercial ones (Liefferinge, et al., 2016) (Shih, et al., 2006). That is why it may be more efficient to produce our own in order to obtain more specific antibodies (Burdo, Dargusch, & Schubert, 2006).

Moreover, based on the same principle but in Western blot this time, I could have used anti-4F2hc antibody to precisely detect this subunit in my samples and to see whether this antibody provides band at its expected molecular weight of 80kDa but also at high molecular weight like 110 or 130kDa. This will indicate that we have detected the heterodimer xCT/4F2hc in the experiments using anti-xCT antibodies.

Another possibility to test our anti-xCT antibodies specificity can be the use of *sut* mice (subtle gray mice) (Liefferinge, et al., 2016). Indeed, these mice present a spontaneous deletion and substitution of the last exon of the gene *Slc7a11* resulting in the lack of xCT protein. Thus, spinal cord tissue from *sut* mice could be used as negative control similarly to xCT-/- mice.

Bibliography

Agamanolis, D. (2016) Chapter 14: cerebrospinal fluid. Neuropathology, http://neuropathology-web.org/chapter14/chaprter14CSF, consulted on 16-11-2016

Ajmone-Cat, M., et al. (2010). "Non-Steroidal Anti-Inflammatory Drugs and Brain Inflammation: Effects on Microglial Functions." Pharmaceuticals (Basel): 3(6): 1949-1964.

Albrecht, P., et al. (2010). "Mechanisms of oxidative glutamate toxicity: the glutamate/cystine antiporter system xc- as neuroprotective drug target." CNS Neurol. Disord. Drug Targets: 9:373-382.

Arulselvan, P., et al. (2016). "Role of antioxydants and natural products in inflammation." Oxidative medicine and cellular longevity: 2016:5276130.

Augustin, H., et al. (2007). "Nonvesicular release of glutamate by glil xCT tra,sporters suppresses glutamate receptor clustering in vivo." Journal of Neuroscience: 27: 111-123.

Baeur, D., et al. (2012). "The glutamate transporter, GLAST, participates in a macromolecular complex that supports glutamate metabolism." Neurochem Int.: 61:566-574.

Baker, D., et al. (2002). "The origin and neuronal function of in vivo nonsynaptic glutamate." The Journal of Neurosciences: 20:9134-9141.

Bannai, S. (1986). "Exchange of cystineand glutamate across plasma membrane of human fibroblasts." J Biol Chem: 261:2256-2263.

Barry, D., et al. (2014). "Radial glial cells: key organisers in CNS development." The internation journal of biochemistry and cell biology: 46:76-79.

Benarroch, E. (2015). "Extracellular matrix in the CNS: dynamic structure and clinical correlations." Neurology: 85:16 1417-1427.

Bernabucci, M., et al. (2012). "N-acetyl-cysteine causes analgesia endogenous activation of type-2 metabotropic glutamate receptors." Molecular Pain: 8:77.

Boundless (2016) Introducing the neuron. Biological foundations of psychology

Bridge, R. and S. Patel (2012). " System X_c^- cys/glu antiporter: an update on molecular pharmacology and roles within CNS." Bristish Journal of Pharmacology.

Burdo, J., et al. (2006). "Distribution of the cystine/glutamate antiporter system X_c^- in the brain, kidney and nuodenum." Journal of histochemistry and cytochemistry: 54(55):549-557.

Butterfield, A. and T. Reed (2016). "Lipid peroxidation and tyrosine nitration in traumatic brain injury: insights into secondary injury from redox proteomics." Clinical Proteomics Journal.

Curt, A. and P. Ellaway (2012). Clinical neurophysiology in the prognosis and monitoring of

traumatic SCI. Spinal cord injury, Elsevier: chapter 4.

Dafny, N. (2000). "Anatomy of the spinal cord." University of Texas, Department of Neurobiology and Anatomy

De Bundel, D., et al. (2011). "Loss of system X_c^- does not induce oxidative stress but decreases extracellular glutamate in hippocampus and influences spatial working memory and limbic seizure susceptibility." Journal of Neuroscience: 31:9134-9141.

de Leon, R., et al. (1998). "Locomotor capacity attributable to step training VS spontaneous recovery after spinalization in adult cats." Journal of Neurophysiology: 79:1329-1340.

Doble, A. (1999). "The role of excitotoxicity in neurodegenerative disease: implications for therapy." Pharmacology therapy: 81:911-920.

Domercq, M., et al. (2005). "Excitotoxic oligodendrocyte death and axonal damage induced by glutamate transporter inhibition." Glia: 52:36-46.

Herculano-Houzel, S., et al. (2006). "Cellular scaling rules for rodent brains." Proc Natl Acad Sci USA: 103(132):12138-12143.

Hulsebosch, C. (2008). "Gliopathy ensures persistent inflammation and chronic pain after SCI." Exp. Neurol.: 214:216-219.

Jiang, L., et al. (2015). "Ferroptosis as a p-53-mediated activity during tumour suppression." Nature: 520(7545): 7557-7562.

Jurewicz, R. (2016) Nerve study. The EMG exam

Kalivas, P. (2009). "The glutamate hypothesis of addiction." Nature Review: 10:561-572.

Kettenmann, H. and A. Verkhratsky (2011). "Neuroglia - Living Nerve Glue." Fortschritte der Neurologie und Psychiatrie 79: 588-597.

Kim, J. Y., et al. (2001). "Human cystine/glutamate transporter: cDNA cloning and upregulation by oxidative stress in glioma cells." Biochemica and Biophysica act: 335-344.

Kim, Y., et al. (2011). "Long-term changes in expression of spinal glutamate transporters after SCI." Brain Research: 1389:1194-1199.

Knierim, J. (2010). "Spinal reflexes and descending motor pathways."

Kuzuhara, S. and S. M. Chou (1980). "Localization of the phrenic nucleus in the rat : A HRP study." Neuroscience Letters: 119-124.

LabCE (2016) Cerebrospinal fluid course. https://www.labce.com/spg90840, consulted on 16-11-2016

Lepore, A., et al. (2011). "reduction in expression of the adtrocyte glutamate transporter, GLT1, worsens functional and histological outcomes following traumatic SCI." Glia: 59:1996-2005.

Li, K., et al. (2014). "Overexpression of the Astrocyte Glutamate Transporter GLT1 Exacerbates Phrenic Motor Neuron Degeneration, Diaphragm Compromise, and Forelimb Motor Dysfunction following Cervical Contusion Spinal Cord Injury." The journal of neuroscience 34(22): 7622-7638.

Liefferinge, J. V., et al. (2016). "Comparative analysis of antibodies to xCT (*Slc7a11*): forward is forearmed." The Journal of comparative neurology: 524:1015-1032.

Linher-Melville, K., et al. (2015). "Signal transducer and activator of transcription 3 and 5 regulate system X_c^- and redox balance in human breast cancer cells." Mol Cell Biochemistry: 405:205-221.

Liverman, C., et al. (2005). Spinal cord injury: progress, promise and priorities. Washington, The national academies press.

Lodish, H., et al. (2000). Molecular cell biology. Section: Overview of neuron structure and function. New-York, W. H. Freeman and Company.

Lopez, M., et al. (2015). "Resveratrol neuroprotection in stroke and traumatic CNS injury." Neurochem. Int.: 89:75-82.

Manzanero, S., et al. (2012). "Neuronal oxidative stress in acute ischemic stroke: sources and contribution to cell injury." Neurochemistry International: 62(65):712-718.

Massie, A., et al. (2015). "Main path and byways: non-vesicular glutamate release by system X_c^- as an important modifier of glutamatergic neurotransmission. ." Journal of neurochemistry: 135:1062-1079.

Massie, A., et al. (2011). "Dopaminergic neurons of sustem xc--deficient mice are highly protected against 6-hydroxydopamine-induced toxicity." The FASEB Journal: 25:1359-1369.

Massie, A., et al. (2008). "Time-dependant changes in striatal xCT protein expression in hemi-parkinson rats." Molecular Neurosciences: 19(16):1589-1592.

McCullagh, E. and D. Featherstone (2014). "Behavioral caracterization of system X_c^- mutant mice." Behavioral Brain Research: 265:261-211.

Melton, N. (2016) The role of the spinal cord. Brain and Spinal cord, http://www.brainandspinalcord.org/the-role-of-the-spinal-cord/, consulted on 19-112016

Mesci, P., et al. (2015). " System X_c^- is a mediator of microglial function and its deletion slows symptoms in amyotrophic lateral sclerosis mice." Brain: 138:153-168.

Mesci, P., et al. (2015). " System X_c^- is a medioator of microglial function and its deletion slows symptoms in amyotrophic lateral sclerosis mice." Brain: 138:153-168.

Myers, E. A. and F. T. Burbrink (2012). "Ecological Opportunity: Trigger of Adaptive Radiation." Nature Education Knowledge: 3(10):23.

Naik, P., et al. (2015). "Effect of full flavor and denicotinized cigarettes exposure on the brain microvascular endothelium: a microarray-based gene expression study using a human immortalized BBB endothelial cell line." BMC Neurosciences: 16:38.

Nakka, V. and P. Prakash-babu (2014). "Crosstalk between ER stress, oxidative stress and autophagy: potential therapeutic targets for acute CNS injuries." Molecular Neurobiology.

Nicaise, C., et al. (2013). "Early phrenic motor neuron loss and transient respiratory abnormalities after unilateral cervical spinal cord contusion." Journal of Neurotrauma: 30:1092-1099.

Nicholls, D. and A. Attwell (1990). "The release and uptake of excitatory amino acids." Trends Pharmacol. Sci.: 11:462.

Oxland, T., et al. (2011). "Biochemical aspects of SCI." Stud Mechanobio Tissue Eng Biomater: 3:159-180.

Pampliega, O., et al. (2011). "Increased expression of cystine/glutamate antiporter in MS." Journal of Neuroinflammation.

Park, E., et al. (2004). "The role of excitotoxicity in secondary mechanisms of SCI: a review with an emphasis on the implications for white matter degeneration." Journal of Neurotrauma: 21:754-774.

Park, S.-C. and J. Krug (2007). "Clonal interference in large populations." PNAS: vol. 104 no. 146.

Piani, D. and A. Fontana (1993). "Involvement of the cystine transport xc- in the macrophage-induced glutamate-dependent cytotoxicity to neurons." Journal of Immunology: 3578.

Poumay, P. Y. (2012-2013). Histologie générale II. Laboratoire cellukes et tissus, Faculté de médecine, UNamur.

Rimmele, T. and P. Rosenberg (2016). "GLT-1: the elusive presynaptic glutamate transporter." Neurochemistry International.

Rio, D., et al. (2010). "Purification of RNA using TRIzol." Cold Spring Harb Protocol.

Rowland, J., et al. (2008). "Current status of acute spinal cord injury pathophysiology and emerging therapies: promise on the horizon." Neurosurgery Focus: 25:25-22.

Saint-Ruf, C., et al. (2010). "Reliable Detection of Dead Microbial Cells by Using Fluorescent Hydrazides." Applied and Environmental Microbiology: vol. 76 no. 75.

Sasaki, H., et al. (2002). "Electrophilic response element-mediated induction of the cystine/glutamate exchange transporter gene expression." Journal Biol Chem: 274:44765-44771.

Sato, H., et al. (2005). "Redox Imbalance in Cystine/Glutamate Transporter-deficient Mice." The Journal of Biological Chemistry: 280: 37423-37429.

Sheperd (2016) SCI: basic facts. Spinal injury

Shih, A., et al. (2006). "Cystine/glutamate exchange modulates GSH supply for neuroprotection from oxidative stress and cell proliferation." The journal of neuroscience: 26:10514-10523.

Silva, N., et al. (2013). "From basics to clinical: a comprehensive review on SCI." Progress in Neurobiology.

Singh, A., et al. (2014). "Global prevalence and incidence of traumatic spinal cord injury." Clinical Epidemiology: 6:309-331.

Soria, F., et al. (2016). "Cystine/Glutamate antiporter blockage induces myelin degeneration." Glia: 64:1381-1395.

Starheim, K., et al. (2016). "Intracellular glutathione determines bortezomib cytotoxicity in multiple myeloma cells." Blood Cancer Journal: 6(7): 446.

Takana, K., et al. (1997). "Epilepsy and exacerbation of brain injury in mice lacking the glutamate transporter GLT-1." Science: 276:1699-1702.

Thirumala, P., et al. (2015). "Diagnostic accuracy of evoked potentials for functional impairment after contusive SCI in adult rats." Journal of Clinical Neuroscience: 25:122-126.

Tomi, M., et al. (2020). "Induction of xCT gene expression and l-Cystine transport activity by diethyl maleate at the inner blood-retinal barrier." IOVS: 43(43).

Tomi, M., et al. (20020). "Induction of xCT gene expression and l-Cystine transport activity by diethyl maleate at the inner blood-retinal barrier." IOVS: 43(43).

Verkhratsky, A. and A. Butt (2013). Numbers: how many glial cells are in the brain ?, John Wiley and Sons.

Wolman, L. (1965). "The disturbance of circulation in traumatic paraplegia in acute and late stages: A pathological study." Paraplegia: 59:213-226.

Xu, G., et al. (2004). "Concentrations of glutamate released following SCI kill oligodendrocytes in the spinal cord." Experimental Neurology: 187:329-336.

Yachi, S. and M. Loreau (1999). "Biodiversity and ecosystem productivity in a fluctuating environment: The insurance hypothesis " PNAS: vol. 96 no. 94

Yuan, Y. and H. He (2013). "The glial scar in SCI and repair." Neurosciences Bull: 29(24):421-435.

Zhang, Y., et al. (2011). "The Multidrug Efflux Pump MdtEF Protects against Nitrosative Damage during the Anaerobic Respiration in Escherichia coli." The Journal of Biological Chemistry: 286(230): 26576–26584.

Zheltova, A., et al. (2016). "Magnesium deficiency and oxidative stress: an update." Biomedicine: (6)4:8-14.